UNIVERSITY OF SOUTHAMPTON

A novel methodology for on-line identification of arcing high impedance faults on overhead power distribution feeders

by

Naser Zamanan

A dissertation submitted for the degree of Doctor of Philosophy at
The University of Southampton
School of Electronics and Computer Science
Electrical Power Engineering Group
United Kingdom
February, 2008

Table of Contents

List of Figures

List of Tables

A novel methodology for online identification of arcing high impedance fault on overhead power distribution feeders

Abstract

Electrical utilities use overhead energized conductors to transport electrical energy to consumers. There are millions of kilometres of overhead distribution lines in the world supplying energy for industrial, commercial and residential customers. In low and medium voltage overhead distribution systems, overhead conductors are exposed to the surrounding elements and to abnormal conditions. High impedance faults (HIFs) on distribution feeders are abnormal electrical conditions that cannot be detected by conventional protection schemes and their detection is considered to be generally a difficult problem. Such faults usually occur when a distribution line conductor is contacted by a high resistance grounded object, such as a tree, or when a conductor breaks and falls on a poorly conducting earth surface. The main problem is that HIFs do not draw sufficient fault current to be easily identified, and the presently available protection systems and relays are incapable of accurately distinguishing high impedance faults, such as a downed power line conductor, from other normal system events and activities. These faults pose a threat to human lives and properties when neighbouring objects come into contact with the lines and energized conductors.

The objective of this research was to study the behaviour of power distribution lines under high impedance fault conditions. An accurate electrical model for HIF was investigated, developed and simulated using computer software to identify special features and patterns of the associated voltages and currents. A genetic algorithm was implemented for the harmonic analysis and tracking of the transients associated with electrical faults on transmission line. This analysis has lead to development of a high impedance fault detection algorithm based on a genetic algorithm. The algorithm was tested on an electrical circuit simulated using Matlab based on real life situations, all of the electrical components and parameters of the circuit were taken from a line in operation which had a history of many high impedance faults, some of them fatal.

Acknowledgment

I would like to thank God for his love and grace which has carried me throughout my life. I treasure the gifts he has given me including my loving and patient wife and family as well as friends and colleagues who have changed my life in so many wonderful ways. I could not have completed this work without the support of my brothers and sisters and persevering love and encouragement of my parents; both inspire me and have served as a model of faith, family, and how to live your life. Most importantly, I would like to thank my wife and this work would not have been possible without her love, patience and constant support.

I thank my supervisor Professor Jan K. Sykulski, who has been more than a supervisor to me. His continuous support helped me grow professionally and personally. Professor Sykulski was always there to listen and to give advice. He taught me how to ask questions and express my ideas. He showed me different ways to approach a research problem and the need to be persistent to accomplish any goal and he was always there to meet and talk about my ideas. He guided me through the writing of academic papers and without his encouragement and constant guidance I could not have finished this thesis.

Beside my Supervisor I would like to also thank Dr. Abdulrahman Al-Othman and Dr. Khaled M. EL-Naggar for their encouragement, support and enlightenment. They had confidence in me when I doubted myself and brought out the good ideas in me.

I also want to thank Mr. Salah Behbehani a senior engineer and general manager of a division at the Ministry of Electricity and Water (MEW) in Kuwait and his staff for their support and for providing me with the necessary information for this research.

The Thesis Contents

A brief introduction is presented in Chapter 1. In Chapter 2 the High Impedance Fault, the identification problems and previous research efforts for the detection are described. In Chapter 3 the physical aspects of the phenomenon of arcing are explained, and analysis of HIF data extracted form previous work is done and a new model that represents high impedance fault is presented, tested and analyzed to prove that it has covered the high impedance signature waveform, harmonics and angle. In Chapter 4 a brief introduction to genetic algorithms is presented. In Chapter 5 a novel method for using a genetic algorithm to track power system harmonics and phase angle is presented with different study cases. In Chapter 6 a comparative study between the genetic algorithm and Fourier transform is presented to demonstrate that the genetic algorithm can perform better than Fourier transform in harmonics analysis. In Chapter 7 the use of the genetic algorithm for tracking harmonics on a power system is put to the test by applying it to track the harmonics and phase angles resulting from arcing high impedance faults.

Chapter 1

Introduction

1.1 General Introduction

From the beginning of widespread distribution of electricity and the increase in power supplied by energy grids, the burden put on the energy system by new developments and consumers in power markets in the world have led to the occurrence of faults. These faults are due to the increased demand on the existing aging electrical infrastructure, continuing low levels of investment, increasing grid congestion and the growing problem of human interference with the electric grid. These faults have caused a great deal of damage to the systems and a disruption of service to the customers. Faults occur on distribution lines as a result of severe weather, lightning strikes, over growing tree branches as seen in Figure 1.1 and the occasional human or animal intrusion.

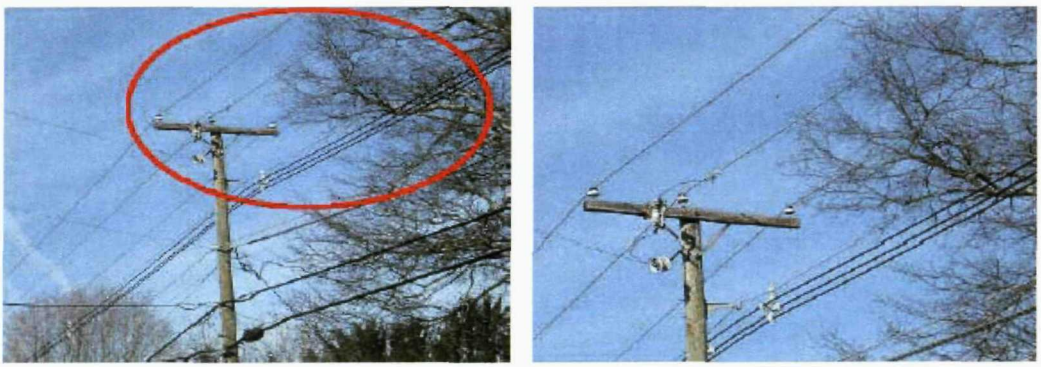

Figure 1.1 Potential HIF Due to Tree-Limb contact

The direct impact of fault currents and their effects on transmission line equipment cannot be underestimated in terms of loss of service and associated costs and it could lead to blackouts that affect a large number of customers at a huge cost to society [1]. Safety and reliability are the two most important aspects in electric power supply systems. Sensitivity and robustness of detecting and isolating faults can influence this safety and reliability.

Fuses and circuit breakers are the protection equipment of choice in power systems as they have been developed over the years. Both, however, have serious limitations and unwanted side effects. Fuses are used extensively in power systems in combination with circuit breakers. The main disadvantage of fuses is that, once they burn out, they must be physically replaced which can lead to even longer periods of interruption of service. Circuit breakers stop the supply of power to the consumer and they are necessary part of any protection system but should be the last alternative. The continuity of supply has long been very important for power engineers; circuit breakers interrupt this supply. Although many protection schemes have been developed, the main reason why these protection devices operate is because of the occurrence of fault currents in the system.

A High Impedance Fault (HIF) on a distribution feeder is an abnormal circuit condition which results in energy being dissipated in a manner other than the serving of the intended load. Most faults can be detected and isolated in time, but high impedance faults and arcing faults are still difficult to detect in practice [2] because the currents the faults produce are small and they mimic normal loads. Distribution feeder conductors are prone to physical contact with neighbouring objects such as overgrown vegetation, building walls, asphalt, a high impedance object or surface, which limits current values for faults on distribution systems and prevents conventional over-current protection from operating. Under these conditions, faults can go undetected [3, 4]. The arcing that

often results from HIFs can have deadly fire and electrocution consequences. A HIF may result in damage to the electrical system, loss of power to customers, public hazard, or possible unsafe conditions due to arcing and flashing and possible property fire [5]. It is estimated that over 60% of fires are electrically caused due to hot neutrals and arcing type faults in low voltage utilization systems [6]. The traditional methods of detecting and isolating such abnormal conditions are over-current protection relays. Conventional protection relays can easily miss these faults because the magnitude of HIF current signals is much lower than their settings (i.e. it produces only slight deviations from steady state current) [7]. Over the years, conventional over-current based protection schemes have been successfully used to detect and protect against "low impedance" faults. However, High Impedance Faults (HIFs) in power systems present a complex and unique challenge for engineers because a HIF does not draw enough current for the protection system to detect it and due to the nature of such faults as they exhibit non-linear characteristics and non-sinusoidal waveforms [8]. A high impedance fault occurs in the event of a still-energized conductor making unwanted electrical contact with many different types of surfaces and objects such as road surface, sidewalk, tree limb and so on. What all these surfaces have in common is that they reduce the flow of current toward the fault point to a level that cannot reliably be detected by conventional over-current protection schemes. The typical HIF current values are shown in Table 1.1 provides typical fault current for downed conductors on different types of surfaces where the system voltage is 12.5kV [4, 5, 9]

Table 1.1 Typical HIF current on various surfaces (system voltage 12.5kV)

MATERIAL	CURRENT (AMPS)
Dry asphalt	<1
Concrete(non-reinforced)	<1
Dry sand	<1
Wet sand	15
Dry sod	20
Dry grass	25
Wet sod	40
Wet grass	50
Concrete reinforced	75

HIFs typically occur on a distribution circuit's voltage level below 15kV. Faults on higher voltage circuits usually exhibit sufficient fault current to be detected by over-current protective devices; generally, there is sufficient voltage to overcome the initial contact impedance and the establishment of a fault current will allow conventional detection and isolation.

Figure 1.2 HIF on tree

Figure 1.3 HIF on gravel surface

The potential hazard to public and property from undetected faulty high voltage wires can lead to very serious consequences and may be fatal. Since high impedance faults can occur on many different surfaces resulting in different arcing and load characteristics, a selection of different test surfaces were utilized during the staged fault test done a few years ago by ABB and the results are shown in Figures 1.2, 1.3, 1.4, 1.5 and 1.6 [10].

Due to the unpredictable nature of HIF behavior, these downed conductors are a major concern to many electric utilities as a public safety hazard. For this reason, the IEEE Power Engineering Society published a Public Affairs Document "Downed Power Lines: Why They Can't Always Be Detected" to address and educate the public about downed conductors and the difficulties in detecting such faults [11]. For a conventional protection device an increase in load current between 0 and 100 Amps can be either a HIF condition or an increase in load demand [12].

Figure 1.4 HIF on sand surface

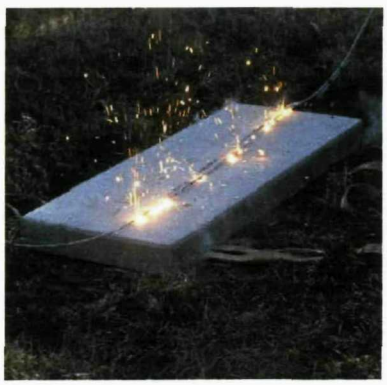

Figure 1.5 HIF on concrete surface

There is no simple way to differentiate between a load and a HIF unless other patterns in the current waveform, besides amplitude, are considered. This leads to decomposing the line current and studying its harmonic content.

Figure 1.6 HIF on asphalt surface

When HIFs are not detected, they create a public hazard and threaten the lives of people. Actually, the desire to improve public safety has been the primary motivator for the development of HIF detectors. Thus a better and more accurate fault detection technique, which has the ability to detect and recognize the behavior of the system under fault conditions, is required. This has become possible thanks to the availability of high-speed digital computers.

1.2 Research Motivation

According to the IEEE Power System Relay Committee report (PSRC) [13], high impedance faults are a growing area of concern for the utility companies. According to their survey on 107 utilities, there were 148 HIFs not detected by relays, 82 HIFs not detected by reclosers and 94 HIFs not detected by fuses. The survey reported the percentage of total recorded ground faults not cleared as between 1.5% and 3.5% depending on voltage classification. The IEEE (PSRC) survey on distribution line protection practices [14] asked 107 utilities to report on whether they had equipment to monitor distribution system harmonics; of those, thirteen utilities reported using portable equipment to monitor harmonics and five more are in the planning stage. When asked if their company has applied any type of protection scheme solely for the purpose of detecting high impedance faults, fourteen utilities responded that they had tried to apply a protection scheme for the sole purpose of detecting HIFs, while 88 of the responding utilities had not applied this type of protection. The schemes that the fourteen utilities use to detect HIFs are relay bias by load current, low pickup ground relays, ground relay blocks reset of reclosing relay, Texas A&M trial installation and open conductor detector. All but one of the reported schemes had coordination or

balance problems, and most appear to have been taken out of service because the problems outweighed the benefits.

Presently, there are no exact statistics on how often HIFs occur. This is because utilities normally record system events that result in a breaker or a fuse operation. Another factor that contributes to scarcity of data on HIFs is the legal issues associated with injuries or damages that might result from an undetected HIF. A report published by General Electric indicates that about 5-20 % of faults on distribution feeders are HIFs [5]. A study of downed conductor faults conducted by Pennsylvania Power and Light Company showed that 32% of these faults were not cleared by overcurrent protection [15]. Another study indicated that approximately 30-50% of the downed conductor events are HIFs [9].

From a questionnaire conducted during this project with Scottish and Southern Energy regarding high impedance faults, it was found that HIFs are considered as a problem to electricity power supply. Their common devices of protection are the Neutral Point Displacement protection for the 33kV transmission lines and Sensitive Earth Fault (SEF) protection for the 11kV transmission lines. In some cases of undetected HIFs the company relies normally on customers reporting the fault. When asked about the identification of the fault location, they replied that they do not have any fault location identification devices for HIFs and the line patrol will manually follow the line and check it to locate the fault before re-energising the line.

The leading expert in this area - when approached by email - B.D Russell at Texas A&M University, replied that "This problem is still a challenge since no full approved method that is 100% had been found".

In an interview with a senior engineer at the Ministry of Electricity and Water (MEW) Kuwait, he said that "high impedance fault is an issue that happens on the network in Kuwait and, on the 27th of February 2005, a fatal accident happened which

involved downed undetected power lines and resulted in one teenage death and one hospitalized".

The nature of HIFs has been studied in detail since the early 1970s in the hope of finding a practical method of detecting such disturbances. Utility protection engineers and researchers have investigated, developed and tested several solutions, and several different techniques for detecting HIFs over the years. The problem is, however, that those HIFs tend to exhibit not only low fault currents but also random behavior, with unstable and wide fluctuations in current levels. The fault signals are also rich in harmonics and have high-frequency components.

It is difficult to reject false trips caused by the many phenomena that have similar electrical signature to high impedance faults. These phenomena occur routinely on all distribution systems, they are generally undocumented and occur at random times because of load variations, capacitor switching or changes in system configuration. Conventional detection schemes monitor only low impedance faults (LIFs that result in instantaneous and large increments of current due to a low impedance path to ground). A HIF seems almost invisible to such detection methods because it presents only a small increment in line current and thus appears to be a normal load increment. With their low current, HIFs can remain undetected for hours or even days in remote areas. The best line of protection to date has been a phone call from a passer by who sees the line on the ground, or from an occupant experiencing a power outage. Even then, the downed conductor can be "hot" on the ground for a considerable length of time before it is noticed. Depending on the surface conditions where a ground fault occurs, conventional detection technologies, which are based on a measurement of current magnitude, may be unable to distinguish between high-impedance faults and load imbalances. The need to find a reliable means to selectively identify HIFs seems to be a growing area of interest to power utilities.

1.3 The research contribution

This research is presenting a new technique for accurate modelling and detection of arcing high impedance faults on overhead power distribution lines. An accurate and reliable method is designed, proposed and tested using Matlab. By observing the current waveforms and frequency spectrum resulting from a high impedance fault, some characteristics are used to identify the existence of such a fault in the system. The problem is formulated as an estimation problem and solved using Real Coded Genetic Algorithms (RCGA) optimization techniques. The goal is to minimize the error in the estimated state parameters via a fitness function. The proposed technique has been tested using simulated cases. The need for a Genetic Algorithm based scheme is discussed. The detection methodology is based on digital current signal analysis. Harmonic contents and other important current characteristics are estimated. The results of the analysis show the way of differentiating between the HIF and other normal and abnormal circuit conditions. The steps of the processing techniques are shown in Figure 1.7.

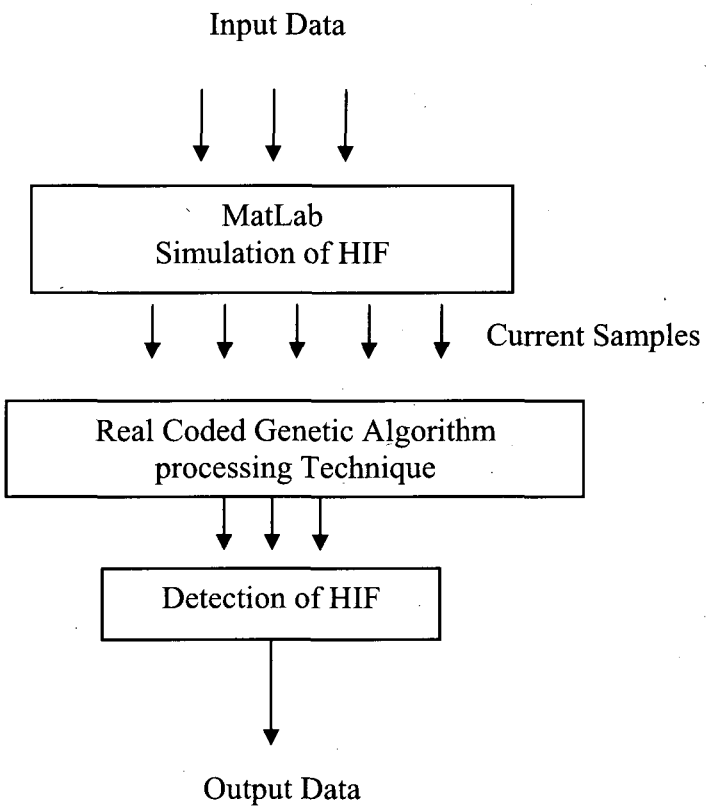

Figure 1.7 Data Processing technique

Chapter 2

High Impedance Faults

2.1 Introduction

In this chapter, the definition of a high impedance fault (HIF) and a description of the problem are presented. The motivation for detection and the various studies under way or recently completed are discussed. Exploring the electrical characteristics of an overhead distribution system that takes place when a HIF occurs is very important. So if the characteristic changes in a way that signifies the onset of a fault, a HIF could be identified. Thus a detection scheme using these changes could be developed.

2.2 Description of HIFs

The detection of HIFs on electrical distribution systems has been one of the most persistent and difficult problems facing the electric utility industry. The clearing of distribution line faults is generally accomplished by a device which senses the overcurrent produced by the fault and then reacts to disconnect the faulted line from the source. Such devices include relay and circuit breaker combinations, reclosers and fuses. Overcurrent protection is achieved by using fuse links, overcurrnet relays and ground current relays to detect faults. In addition, for providing overcurrent protection, the phase overcurrent relay must be capable of carrying normal and emergency load currents and transient overcurrent, they must not trip on inrush and surge currents; thereby causing unnecessary service interruptions. Because of this, the threshold of

operation must be set at relatively high current level in relation to the load current as seen in Figure 2.1 (i.e above load currents). The current which flows during a fault depends on many variables, one of which is the impedance of the fault itself. High impedance can limit the fault current to values which are below the threshold of operation of the fault clearing devices. In such a case the fault cannot be recognized and will persist until some external event clears it. Often this is a manual operation which may take a considerable length of time to be performed.

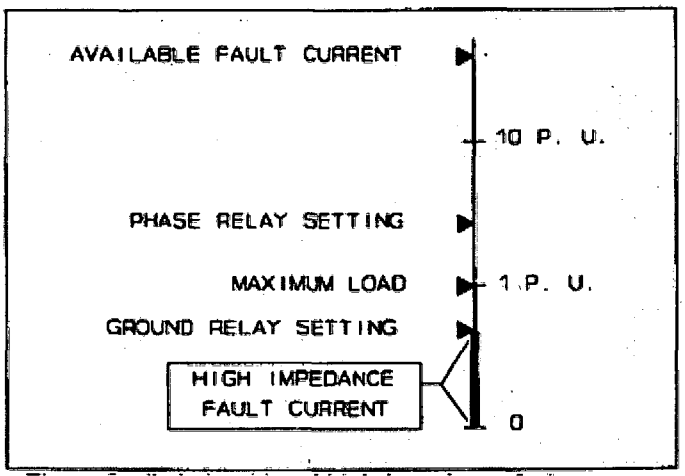

Figure 2.1 Relationship of high impedance fault currents to overcurrent device settings

Typical measured values of the primary fault currents for a 12.5kV distribution feeder conductor in contact with various surfaces were shown in Table 1.1 in Section 1.1.

A HIF may be broadly defined as one that cannot be detected and cleared by conventional fault clearing devices [16, 17]. Such a fault usually occurs when a distribution line conductor is contacted by high resistance grounded object. These faults often exhibit arcing phenomena when no solid return path for current is available. In addition to service interruption they can cause many unsafe and hazardous situations.

2.3 Physical Aspects of HIFs

HIF is a generic term which can be applied to a number of abnormal system conditions caused by a wide variety of circumstances. The main difficulty in detecting HIFs is the lack of knowledge about the electrical characteristics and behavior of this type of fault. In this section the variables associated with HIFs are categorized as a first step towards specifying a detection scheme.

2.4 Mechanisms of occurrence of HIFs

A HIF is typically characterized by a low magnitude of fault current, sometimes of an order of milliamperes. A low current magnitude might be caused by one of three conditions:

1. A high resistance or high impedance return path for the fault current.
2. The fault occurring at a location electrically remote from the source thereby reducing the available short circuit current.
3. A combination of both of the above.

A HIF can occur in various ways and can be a permanent or a temporary fault. These faults could be caused by:

1. The physical separation of conductor resulting in the conductor falling to the ground.
2. A break in the conductor insulation which results in a fault.
3. Contact of conductor with foreign objects such as tree limbs, animals, and buildings.

HIFs caused by separated and downed conductors are usually permanent faults, as they require knowing their locations and repair of the break by a repair crew. The faults caused by contact could be permanent or temporary. For example, if a tree limb

grows near a power line and contacts a conductor, the fault will persist until either the limb burns off or the fault is located by a crew and removed. If the fault is caused by an animal crossing between phases or a phase and ground, the fault would persist until the animal burns free of the line. A recloser operation would eventually restore power to the line, making the fault temporary. This research is directed towards permanent HIFs since they present the greatest risk to public safety.

2.5 Operational problems caused by HIFs

Conventional protection devices operate when the line that is protected exceeds the system's normal value (voltage unbalance, current, impedance, etc.) for operation. In the case of an over-current relay, a gross positive deviation of current must occur in order to cause the relay to operate. The relay must be set to operate above the normal load current, the emergency load current and occasional positive excursions from the system normal current. For example, a system is supplying 600 Amperes of load current and a HIF occurs on this system producing a few amperes. By comparing the HIF current and the normal load current it is found that the HIF current will remain un-measurable and undetectable using conventional protective devices.

A HIF caused by a downed conductor could produce as little as a few milliamperes of fault current, which is essentially a zero-current condition. It is difficult to discriminate this type of fault from normal load switching even during times of low consumption, or from the altering of circuit geometry caused by the operation of a circuit interrupter.

Over a period of years, researchers at Texas A&M University staged approximately 200 high impedance faults, under various operation conditions. Of these 200, less than 10% were cleared by conventional protection. Pennsylvania Power & Light Company, in a survey of electric utilities found that 61% of overhead distribution

lines had problems with HIFs. The survey also found that on a 12kV overhead distribution system, up to 32% of faults produce currents too low for detection by overcurrent devices [15, 18].

Sometimes HIFs exhibit arcing of a highly random nature, resulting in fault currents with noticeable high frequency components. The same behaviour can result from normal operations such as capacitor switching and transformer tap changing. If the fault occurs within 20 miles of the substation, the resulting high frequency noise can sometimes propagate back to the substation, allowing for detection there. However, grounded capacitors along the way can sharply attenuate the signal. These attributes of HIFs make them very difficult to detect.

Faults on primary distribution feeders are commonly cleared by devices on overhead lines which sense over-current conditions. These devices are placed to interrupt fault currents, which may constitute 150-300% of normal load currents, but they should not interrupt normal or emergency load currents and transient over-currents. Over-current devices are commonly set to operate at 125-200% of rated line current for a given feeder section [7, 15, 16]. Since most HIFs involve current levels much less than those of bolted (short-circuit) faults, they cannot be reliably detected by conventional devices.

Ground relays, which can sometimes be set more sensitively than phase relays, are often used to help clear HIFs. However, these relays must be set high enough to carry the neutral currents resulting from phase unbalance, and coordinate with other circuit protection devices. Tripping on large inrush currents during cold load pick up and normal circuit switching must be prevented as well. In some distribution circuits, an unbalanced load could require a ground current relay setting as high as one half of the phase relay setting. In other distribution circuits, the ground relay may be omitted entirely because of severely unbalanced conditions that make it no more effective than

the phase relay. Practically, since there are unbalanced loads on the electrical network (in some cases as much as 50-75% unbalance), utilities must set ground relays to allow for some unbalance in the phase loads which can produce a large normal neutral or earth return current. Although ground relays do detect many current faults, these relays still do not detect faults with very low current [15].

2.6 Symmetrical Components

The method of symmetrical components is very important in the analysis of three phase electrical systems. It provides a practical tool for understanding and analysing electrical power system operation during unbalanced conditions. The principle of symmetrical components, as applied to three phase circuits, is that an unbalanced group of three related phasors (for example, three unsymmetrical and unbalanced phasors of voltage or current in a three phase system) can be resolved into three sets of phasors, of equal magnitude and phase shift of either zero or 120° as shown in Figure 2.2. Each set is a "symmetrical component" of the original unbalanced system with the following properties:

1. The positive-sequence components consist of three phasors equal in magnitude, displaced from each other by 120° in phase, and have the same phase sequence as the original phasors (a-b-c).
2. The negative-sequence components consist of three phasors equal in magnitude, displaced from each other by 120° in phase, and have the phase sequence opposite to that of the original phasors (a-c-b).
3. The zero-sequence components consist of three phasors equal in magnitude and with zero phase displacement form each other.

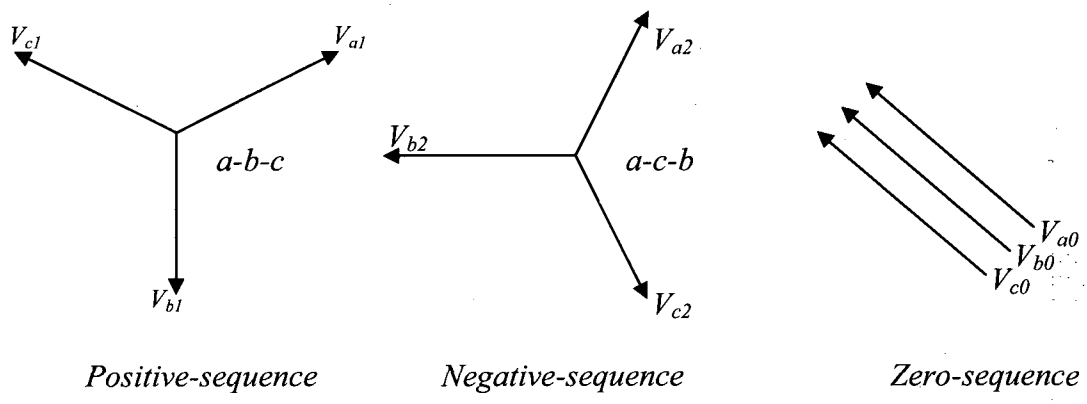

Figure 2.2 Three sets of balanced phasors which are the symmetrical components of three unbalanced phasors

For the full mathematical description of symmetrical components refer to Appendix 1.

In the case of a single line to ground fault through an impedance, as for the case of the high impedance fault, the hypothetical impedance Z_f is connected to the line as shown in Figure 2.3

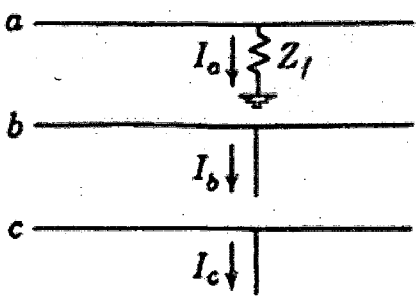

Figure 2.3 Single line to ground fault

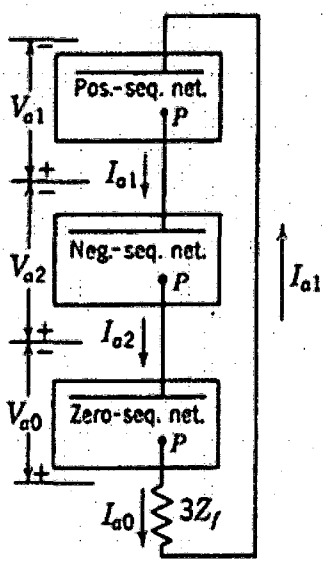

Figure 2.4 Single line to ground fault sequence network

The following relations exist at the fault:

$I_b = I_c = 0$

$I_{a1} = I_{a2} = I_{a0} = I_a/3$ means that all sequence circuits are in series at the fault point as shown in Figure 2.4

$$V_a = V_{a1} + V_{a2} + V_{a0} = Z_f I_a = 3 Z_f I_{a1}$$

$$I_{a1} = \frac{V_f}{Z_1 + Z_2 + Z_3 + 3Z_f}$$

As mentioned for example in [19], by applying the symmetrical components method, faults through an impedance may be treated as a single phase load. The single line to ground fault impedance Z_f is equivalent to connecting a single phase load from line a to neutral. In the case of detecting high impedance faults, the method of symmetrical components in its standard formulation does not include the analysis of the harmonics, or their angle shifts, therefore by itself does not offer any particular possibility to detect HIF without other measurements such as harmonic content and phase shift of such faults.

2.7 Harmonics and their generation

Over the past several years, electric utilities have experienced an increase in the use of harmonic producing equipment. Harmonic distortion is caused by nonlinear devices in the system. A nonlinear device is one in which the current is not proportional to the applied voltage. More recently the range of types and the number of units of equipment causing harmonics have risen sharply, and are likely to continue to rise. Harmonic load currents are generated by all non-linear loads. These include:

Single phase loads, such as:

- Switched mode power supplies (SMPS)
- Electronic fluorescent lighting ballasts
- Small uninterruptible power supplies (UPS) units

Three phase loads, such as:

- Variable speed drives
- Large UPS units

Since harmonic voltages produce harmonic currents with frequencies considerably higher than the power system fundamental frequency, these currents encounter much higher impedances, as they propagate through the power system, than does the fundamental frequency current. One of the reasons is the skin effect, which is the tendency for higher frequency currents to flow near the surface of the conductor. Since little of the high-frequency current penetrates far beneath the surface of the conductor, less cross-sectional area is used by the current. As the effective cross section of the conductor is reduced, the effective resistance of the conductor is increased. This increased heating effect is often noticed in two particular parts of the power system: neutral conductors and transformer windings. These harmonics flow in the system neutral and circulate in delta-connected transformer windings, generating excessive conductor heating in their path [20].

Other sources of harmonics on distribution system are transients due to capacitor or load switching. Although transient disturbances contain high-frequency components, transients and harmonics are distinctly different phenomena and are analyzed differently. Transient waveforms exhibit the high frequencies only briefly after there has been an abrupt change in the power system. The frequencies are not necessarily harmonics; they are the natural frequencies of the system at the time of the switching operation. Transients are usually dissipated within a few cycles and they are usually associated with changes in the system such as switching of a capacitor bank. Harmonics are associated with the continuing operation of a load [21].

Because of the adverse effect of harmonics on power system components, many companies and countries have established limits of harmonics on the distribution systems. In France the limits of harmonics on the distribution system are 0.6% of fundamental for even harmonics, 1% of fundamental for odd harmonics, and 1.6% total harmonic distortion. In Germany the individual harmonic level are set at 5% of the

fundamental voltage level up to the 15th harmonic. In Australia the limits of harmonics in a distribution system up to 33kV is 4% for the odd harmonics and 2% for the even harmonics [20].

The IEEE developed the standard 519-1992 [22] to define recommended practices for harmonic control. This standard also specifies the maximum harmonic distortion allowed in the voltage and current waveforms for various types of systems. The maximum harmonic current distortion in power systems is shown in Table 2.1.

Table 2.1 Current Harmonic limits as per IEEE 519-1992

Maximum Harmonic Current Distortion in % of I_L						
Individual Harmonic Order (Odd Harmonics)						
I_{sc}/I_L	< 11	11≤h <17	17≤h <23	23≤h <35	35≤h	TDD
<20*	4.0	2.0	1.5	0.6	0.3	5.0
20<50	7.0	3.5	2.5	1.0	0.5	8.0
50<100	10.0	4.5	4.0	1.5	0.7	12.0
100<1000	12.0	5.5	5.0	2.0	1.0	15.0
>1000	15.0	7.0	6.0	2.5	1.4	20.0
Even harmonics are limited to 25% of the odd harmonic limits. TDD refers to Total Demand Distortion and is based on the average maximum demand current at the fundamental frequency taken at the Point of Common Coupling PCC.						
* All power generation equipment is limited to these values of current distortion regardless of I_{sc}/I_L						
I_{sc} = Maximum short circuit current at the PCC I_L = Maximum demand load current (fundamental) at the PCC h = Harmonic number						

High impedance faults are dominated by odd harmonics as will be shown in Section 3.4 of this thesis using real HIF data collected by KEPCO. The typical magnitudes of the 3rd and 5th harmonics with respect to the fundamental current exceed most of the limits allowed in the distribution systems by the countries mentioned above. Thus the presence of harmonics due to non-linear loads, although inconvenient, is unlikely to pose a significant problem in the proposed HIF detection scheme. This view is reinforced by the study in [23] which emphasises the differences between high impedance fault harmonics and the harmonics which occur from other causes in the

system. The study suggested preferred criteria to distinguish HIF from other events in the system. These criteria are:

1- the change in the ambient 3rd harmonic current magnitude

2- the change in the ambient 3rd harmonic current phase angle

The study concluded that there is a unique signature of a high impedance fault due to a combination of the magnitude and phase angle of a single harmonic current and thus an accurate measurement makes the 3rd harmonic current a viable and reliable parameter for detection of HIFs.

The problem of correctly identifying a system disturbance, which at least superficially may appear to be the same as the normal system operating condition, is compounded by the different types of distribution systems. Ungrounded systems can behave considerably differently from grounded systems during a HIF. If a conductor breaks and makes a contact with the ground, the ungrounded system reacts with a neutral voltage shift while the grounded system reacts with the change in phase currents. It is obvious that neither the phase current nor the neutral voltages are sufficient by themselves for detection purposes. During a bolted fault, the thermal effects of faulted lines are dangerous, causing possible destruction of the interconnected system. So detection and clearing of these faults is necessary for the integrity of the entire feeder. On the contrary, HIFs pose no direct danger to the system, although electric shock and fire hazards still exist. Hence, system protection is not the prime goal of HIF detection. Even though the actions taken to detect these faults may be identical to those of bolted fault clearance, the motivation for HIF detection is to improve public safety.

2.8 Previous High Impedance Fault investigations and research

The fault conditions can adversely affect the quality of electrical service and under some conditions present safety hazards such as arcing and fire as shown in Figure 2.5. Various utilities and research institutions have long sought an appropriate fault detector. In power systems, most faults are detected by an increase in current flow towards the fault point. The most common method of detecting and isolating an abnormal condition on a distribution line is an over-current protection relay [2, 7]; however, since most HIFs produce current levels indistinguishable from normal loads, this method causes frequently unnecessary service interruptions. Lowering the settings on ground relays in the hope of detecting abnormal ground currents is impossible for multiple grounded systems and unreliable for feeders with a normally high degree of unbalance.

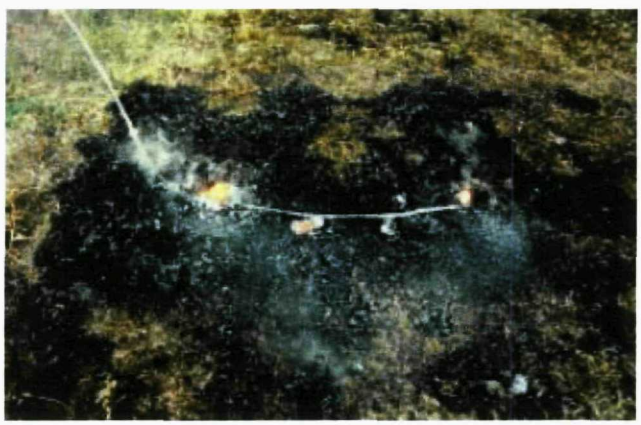

Figure 2.5 Arcing power line

Mechanical detection usually involves some way of forcing contact with a solid ground in order to allow conventional over-current protection to operate. The first type of mechanical HIF detection method consists of a device or devices mounted to a cross arm or a pole [3, 5]. The device is mounted under each phase wire in order to catch the conductor as it falls to the ground. The force of the falling conductor releases an internal spring that ejects a bus bar to make contact with the fallen wire and create a low

impedance ground fault. The ground fault created will cause conventional over-current protection to operate. However, sagging conductors that do not come in contact with earth or a grounded object could be detected by this mechanical method by mistake. Moreover, the installation and maintenance costs are high. For bi-directional coverage, six units would have to be mounted on each pole. Even though the cost is high to allow usage on every pole, utilities may install the system in certain areas, such as churches, schools, or hospitals.

A second type of mechanical HIF detection method uses a pendulum mounted aluminum rod with hooked ends [3]. It is suspended from an under-built neutral conductor. The falling conductor is caught and produces a low impedance ground fault, which operates conventional over-current protection. Typically, two units are mounted per span. Again, sagging conductors that do not come in contact with earth or a grounded object could be detected by this mechanical method. Also ice, wind and tree growth could cause a false detection.

The Ratio Ground Relay detection method is an electromechanical relay [4, 24, 25] based on the concept that the amount of load unbalance on a given feeder is invariant over a small time interval. This is done by computing the ratio of neutral current to positive sequence current. Another technique involves finding a chi-squared test statistic using 60 Hz sequence components and harmonics to detect HIFs. This technique seeks a change in feeder unbalance to indicate the presence of a fault. After implementation, the method failed in 60% of cases [17]. Yet another scheme uses increases in frequency components near 60 Hz to detect faults. However, the 60 Hz parameters normally dominate the frequency spectrum, so it is difficult to detect meaningful changes in them [26].

Some other methods try to solve the problem using different approaches as shown in Figure 2.6 and amongst past HIF works published in IEEE transactions it is

documented that the fault current harmonics are a function of the system voltage and not of the load current [8]. Phase information in the harmonics is shown to be significant in evaluating if a HIF exists. The phasor changes of the 3rd harmonic are measured in addition to its magnitude or phase position. High-impedance faults are non-linear and always result in distorted currents, so harmonic analysis is critical in the estimation and determination of HIFs. This is in part the reason why lower spectral components are preferred for HIF measurements. Also, the 3rd harmonic is a good measurement factor since it is the least disturbed by a resonant condition. A signature of a HIF, as described in [23], can be detected by the change in the ambient 3rd harmonic current magnitude and its relative phase to the system voltage.

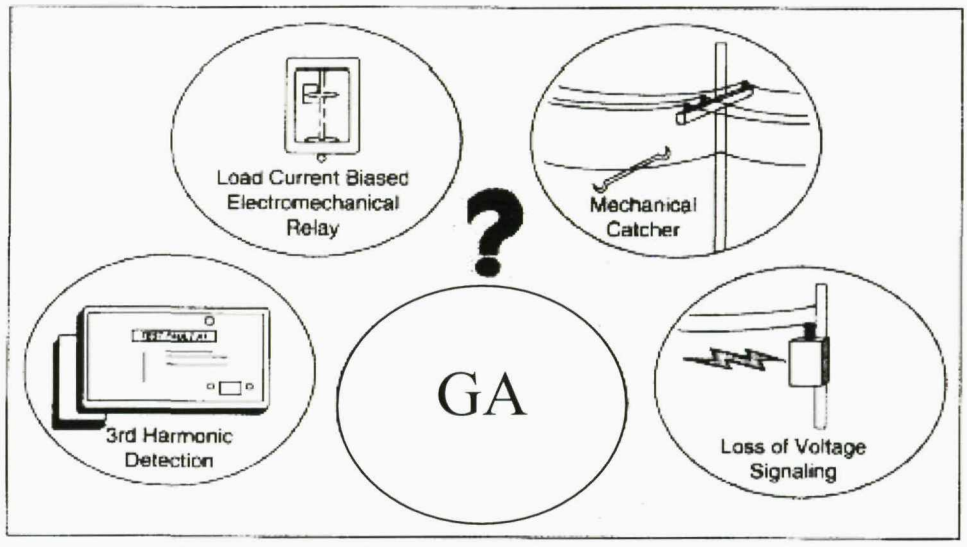

Figure 2.6 Some approaches for HIF detection

Researchers from Texas A&M University have investigated high impedance faults since the early 80s and are pioneers in HIF detection and developed algorithms based on current magnitudes and waveforms. Mixtures of algorithms to evaluate HIF have been implemented, but only two are detailed and described in some depth. The energy algorithm [4, 25] method monitors a specific set of non-fundamental frequency component energies of phase and neutral currents. After establishing an average value

for a given component energy, the algorithm indicates arcing if it detects a sudden, sustained increase in the value of that component. The randomness [4, 25] algorithm, on the other hand, calculates the amount of randomness associated with a fault using the energy contained at a non-fundamental frequency as the monitoring quality. The detection logic used by their microprocessors uses two (or more) algorithms for analyzing four currents (3 phases + neutral) and their three spectral groups (odd, even, and none). A total of 24 inputs are taken into the microprocessor to determine a HIF (two algorithms * four currents * three frequency components). Timers are intended to rule out normal system activity such as bank switching, motor starting, or load shifting. It is considered that nominal system disturbances such as the aforementioned are occasional and momentarily only. High-impedance faults must be detected within the first minute of incidence; otherwise due to changing media conditions (chemical properties in the fault location due to heat, and ionization) they will never be detected since the current may level off to normal again while the HIF still exists. When the pre-programmed logic believes that there is a HIF, the system's alarm state changes. If the confidence level reaches 100% (first presence of a HIF), the algorithm resets the flags and tests the system all over again. If the HIF still exists, and the second confidence level is again acceptable (i.e. >80% of confidence), it tries one last time. If the detection is acceptable again, an alarm triggers. This system was developed by Texas A&M Power System Automation Laboratory (PSAL) and it is currently licensed to General Electric (GE). Ever since GE's acquisition of this product [8], HIF research de-intensified as the end-product detects a good number of HIFs today.

The Digital Feeder Monitor system is a method that analyses harmonic and non-harmonic components of the feeder's current between 30 and 780Hz through the use of pattern recognition. Down conductors are differentiated from arcing conductors by looking for a loss of load or a high current fault prior to the HIF event.

The Load Analysis Algorithm [25] method differentiates between arcing downed conductors and arcing intact conductors by looking for a precipitous loss of load and/or an overcurrent disturbance at the beginning of an arcing episode.

Other researchers investigated the use of wavelet transforms [27-31] where the detection process is preformed through signal decomposition. However, wavelet analysis has three severe disadvantages. The first problem is lack of phase information that accurately describes non-stationary signal behaviour. The second drawback is to do with the shift sensitivity which implies that wavelet transform coefficients fail to distinguish between input signal shifts. Finally, the third difficulty is poor directionality because wavelet transform coefficients reveal only three spatial orientations.

Artificial neural networks, which are based on the structure and function of human brains in physiology [32-39], are also used to detect high impedance faults and the method is to train the neural network for as many HIF cases as possible so when the network is then presented with an input it has seen before, it will (hopefully) produce the right output. Again, there are problems with this approach, the training sample size used has to be large to ensure that the results are statistically accurate and that requires a lot of computational power. Moreover, as individual relations between the input and output variables are not developed by engineering judgment, the model tends to be a black box or table without analytical basis. Another disadvantage of the neural networks is the complexity of hardware and software necessary to enable it to deal with industrial applications. For example, if process conditions change from those used when training the neural network, data must once again be collected, analyzed and used for retraining the system.

Table 2.2 Summary of some HIF detection methods

Methods	Description	Reference
Mechanical methods	In these methods some devices are use to provide low impedance by catching the fallen conductors	[5]
Electrical methods		
Time Domain	Ratio ground relay	[40]
	Proportional relay algorithm	[24]
	A smart relay based on time domain feature extraction	[41]
	Arc detection method	[42]
Frequency Domain	Several papers have been published based on harmonic component using Fourier transform	[43, 44]
	Inter harmonic component	[45]
	High frequency spectra	[46]
	A method based on Kalaman filtering	[47]
	A method based on fractal theory	[48]
Artificial neural networks	its method is to train the neural network for as many HIF cases	[32-39]
Wavelet transform	Wavelet transform (WT) can be used to analyze the transient behavior of a signal in both time domain and frequency domain	[27-31]

When a downed conductor HIF occurs, energized high voltage conductors may fall within the reach of the public which may cause electric shocks and threaten lives in addition to power supply interruption. Moreover, because arcing often occurs with HIFs, these faults can result in fire and property damage and endanger public life many researchers have studied HIF and proposed detection methods and they are summarized in Table 2.2. Therefore, the challenge to provide a reliable detection method that responds to the system requirements still exists because in most cases power companies rely on being notified of down conductor by customers. Better techniques need to be developed so that power companies can benefit from the improved detection of HIF with no damaging effect on service reliability.

Chapter 3

Modelling arcing high impedance faults in relation to the physical processes in the electric arc

There is an increasing demand for more detailed and accurate modelling techniques for predicting transient response of power systems caused in particular by high impedance arcing faults (HIF). This is particularly so in relation to the design and development of improved equipment and new protection techniques. Accurate prediction of fault transients requires detailed and comprehensive representation of all components in a system, while the transient studies need to be conducted into the frequency range well above the normal power frequency. The HIF is a very complex phenomenon and exhibits highly nonlinear behaviour. The most distinctive characteristics are nonlinearity and asymmetry. The nonlinearity arises from the fact that the voltage-current characteristic curve of the HIF is itself nonlinear. It is also observed that the fault current has different waveforms for positive and negative half cycles, which is called asymmetry. The nonlinearity and asymmetry exist in every cycle after the HIF. In order to obtain a good representation of a HIF, it is necessary to develop a model that gives the above mentioned characteristics, as well as the harmonic content of the HIF.

3.1 Introduction

In the case of an arcing HIF, when an energized conductor contacts the ground, the electric contact is not solid. Due to the existence of air between the ground and conductor, the high potential differences in such a short distance cause a breakdown of the insulating properties of the air and excite the appearance of an arc. This occurs when a conductor breaks and falls on a non-conducting surface such as an asphalt road, sand, cement, grass or perhaps a tree limb, producing very little measurable current.

HIFs have characteristics in their transient and steady states that make them identifiable. An accurate modelling method for a HIF is essential for the development of reliable detecting algorithms. The HIF model's data should contain the complex characteristics of HIFs such as nonlinearity, asymmetry, the low frequency phenomena typical of an arcing fault and the angle shift of the third harmonic. Some models of HIFs have been proposed in literature. For example, in the past and for the purpose of simulation or calculation in reference [49] the HIF was simulated by connecting a resistance to the network at the fault point. Later on, a model based on a diode was presented in [50]. Other researchers had modelled HIF as a voltage source in [51, 52]. another model in [53] uses two time-varying resistances (TVR) in series. One TVR is used for buildup and shoulder from the waveforms in the transient state after HIF and then the other TVR for nonlinearity and asymmetry from the voltage-current characteristic for one cycle in the steady state after HIF. Although these methods represent the nonlinear behaviour of HIFs well, they are not capable of representing the other important characteristics mentioned above.

According to the experimental work of the Korea Electric Power Corporation (KEPCO) [53], the HIF experimental data was collected on a 22.9kV distribution system. The total number of experiments was thirty two and the sampling frequency

10kHz. Figure 3.1 exemplifies the currents for the 20th and 40th cycle after the HIF has occurred; both currents exhibit some asymmetry. Figure 3.2 shows the voltage-current curve and demonstrates the degree of nonlinearity. The "signature" of the current curve and the current-voltage curve for HIF has a unique shape.

While designing a model for HIF, it must be taken in consideration that the developed model should give the above mentioned characteristics and harmonic content of HIF.

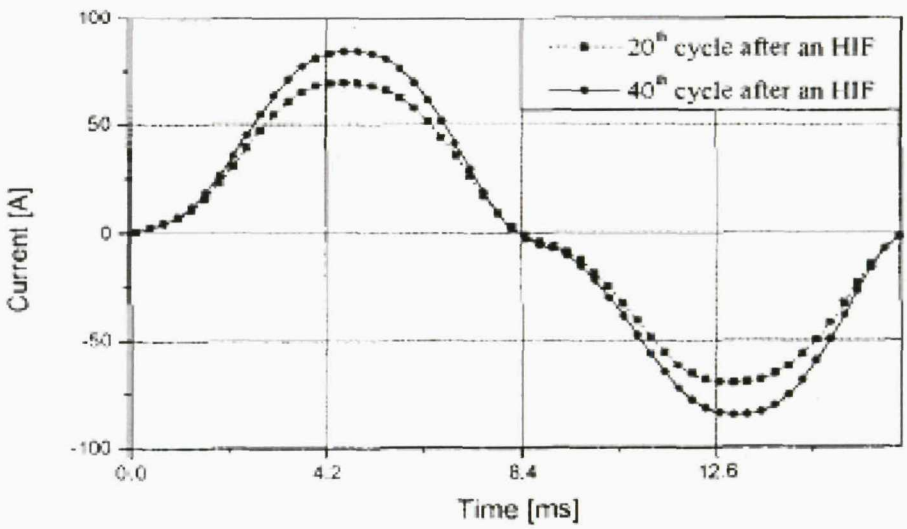

Figure 3.1 Current for the 20th and 40th cycle after HIF (asymmetry) [53]

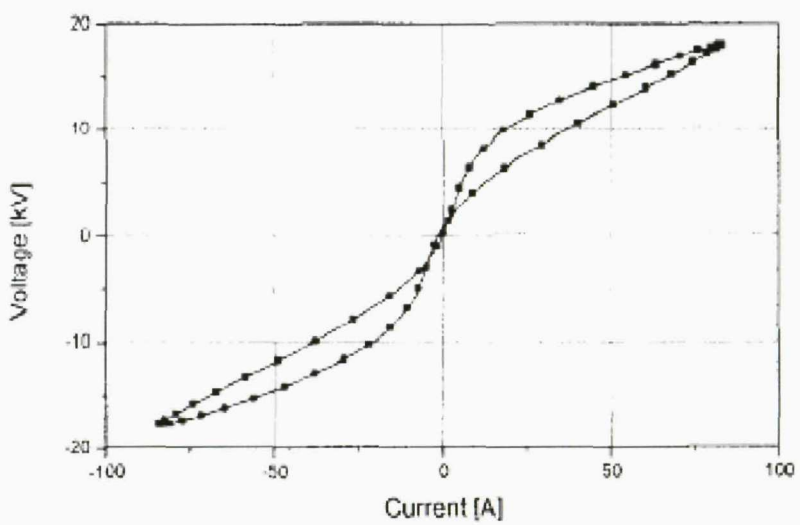

Figure 3.2 Voltage-current characteristic curve for one cycle in the steady state after HIF (nonlinearity) [53]

3.2 Physical processes in an arc

By their nature all gases are normally good electrical insulators and molecules in gases at low pressures are widely spaced so that they can be considered independent of one another except for occasional collision due to random thermal motions. But it is well known that the application of a sufficiently high electric field may cause a breakdown of the insulating properties, after which current may pass through the gas as an electric discharge. The term arc is usually applied only to stable discharges, and an arc may be regarded as the ultimate form of discharge; it is defined as a luminous electrical discharge flowing through a gas between two electrodes. Electric discharges are commonly known from natural phenomena like sparks whose lengths can vary.

Discharges can occur not only in gases but also in fluids, solids or in almost any matter that can turn from a state of low vanishing conductivity to a state of high conductivity, when a sufficiently strong electric field is applied. The first theories that introduced a satisfactory explanation of the electrical breakdown of air were put forward by Townsend [54, 55] and later by Slepian [56].

Figure 3.4 shows the three general regions of an arc: the anode, the cathode and the positive column. The voltage drop in the cathode region is much larger than the voltage drop in the anode region, which is usually considered to be smaller. The positive column, or plasma, has a fairly uniform voltage gradient [57]. Arcs may be initiated in three ways: physical contact, spark discharge, and glow-to-arc transition.

Accidental physical contact, such as a dropped screwdriver shorting two bus bars, is the most common method of initiating an arcing fault in a low-voltage system. The spark discharge may initiate an arc when a large voltage potential breaks down the air between two electrodes. Normally, the voltage potentials associated with low voltage systems are incapable of spark-discharge initiation; however, arcs may develop

from a spark when arc tracking occurs across a partially conductive surface, such as damaged insulation, or when electrodes are loosely touching, such as a wire touching a grounded circuit. The other possible method is a glow-to-arc transition. As seen from Figure 3.3. an arc is characterized by a smaller voltage potential and a larger current flow (>10 A) [58], while a "glow" state is characterized by a relatively high voltage potential and small current flow (<1 A). A "glow" discharge develops into an arc when large numbers of electrons are released by the cathode. Certain conditions at the cathode, such as surface impurities and scratches [59], local hot-spots and deteriorated insulation increase the likelihood that an arc will develop.

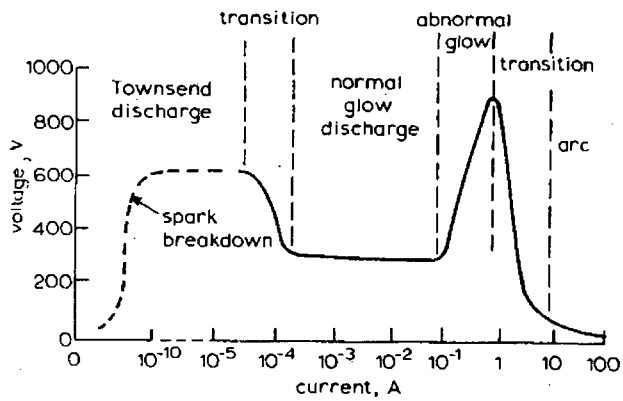

Figure 3.3 Steady state voltage-current characteristics of discharge

According to [54, 56, 58, 60-62], starting with a uniform distribution of ions when the current and voltage are zero, the increase in voltage will cause space charge sheaths to form next to the electrodes. Three regions between the electrodes will be formed through which the discharge current passes. These are (1) the cathode fall space (2) the plasma, and (3) the anode fall space (Figure 3.4). The total voltage drop across the discharge is the sum of the drops across the three regions. In the low intensity arc the

drop across the anode and the cathode are generally equal and the drop across the plasma is the largest of the three and accounts for the major portion of the arc voltage. The current densities in this sheath are very small and in order to 'restrike' the arc, the space charge sheath must be broken down. If there are no ionizing agents, the breakdown must be ionization by collision; it will therefore require a minimum of several hundred volts. Under the action of the electric field strength, electrons are emitted from the cathode spot. These collide with neutral molecules, thereby ionizing them electrically. The arc column is an electrically neutral mixture of ions and electrons and the mobility of electrons is higher than ions so they carry most of the arc current and the heat generated in this process developed at the anode (electron heating). The ions in the arc column move under the effect of the field strength towards both electrodes and heat them by impact to high temperature. The negative electrons hit the anode, and the positive ions hit the cathode. In this way new electrons are liberated within the arc column and at the electrodes; the process starts again.

From Figure 3.4 the following part of the arc may be identified:

- Cathode spot - part of the negative electrode where electrons are generated,
- Cathode drop zone - gas region next to the cathode in which a sharp potential drop occurs (electrons accelerated),
- Arc column - bright visible portion of the arc, high temperature (plasma),
- Anode drop zone - gas next to the anode where a further potential drop occurs,
- Anode spot -position where electrons are absorbed.

According to [63] the dynamic characteristics of arcs may be represented as in Figure 3.5

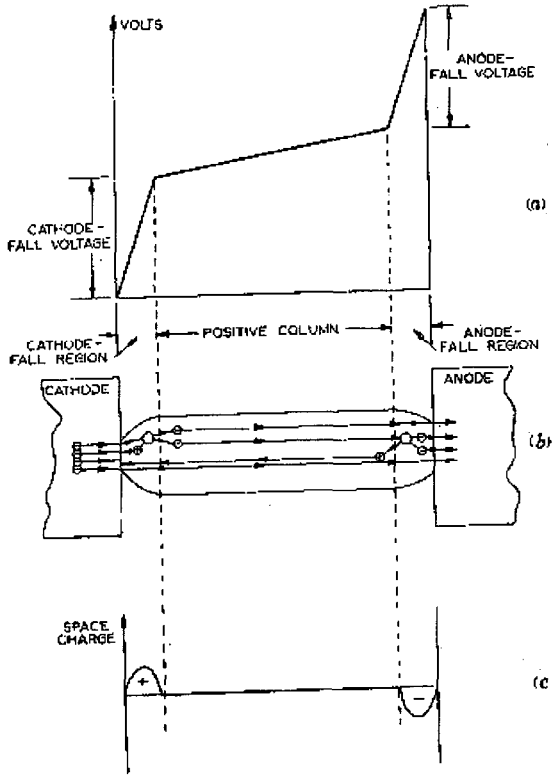

Figure 3.4 Ions and potential distribution in arc discharge through gas [59]
a- potential
b- current
c- space charge

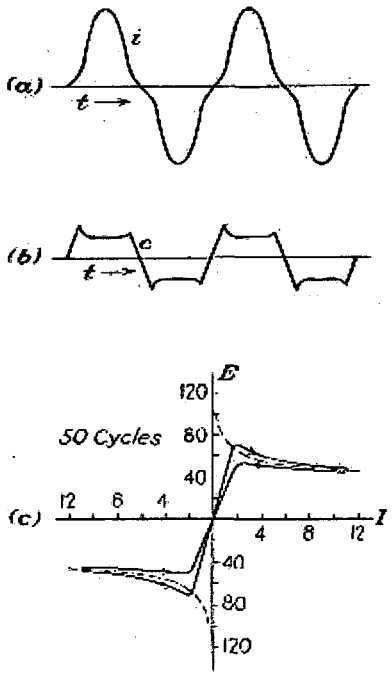

Figure 3.5 (a)&(b) Current and Voltage during electric arc, (c)V-I characteristics during arc [63]

3.3 Physical processes in the HIF arc

Arcing associated with the HIFs results in energy dissipation, in the form of heat, which turns the moisture in the soil into steam and burns the grass into smoke. In the arcing phenomenon associated with downed power lines, due to the existence of air between ground and conductor, the high potential difference in such a short distance excites the appearance of the arc (it resembles anode-cathode phenomenon). This normally occurs in a largely resistive circuit and is characterized by a short arc length, small current magnitude and could persist for a long period of time [64]. The arc which penetrates the soil has typical temperature values at the arcing spot in the order of 5000 to 8000°C in the gas column, 3000 to 4000°C for carbon electrodes and 2000 to 3000°C for metallic electrodes [65]. The heat generated from the arc is sufficient to melt the sand and silica in the soil into a glass-like substance as seen in Figure 3.6, silicon carbide tubes (carbide is a compound of carbon with a less electronegative element). These glass-like tubes reach a length of 5cm and they were found to have a linear resistance of the order in 2 to 100 kΩ/ m [50].

Figure 3.6 Molten material due to arcing creates a tube-like formation

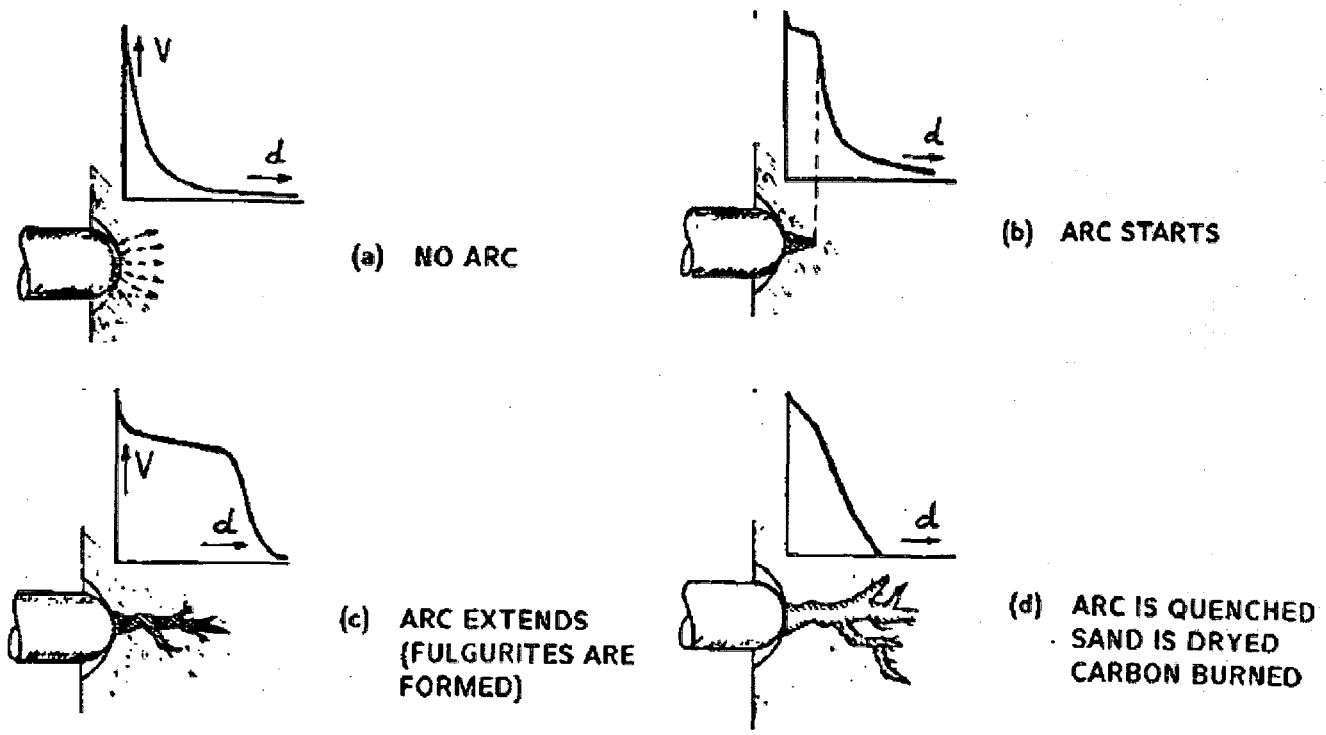

Figure 3.7 Physical characteristics of arc environment vs. time

According to references [50, 56, 58, 60, 63] when an energized conductor touches the ground no arcing will take place immediately (Figure 3.7 (a)), but after a few seconds the temperature of the soil surrounding the electrode will rise. Due to the rise of temperature a steam will develop and cause a local increase in spacing between the soil particles and the arc is triggered. In time the arc voltage increases as the arc starts to penetrate in the soil.

When the arc is triggered, Figure 3.7(b) the arc penetration of the soil will significantly change the local electric field distribution, causing a field of enhancement at the tip of the arc. High field gradient, thermionic emission and the fact that the conductive layer of soil move away from the electrode causes the arc to expand and penetrate further into the soil (Figure 3.7(c)). The area surrounding the arc will turn to glowing hot silica that acts like a cathodic spot which emits electrons causing a smaller

voltage drop when the conductor (high voltage electrode) is positive. As the arc extends further into the soil two factors are changing:

1. Due to the soaring heat the soil surrounding the arcing area becomes dry;
2. The balance between the transferred heat to the environment and the rate of generation of the heat of arcing is disturbed. These result in the arc being extinguished, Figure 3.7(d). From this stage two situations are possible:

A. The arc will be reignited when humidity penetrates back into the dry soil and once the front boundary of the moist (conductive) layer is close enough to the high voltage electrode. The arc however, will be re-triggered on a different path than the previous one. The preliminary arcing path is now a solidly vitrified form of fulgurites tubes.

B. If the energized conductor that touches the ground has multiple points of contact with the soil, then another point which was before inactive may start arcing if the local field has increased due to changes in the potential distribution.

The arcing faults voltage-current characteristic and the behaviour of the fault current signal will be a result of a complex interaction of:

- soil material itself.
- particle movement in the soil.
- moisture content in the soil.
- generation of smoke and steam.
- development of silicon carbide tubes.
- nonlinearity of the arc and soil-conductor interface [64].
- bounce of the conductor on the ground surface.
- heat capacity of the conductor, arc gas and earth.

As for the fault current behaviour, it has been observed that the positive half-cycles of the current may be greater in magnitude than the negative half-cycles, or vice versa, and the fault current magnitude may vary greatly from one cycle to the other as seen in Figure 3.8 [50].

The asymmetry of the fault current in some cases could be a result of the rectifying action by the soil. The glass-like tubes surrounding the conductor act as hot cathodic spots that emit electrons. The voltage drop across the cathode spots is small when the conductor is positive. The arc voltage in the negative half-cycle is thus larger than that during the positive half-cycle. Consequently, the current conduction period, and hence its magnitude, are smaller in the negative half-cycle. The amount of moisture in the soil and the packing of its particles affect the values of the arc voltage in each half-cycle. Drier soil yields higher difference in arc voltages and, therefore, a larger degree of asymmetry than wet soil; harmonics are generated on account of this asymmetry [50, 65]. The varying current magnitude could be explained as a result of arcing at the fault, which rearranges the characteristics of the air gaps surrounding the downed conductor as well as accumulation of silicon carbide tubes around the conductor.

In a field test reported in reference [50], measured values of current harmonics at a staged high impedance ground fault are presented and the measured low frequency spectrum is compared with current harmonics recorded continuously for one week at the substation. It has been confirmed that faults with currents above 1A have a stable arc with nearly constant rms value for long periods of time, whereas arc currents lower than 1A are characterized by shorter periods of stable arc current and by random initiation and quenching of the arc. Based on the laboratory measurements conducted by the authors in [50], Figure 3.8 shows oscillograms of currents and voltages which illustrate

and validate the characteristics for large as well as small fault currents. In Figure 3.9 the asymmetry is also noticeable in the *V-I* curve of the arc as well as in the arc voltage.

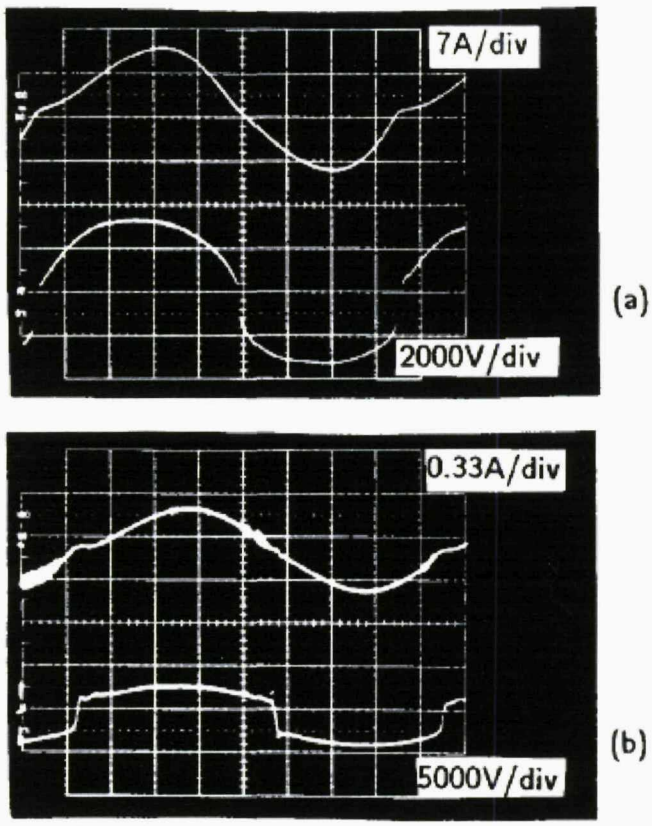

Figure 3.8 Oscillograms of laboratory arc currents; (a) large arc current (b) small arc current [50]

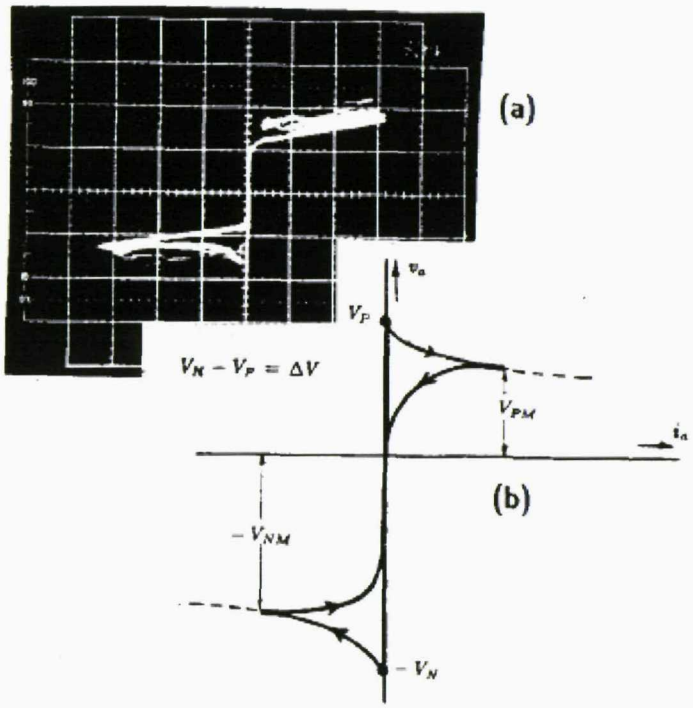

Figure 3.9 V-I characteristic of arc; (a) laboratory oscillogram; (b) theoretical description [50]

3.4 Harmonic analysis of practical data from KEPCO [53] and Emanuel et al [50]

To assist in developing a model for HIFs, many attempts have been made to obtain practical HIF data from different power companies but unfortunately no company was willing to supply the necessary data. It was therefore decided to use the published results already reported in Figures 3.1 [53] and 3.8 [50]. The approach used involved tracing and digitising the relevant curves and then finding the harmonic content of the extracted waveforms. Using printed curves is unlikely to yield accurate results but should at least provide some level of confidence in the proposed model.

Figure 3.10 represents the extracted data from Figure 3.1 as reported by Korea Electric Power Corporation (KEPCO). The two current signals in Figure 3.10 are separated, plotted and harmonically analyzed. The results of the harmonics analysis are shown in Figure 3.11. Figure 3.11A represents the 20^{th} cycle after HIF, while the harmonics are shown in Figure 3.11B. The harmonic analysis reveals that the 3^{rd} and 5^{th}

harmonics have a magnitude of 14% and 5%, respectively, taken as a percentage of the fundamental current.

The second current signal, which represents the 40th cycle after HIF, is shown in Figure 3.11C. The harmonic analysis of this current as shown in Figure 3.11D, gives the 3rd harmonic as 16% and the 5th harmonic as 5% with respect to the fundamental current.

The reason that the 3rd and the 5th harmonics of Figures 3.11B & D are slightly different in magnitude (with respect to fundamental current) is likely to be related to the intensity of the arc or the surface conditions, or some other factors mentioned in Section 3.3.

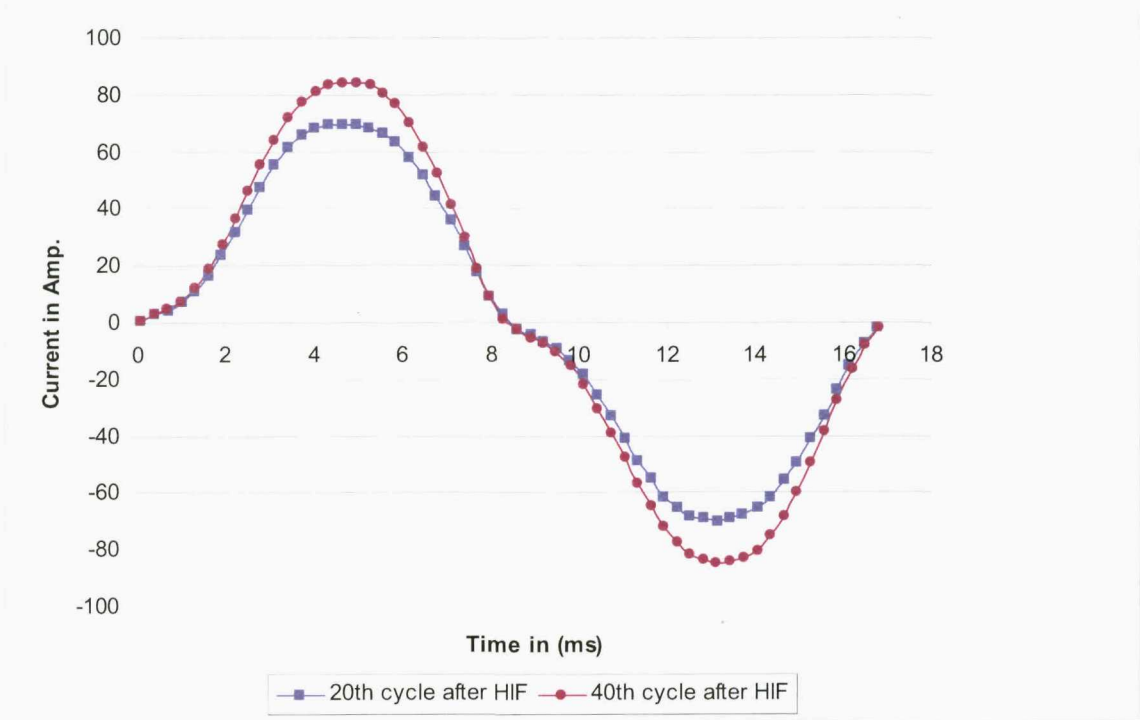

Figure 3.10 HIF extracted data from Figure 3.1 which represents real data collected by KEPCO

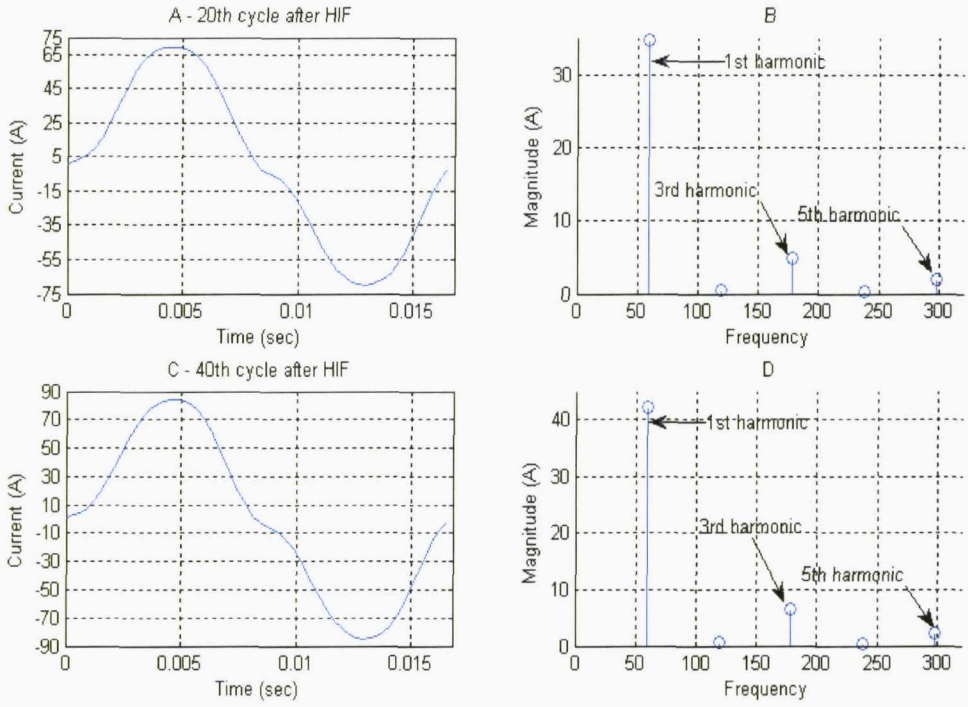

Figure 3.11 Time and frequency plots for both signals shown in Figure 3.10

Similarly, Figure 3.12 represents the extracted arcing HIF current waveform from Figures 3.8a and b [50].

Figure 3.12A is the time plot of the small arc current extracted from Figure 3.8(b), and its harmonic analysis is shown in Figure 3.12B. The harmonic analysis shows that the small arc current signal contains the 3rd harmonic of 36% and the 5th harmonic of 12% with respect to the fundamental current.

For the large arc current (Figure 3.8a), the time plot of the extracted waveform is shown in Figure 3.12C and its harmonic analysis in Figure 3.12D. It is found that the large arc current signal contains the 3rd and the 5th harmonic with magnitude of 53% and 15%, respectively.

It should be noted that the plots in Figure 3.8 are not real data collected from the field but a result of an experiment data conducted in a lab controlled environment.

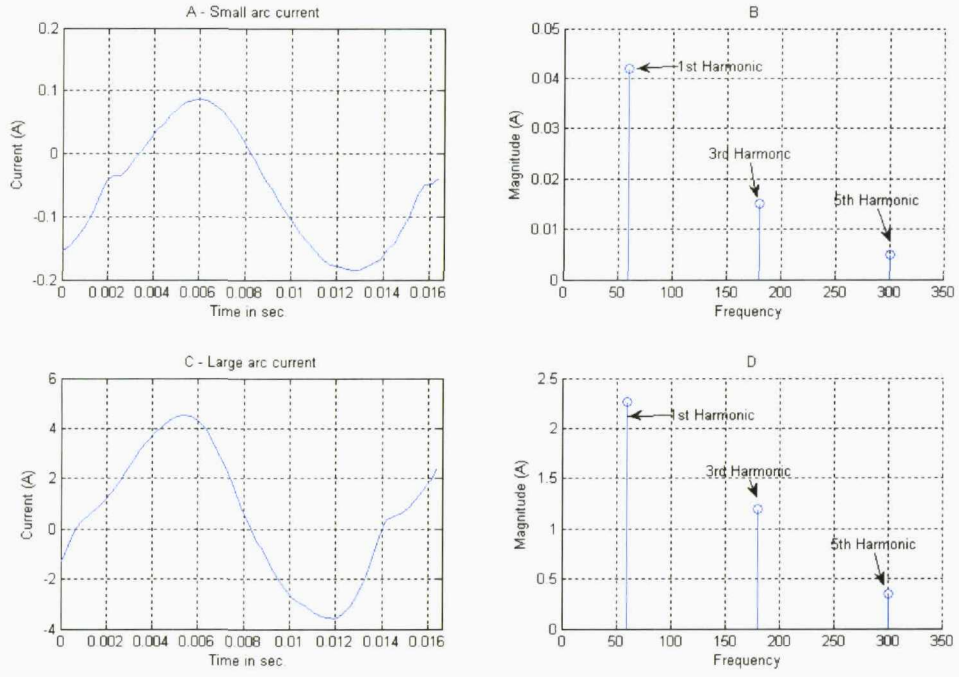

Figure 3.12 Time and frequency plots for both signal shown in Figures 3.8 a & b

In conclusion, the analysis of the extracted current waveforms of both signals reveals that the arcing HIF current contains both the 3^{rd} and the 5^{th} harmonics. In the KEPCO extracted data, the 3^{rd} and the 5^{th} harmonic in both cases did not exceed 16% and 6 %, respectively, of the fundamental current. Regarding the data from Emanuel et al [50], the results from their controlled experiment show that the 3^{rd} and the 5^{th} harmonics for both cases do not go above 53% and 15%, respectively, of the fundamental current.

The magnitude of the 3^{rd} and 5^{th} harmonics depends on many factors including the intensity of the arc and the material and condition of the surface where the arc took place.

Since the KEPCO experiment is based on real data, rather than data collected from a lab controlled environment, then to validate any HIF model the KEPCO results should be considered as more reliable and thus of particular importance.

3.5 A new model of an arcing HIF

Many authors have worked on the theory and dynamics of voltages and currents in an electric arc based on laboratory studies. References [66, 67] propose a model explaining this phenomenon using a spark gap: the air gap will not conduct until the applied voltage reaches the breakdown point. Then the current flows and reaches a maximum when the applied voltage equals the arc voltage. After that, the arc current decreases and becomes zero, i.e. the arc is extinguished. When extinction occurs, the arc requires a potential known as *restrike voltage* to re-ignite. This re-ignition will have an opposite polarity. This procedure explains the typical voltage–current waveform of an arc shown in Figure 3.13. Electric models have been proposed describing arc behavior, and they have been recently collected and published in [68, 69].

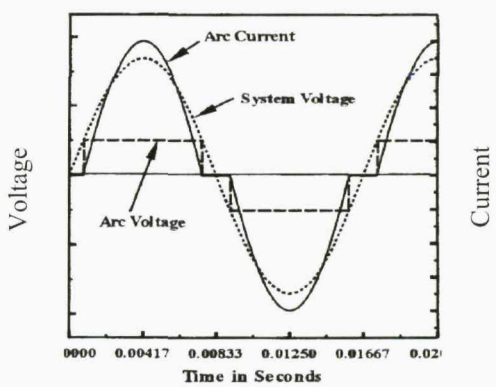

Figure 3.13 Electric arc voltage and current shapes

The high impedance fault model proposed by this chapter is shown in Figure 3.14. The values of V_p, V_n, R_p, R_n, L_p, and L_n are chosen after several Matlab simulation to match the harmonic content of the extracted signal from KEPCO collected data in section 3.4. The model includes two DC sources, V_p=3000 V and V_n=3000 V, which represent the arcing voltage of air in soil and/or between trees and the distribution line and the values of the DC voltage sources chosen according to many experimental simulation conducted by this research and experimental findings in [50]. Two

resistances R_p =104Ω and R_n =104Ω between the diodes which represent the resistance of trees and/or the earth resistance. The values of the resistors have been chosen according to the resistance of the glass-like substance mentioned in Chapter 3.3. Since most observed arcs occur in highly inductive circuits and due to the inductance of the discharge in the spark gap [64, 70] two inductances, L_p =0.04H and L_n =0.04H were added to the circuit and their values been chosen according to extensive simulation to give us the desired current effect. The effect of the inductances leads to the nonlinearity loop shape in the *V-I* curve and the desired asymmetrical shape for the HIF current. When the line voltage is greater than the positive DC voltage V_p, the fault current starts flowing towards the ground. The fault current reverses backward from the ground when the line voltage is less than the negative DC voltage V_n. In the case when the line voltage is in between V_p and V_n, the line voltage is counter-balanced by V_p or V_n so that no fault current flows. Typical fault current and *V-I* curves are shown in Figures 3.15 and 3.16.

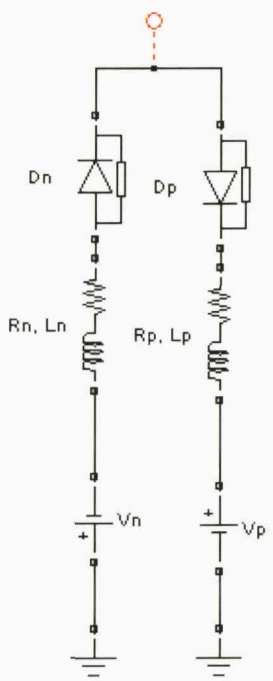

Figure 3.14 Two diode fault model for HIF with Rn, Rp, Ln, Lp

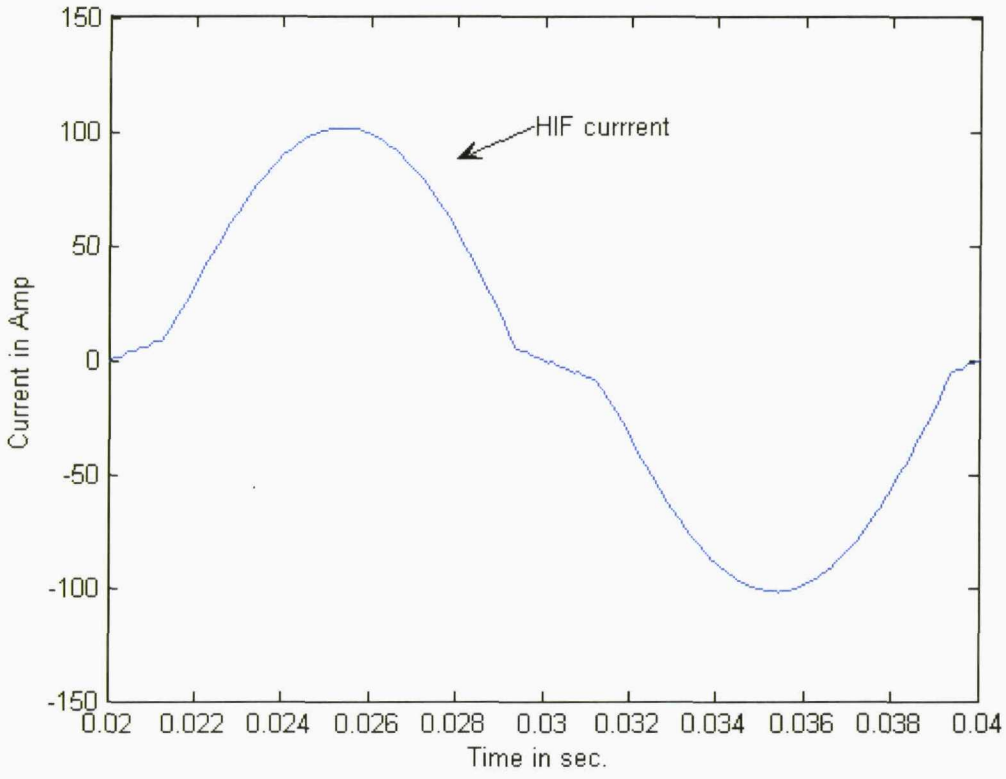

Figure 3.15 A typical current curve for HIF based on the model of Figure 3.14

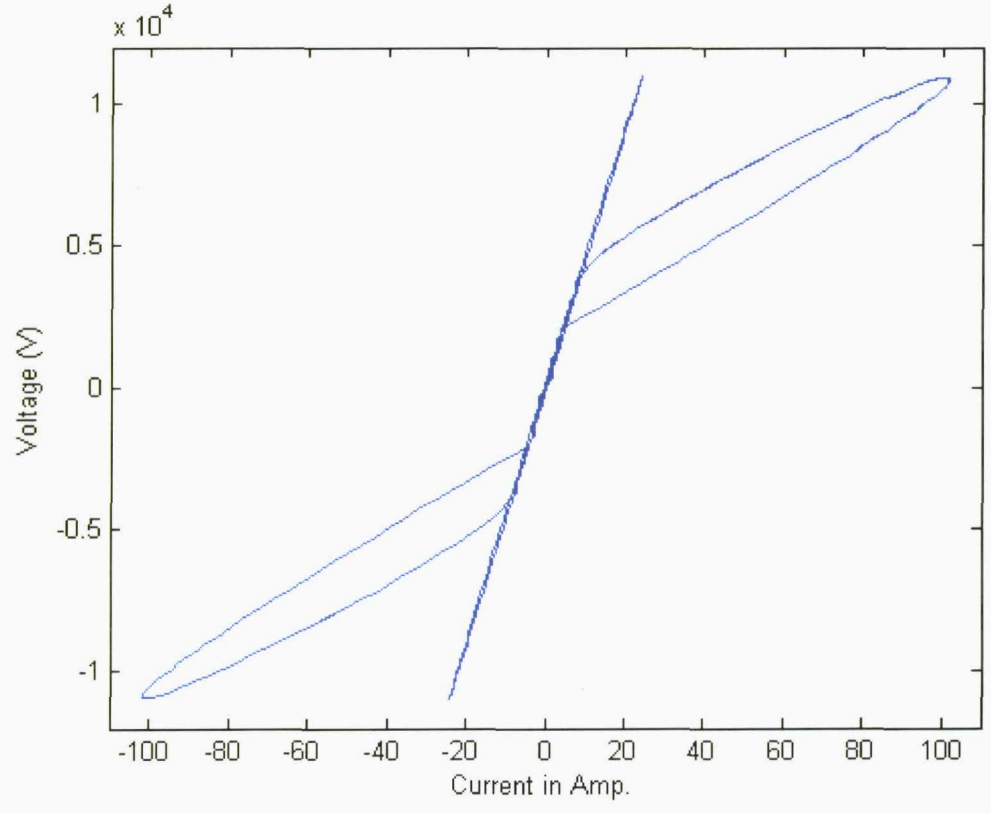

Figure 3.16 A typical voltage-current characteristic of HIF

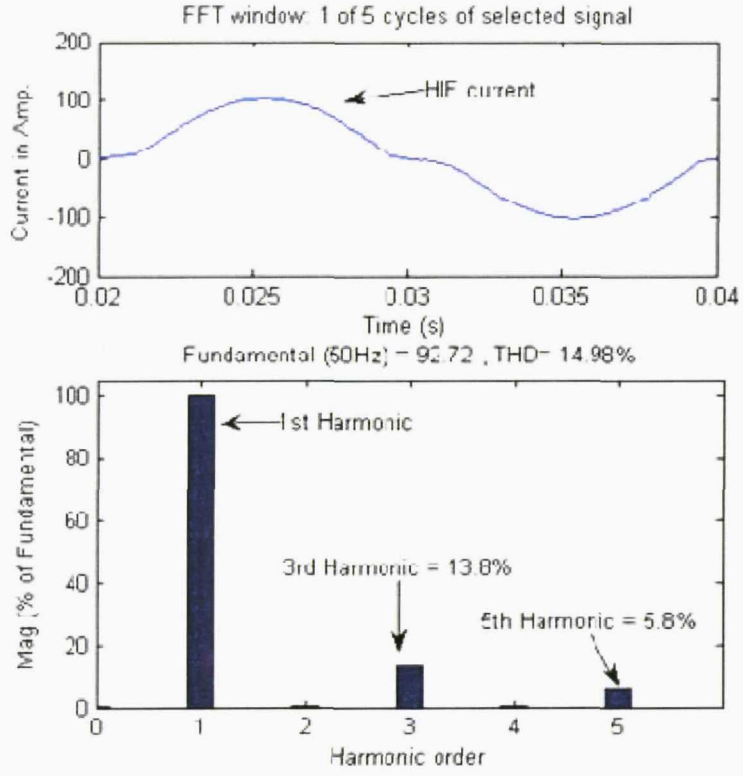

Figure 3.17 Harmonic content of the HIF model

The HIF harmonic content produced by the proposed model is shown in Figure 3.17. The 3rd and the 5^{th} harmonics are 13.8% and 5.8%, respectively, with respect to the fundamental current. Comparing the results of KEPCO extracted data from Section 3.4 with the results from the HIF model above shows an encouragingly good match, especially in the harmonic content. In other words, the proposed model is capable of reproducing the experimental results reported earlier. It is also important that the adjustable parameters of the model allow variation of the resultant HIF characteristics. To demonstrate this, a sensitivity analysis has been undertaken and is reported in the next section.

3.6 The sensitivity of the results to the values of R, V, L chosen in the HIF model

3.6.1 The effect of varying the resistances (Rp, Rn)

In Figure 3.18 the value of Rp and Rn are changed from 90Ω to 150Ω with a 20Ω increment while Vp=Vn= 3500V and Lp=Ln= 0.04H. As may be seen, the higher the values of Rp and Rn the lower the current. Clearly the resistances in the model control the flow of the current. Furthermore, the current harmonics when Rp=Rn= 90Ω are shown in Figure 3.19. The value of the 3rd harmonic is 13.5% of the fundamental current while the 5th harmonic is 5.6% (for the purpose of clarity the first harmonic will be shown only in Figure 3.19, for the rest of the report only the 3rd and the 5th harmonic will be shown). When Rp=Rn= 150Ω, the 3rd and the 5th harmonics are 11.8% and 5.1%, respectively, as shown in Figure 3.20. As a result of this analysis, it may be concluded that the values of Rp and Rn mainly control the flow of the current through the model whereas it have relatively small effect on the harmonics produced by the model.

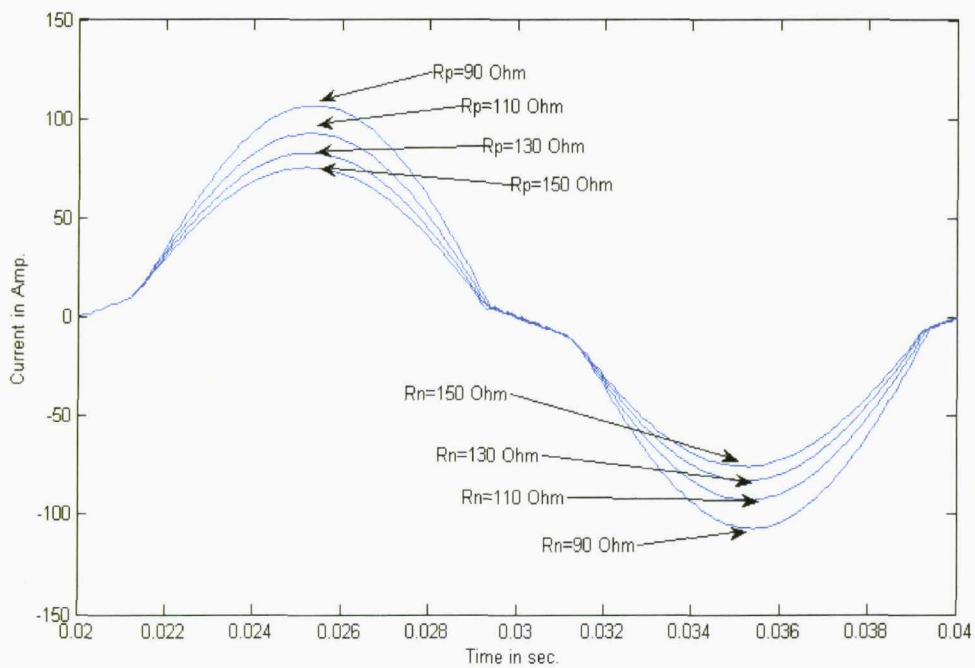

Figure 3.18 The effect of Rp and Rn on the value of the HIF current

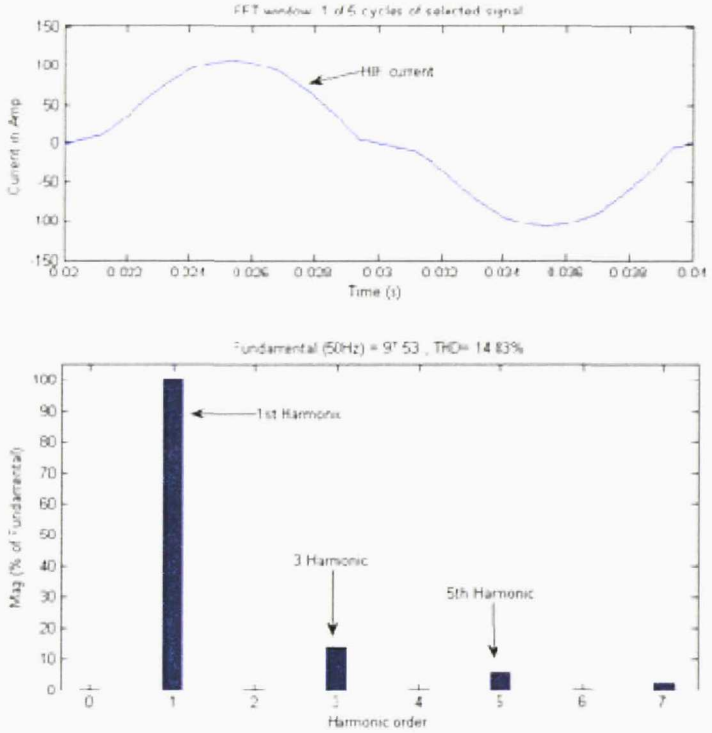

Figure 3.19 The magnitude of the harmonics when Rp=Rn = 90 Ω

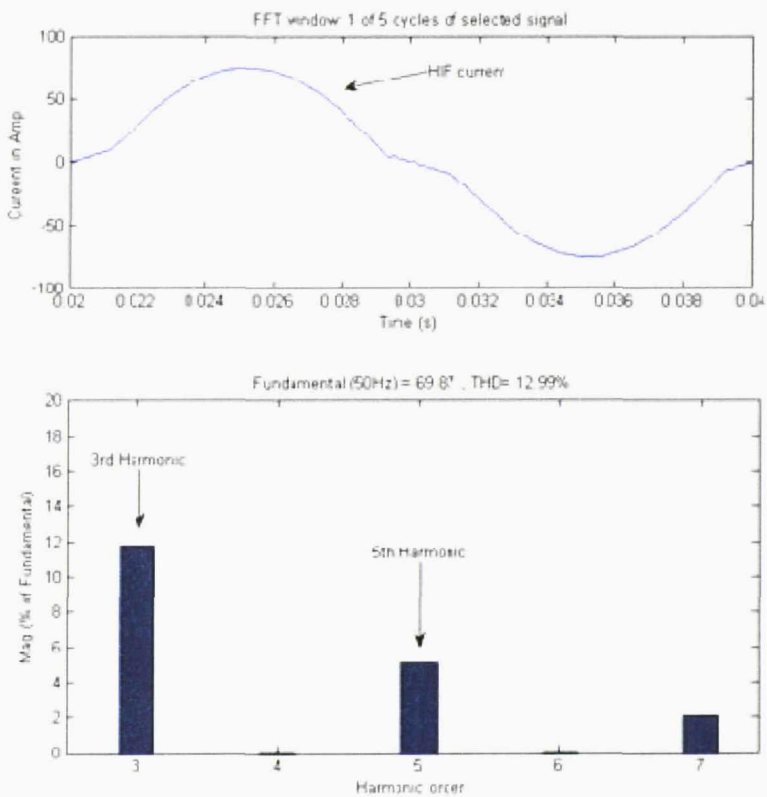

Figure 3.20 The magnitude of the harmonics when Rp=Rn = 150 Ω

3.6.2 The effect of varying the Voltages (Vp, Vn)

Figure 3.21 shows the effect of the values of Vp and Vn on the current flowing through the model. The values of Vp and Vn are changed with an increment of 1000V and for this test Rp=Rn=104 Ω and Lp=Ln=0.04H (the values were assumed here to provide best match for the KEPCO case, section 3.4). As may be seen the higher the values of Vp and Vn the less current flows through the model. The effect of Vp and Vn on the harmonics is shown in Figures 3.22 and 3.23. When Vp=Vn=2000V the 3rd and 5th harmonics are 7% and 4% respectively. However, when Vp=Vn=5000V, the 3rd harmonic is 19% while the 5th harmonic is 5%. The analysis shows that the values of Vp and Vn influence both the amount of current and the harmonics produced by the model.

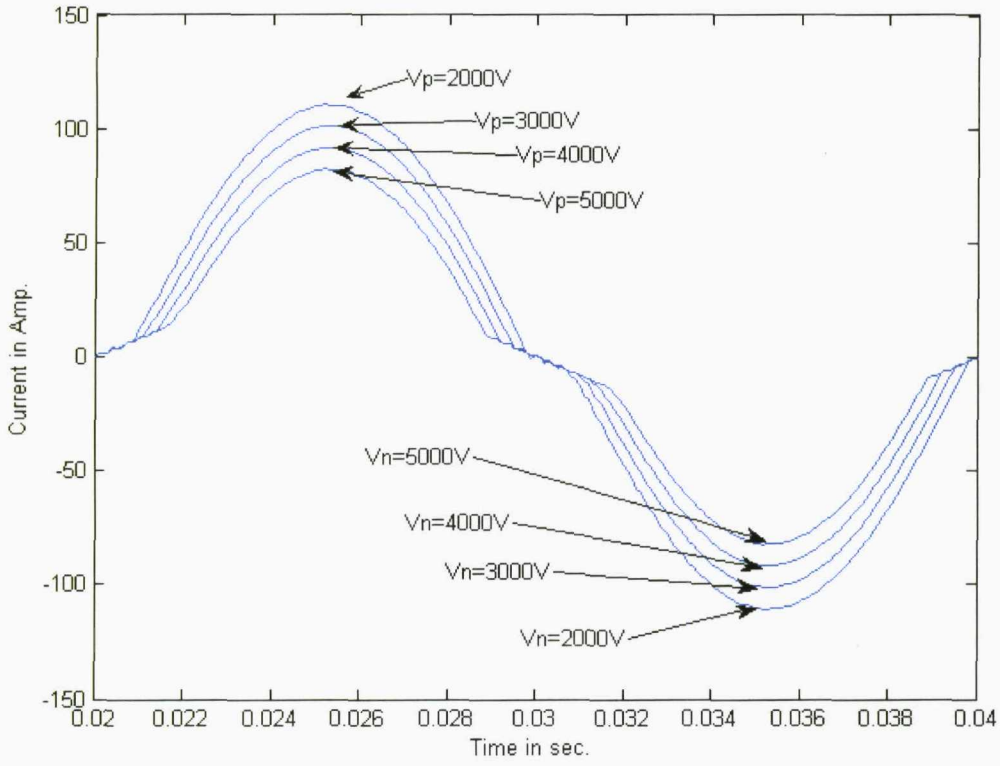

Figure 3.21 The effect of Vp andVn on the value of the HIF current

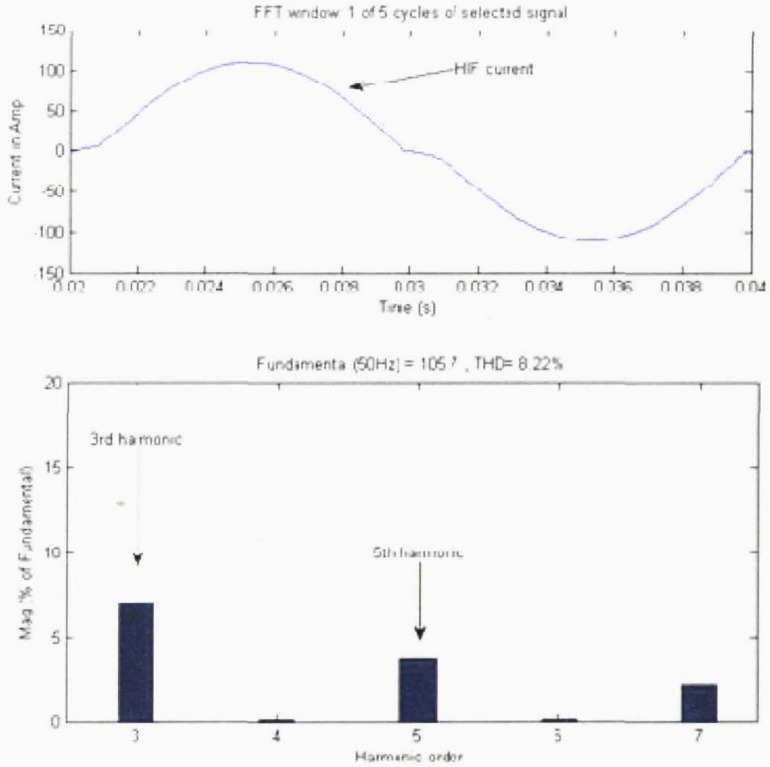

Figure 3.22 The magnitude of the harmonics when Vp=Vn = 2000V

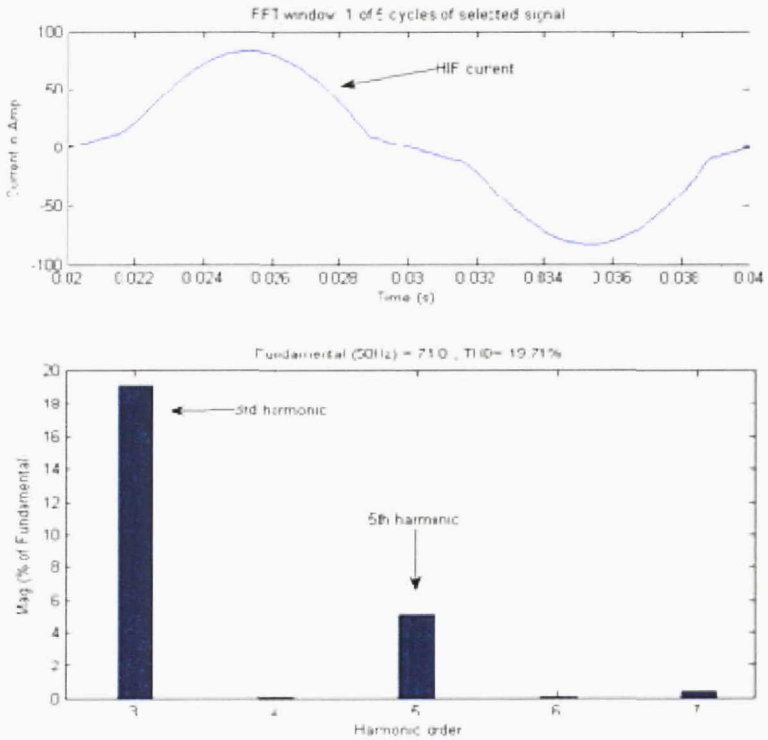

Figure 3.23 The magnitude of the harmonics when Vp&Vn = 5000V

3.6.3 The effect of varying the inductances (Lp, Ln)

Figure 3.24 shows the effect of increasing the values of Lp and Ln. Increasing the values of Lp and Ln has a shifting affect on the current due to the increasing inductance. In order to see the effect of the increasing inductance on the harmonic content of the current, the current in Figure 3.24 is analyzed for the highest and lowest values of Lp and Ln. Figures 3.25 and 3.26 show this harmonic content and in both cases the 3rd and the 5th harmonics are about 11.8% and 5%, respectively. Therefore the changing in the values of Lp and Ln has no effect on the harmonic content of the current and has almost no effect on the amount of current passing through the model but it has a direct effect on the V-I curve as shown in Figure 3.16.

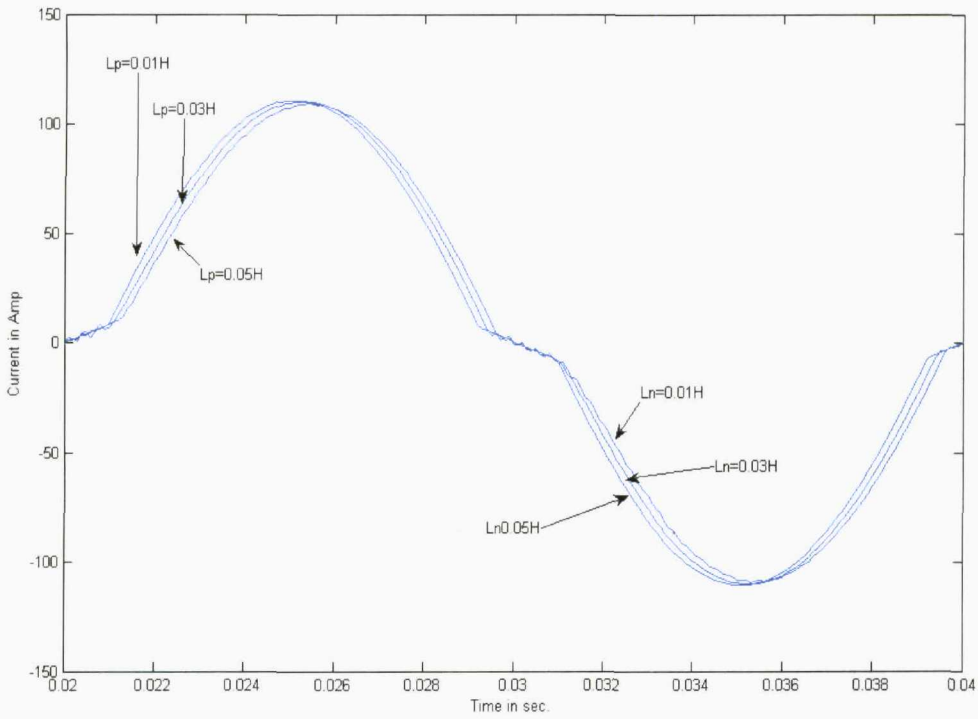

Figure 3.24 The effect of Lp&Ln on the value of the HIF current

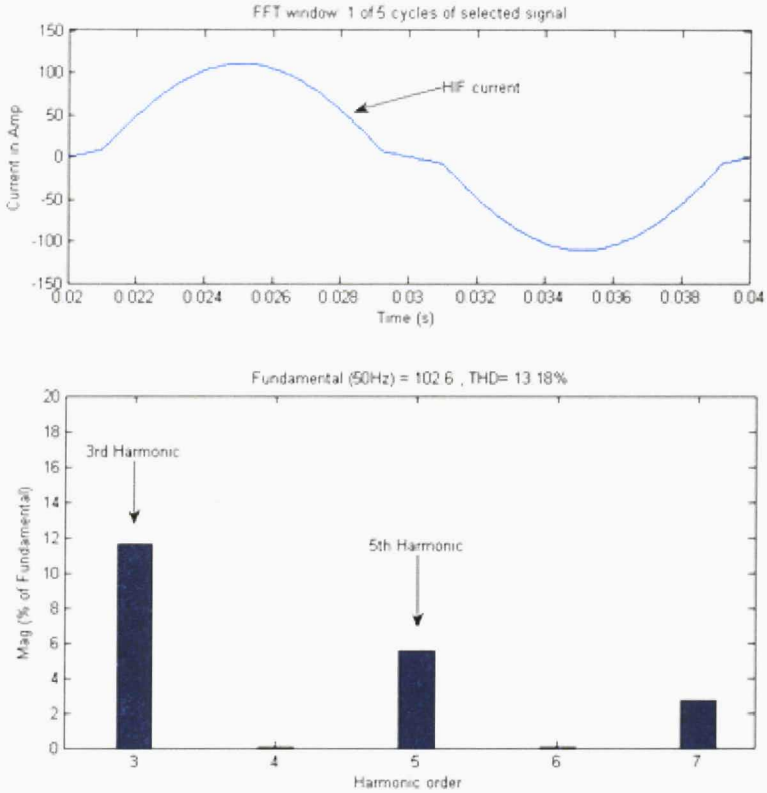

Figure 3.25 The magnitude of the harmonics when Lp=Ln = 0.01H

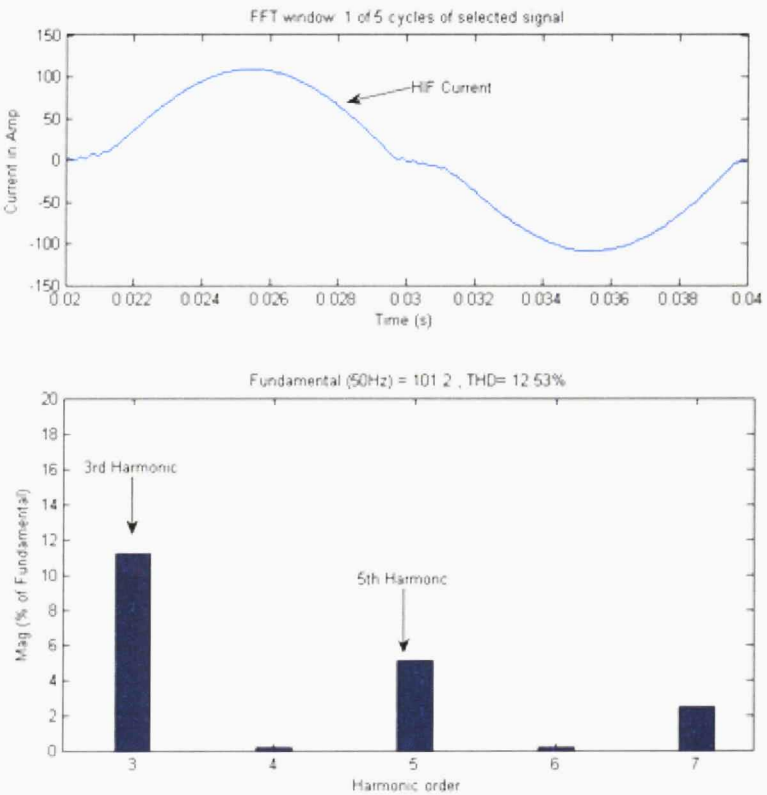

Figure 3.26 The magnitude of the harmonics when Lp=Ln = 0.05H

In conclusion, varying the value of V_p and V_n has the greatest effect on the amount of current passing through the model and on the percentage of harmonics produced by the model (this is due to the intensity of the arc). The higher the V_p and V_n the higher the harmonics but less current will pass through the model. Varying the values of R_p and R_n has a direct effect on the current. However, no direct relation was found between the harmonic content and the values of R_p and R_n. As for changing the values of L_p and L_n, there was no effect on the harmonic content or the amount of current passing through the model, but there was a noticeable shift in the current signal and thus the values of L_p and L_n have a direct effect on the V-I curve characteristics shown in Figure 3.16.

3.7 The harmonic content of HIF model

This section shows the harmonic content of the HIF model and its current curve, after decomposing the line current into its spectral content and studying its harmonic content. Harmonic analysis involves the use of Matlab to identify the harmonics and their magnitudes with respect to the fundamental frequency. In the HIF model test the lower harmonics are analyzed, starting from the 1^{st} to the 7^{th} , and changes are monitored that happen in that range under different system conditions, including any angle shift for the 3^{rd} harmonic. By observing the current signal a method is developed to try discriminating against normal and abnormal behaviour in distribution feeders by analyzing the harmonic content of such events. The most common cases performed on a distribution line are:

A. Normal load switching. (switched on at 0.035s)

B. Normal load and capacitor switching. (switched on at 0.025s- 0.035s)

C. High impedance fault. (switched on at 0.03s)

D. High impedance fault with load switching. (switched on at 0.03s– 0.025s)

E. High impedance fault with load and capacitor switching. (switched on at 0.03s – 0.025s – 0.035s)

All of these cases have been monitored over a period of three cycles (a cycle before the event, a cycle during the event, and a cycle after the event). The detailed analysis follows.

3.7.1 Normal load switching

In the normal load switching, during the cycle before switching on the load, there are no harmonics on the line except for the fundamental current (Figure 3.27A). During the cycle in which the load is switched on there is a noticeable change in the magnitudes of the 2nd to the 7th harmonics as seen in Figure 3.27B and an increase in the line current at the moment of switching as seen in Figure 3.27D. In the cycle after the event has happened the only harmonic there is the fundamental current (Figure 3.27C).

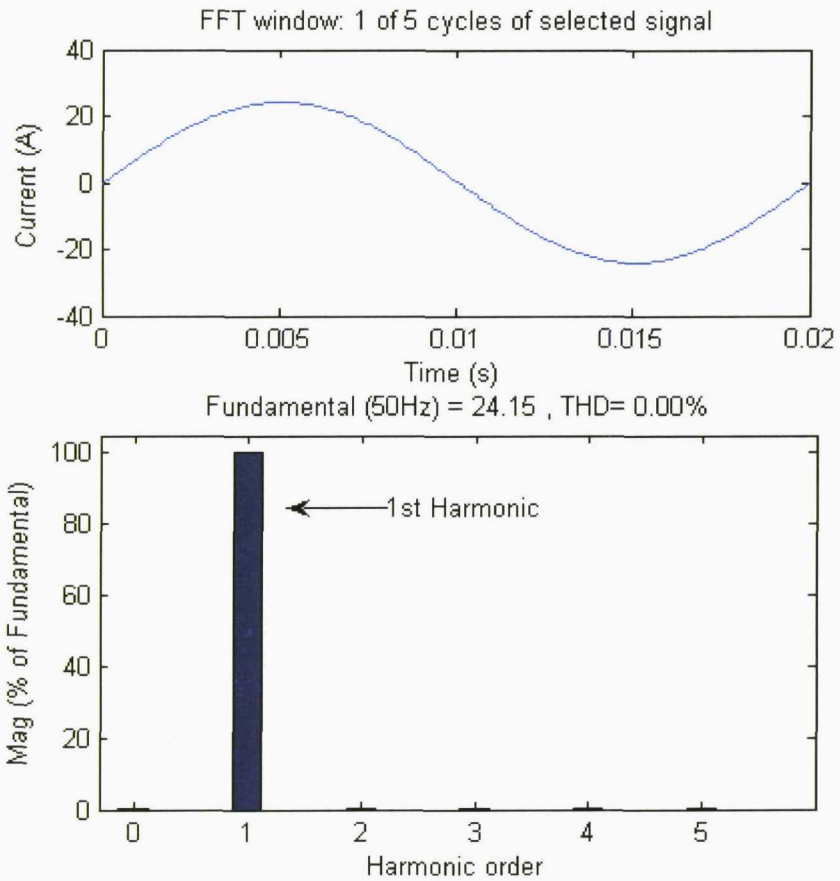

Figure 3.27A Line harmonics and current before load switching

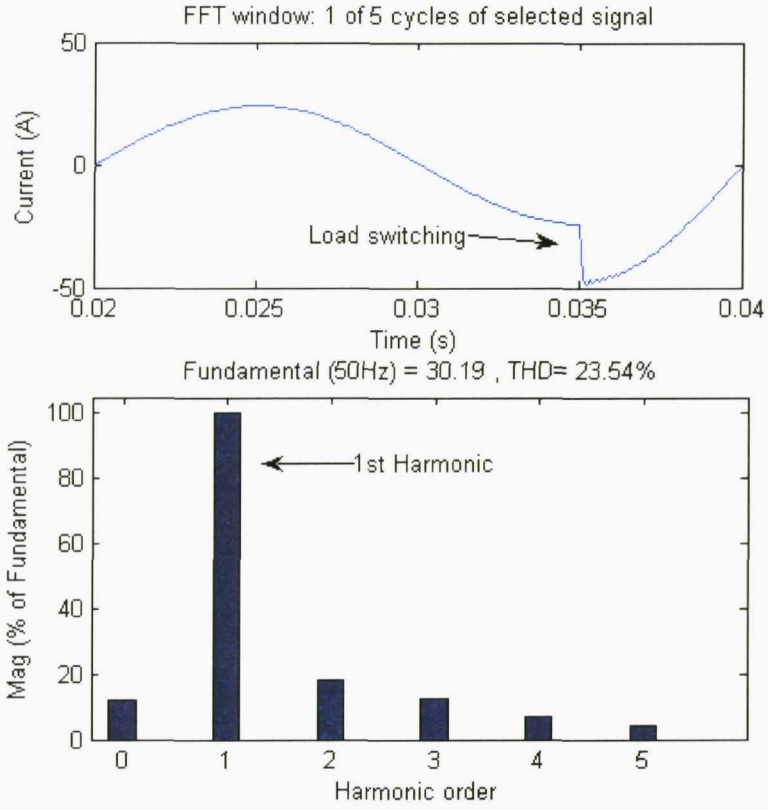

Figure 3.27B Line harmonics and current during load switching

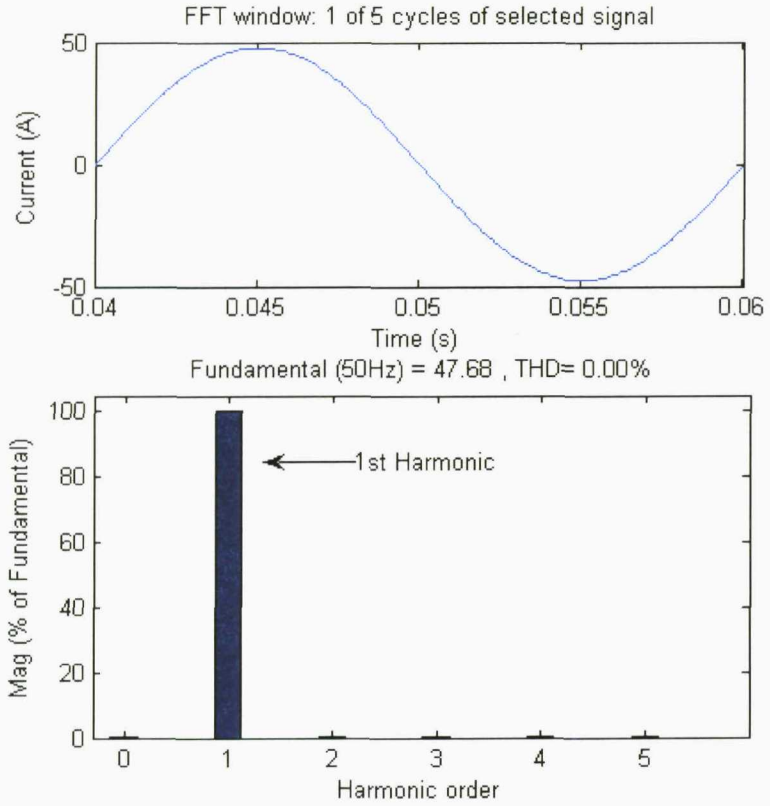

Figure 3.27C Line harmonics and current after load switching

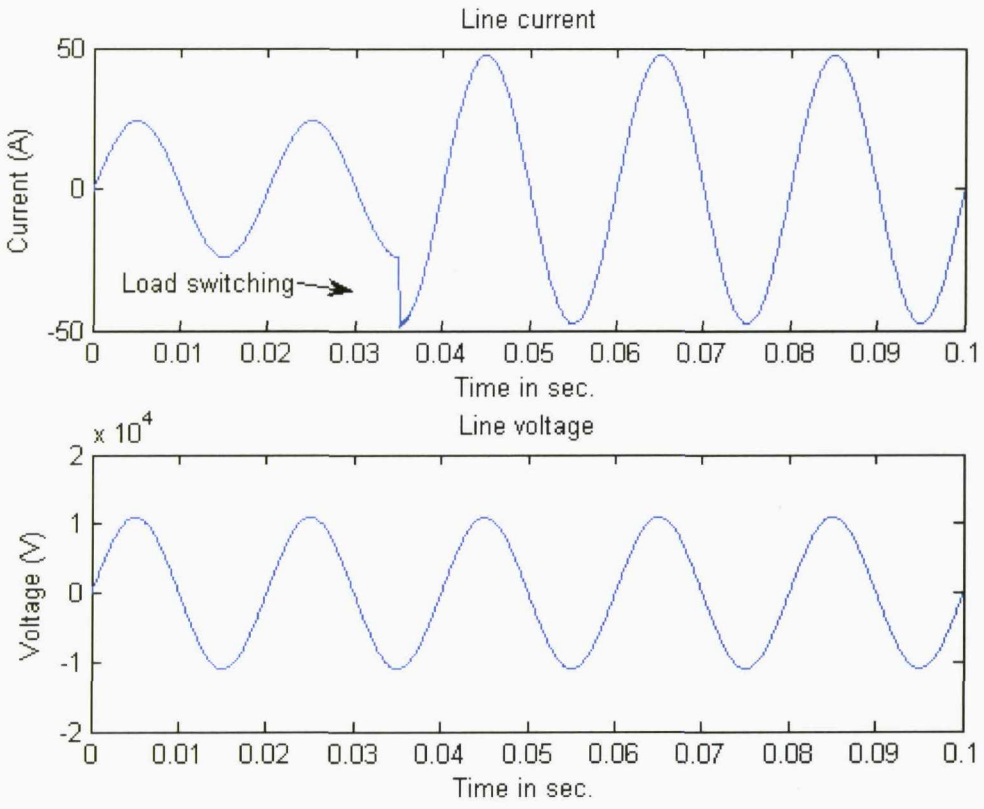

Figure 3.27D Line voltage and current for load switching

3.7.2 Normal load and capacitor switching

In this numerical experiment, before switching on the load and the capacitor, the current signal is normal and there are no harmonics with only the fundamental current present as seen in Figure 3.28A. After switching on the load, and 0.01s later switching on the capacitor, there are many harmonics within the current signal due to the switching as seen in Figure 3.28B. The increase of the line current and the transient due to capacitor switching are shown in Figure 3.28D , but a cycle later the signal is clear of any distortion except for the fundamental current, as shown in Figure 3.28C.

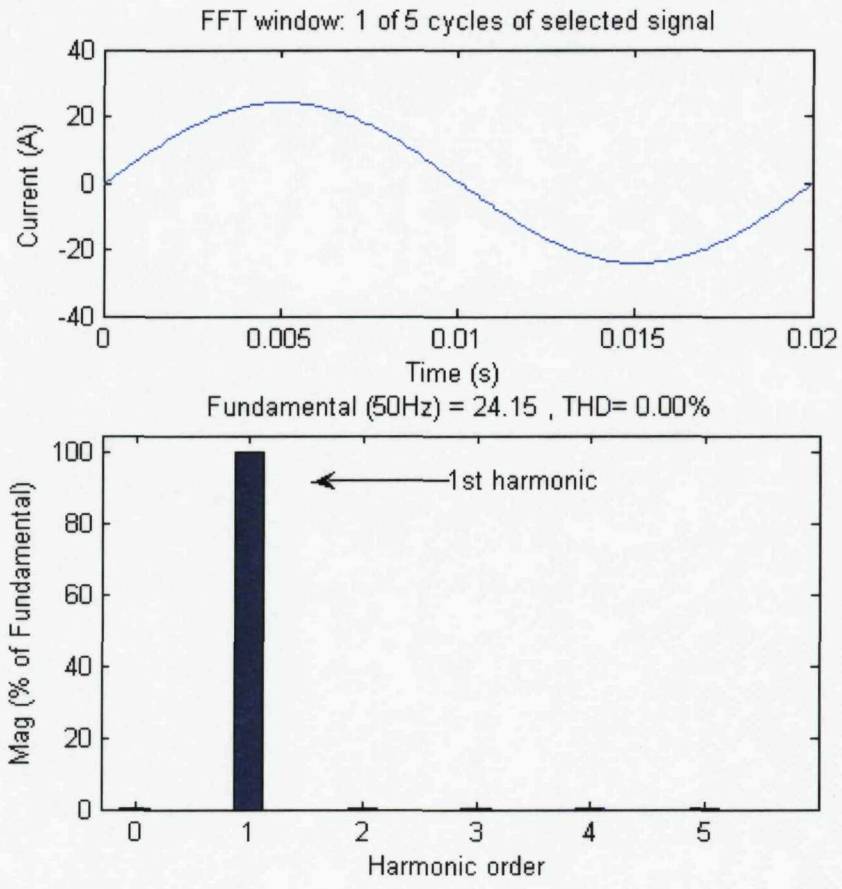

Figure 3.28A Line harmonics and current before the load and capacitor switching

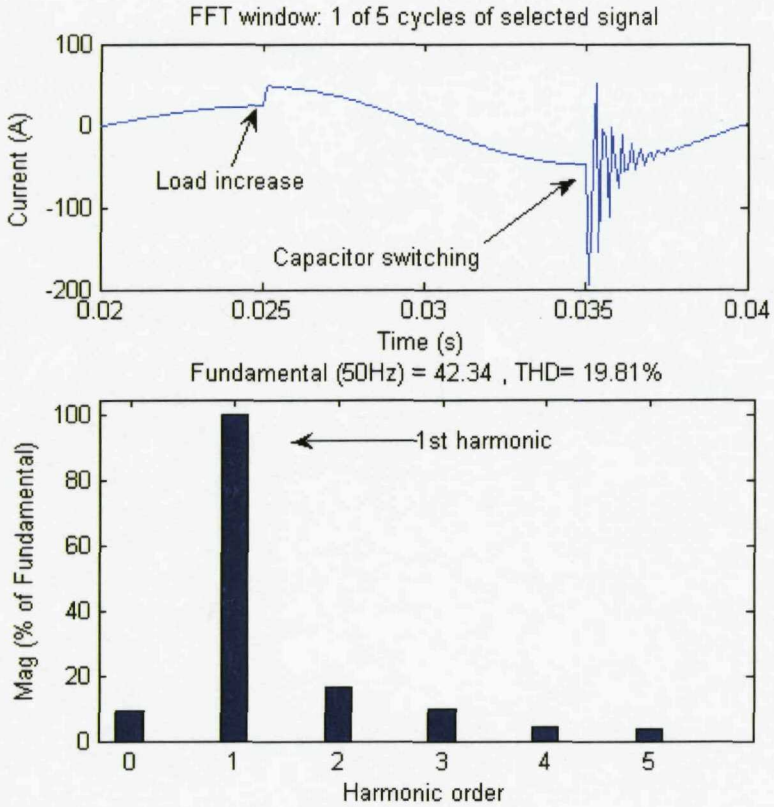

Figure 3.28B Line harmonics and current during the load and capacitor switching

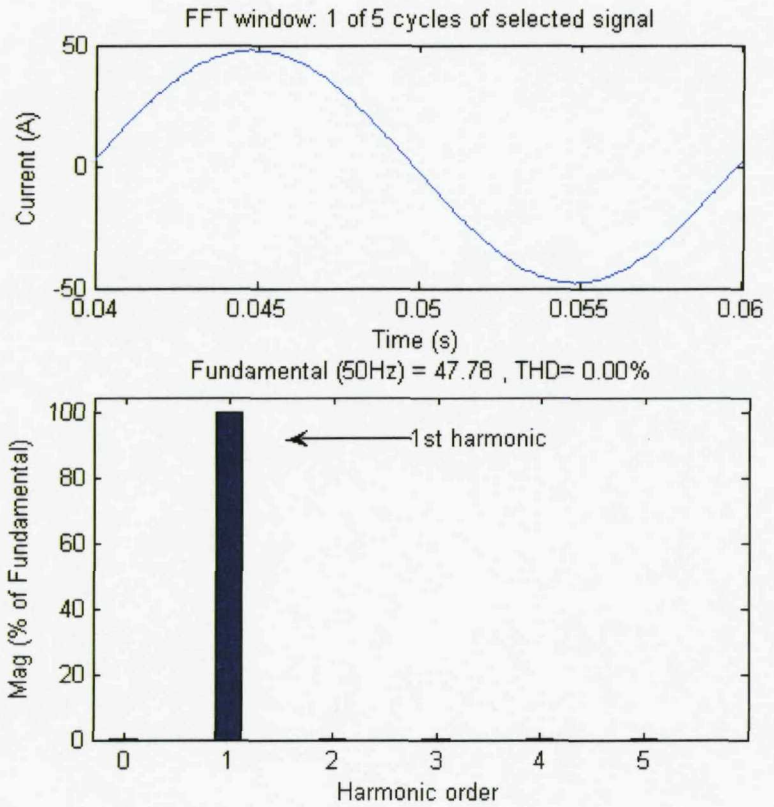

Figure 3.28C Line harmonics and current after the load and capacitor switching

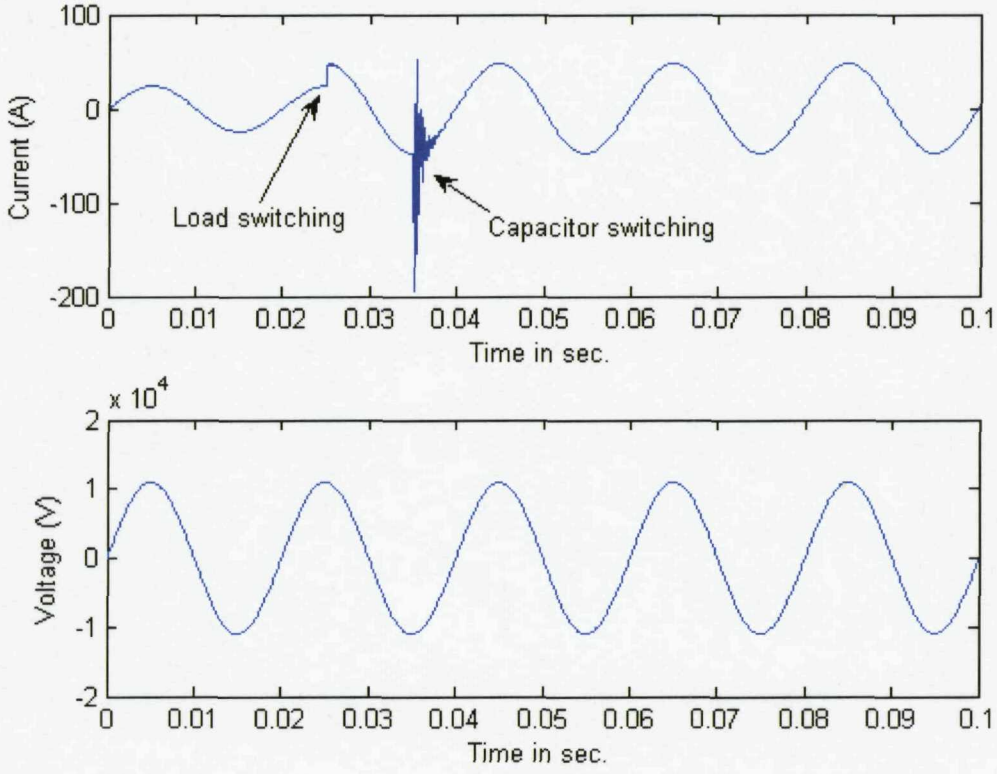

Figure 3.28D Voltage and current for load and capacitor switching

3.7.3 High impedance fault

In the case of a high impedance fault, during the cycle before the fault, there are no harmonics in the line except for the fundamental current (Figure 3.29A). For the period of the cycle in which the fault exists there is a noticeable change in the magnitudes of the 2nd to the 7th harmonics as shown in Figure 3.29B. In the third cycle after the event has happened, the existence of the odd harmonics and the asymmetrical shape in the fundamental current can be noted as shown in Figures 3.29C and D. Moreover, a phase shift for the 3rd and 5th harmonics current with respect to the fundamental current has also been observed and is shown in Figures 3.29E and F.

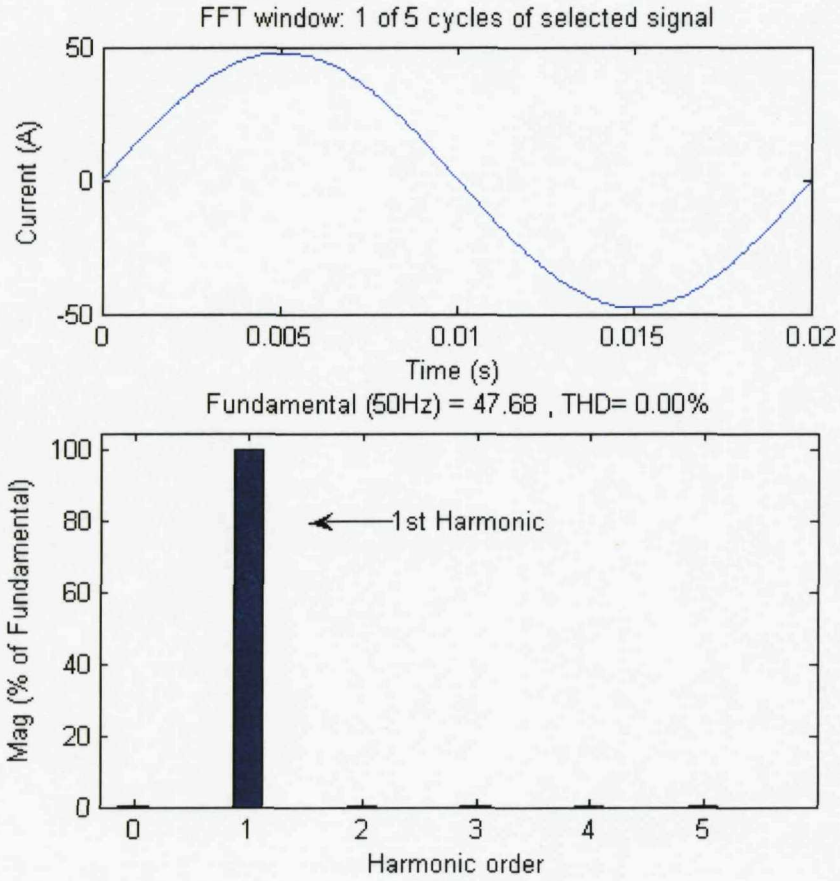

Figure 3.29A Line harmonics and current before HIF

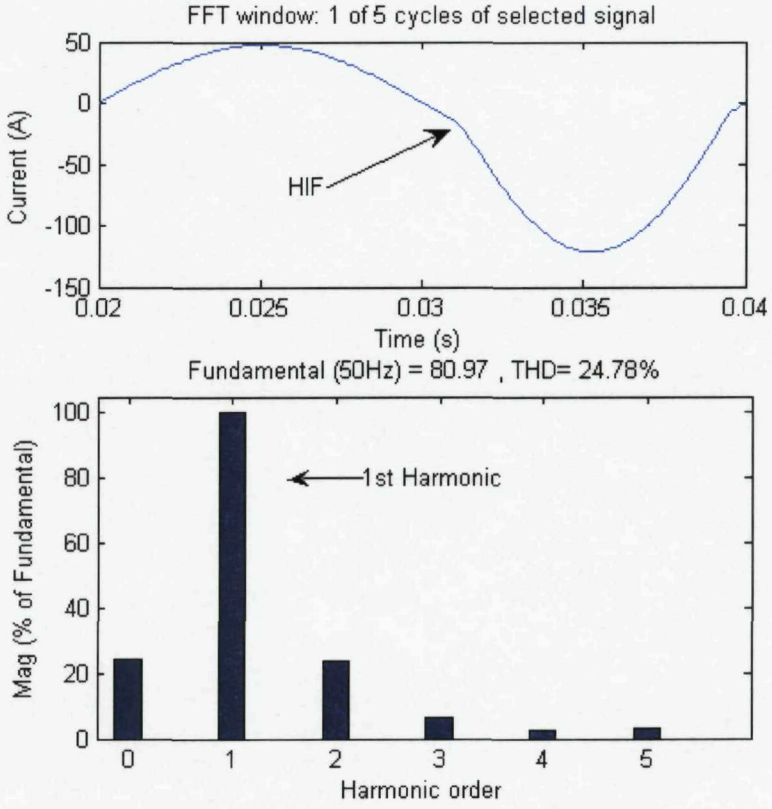

Figure 3.29B Line harmonics and current during HIF

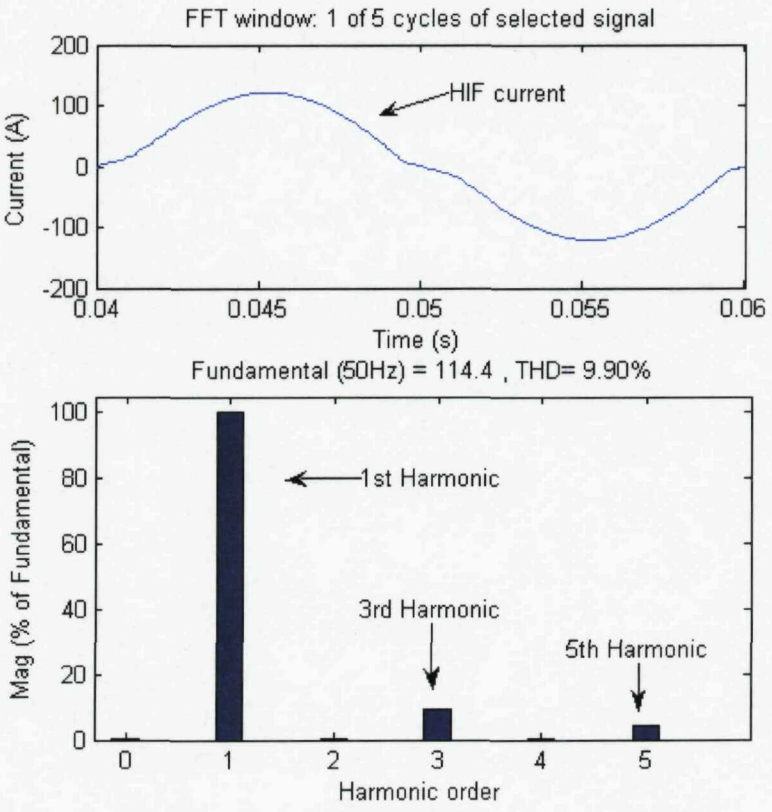

Figure 3.29C Line harmonics and current a cycle after the existence of HIF

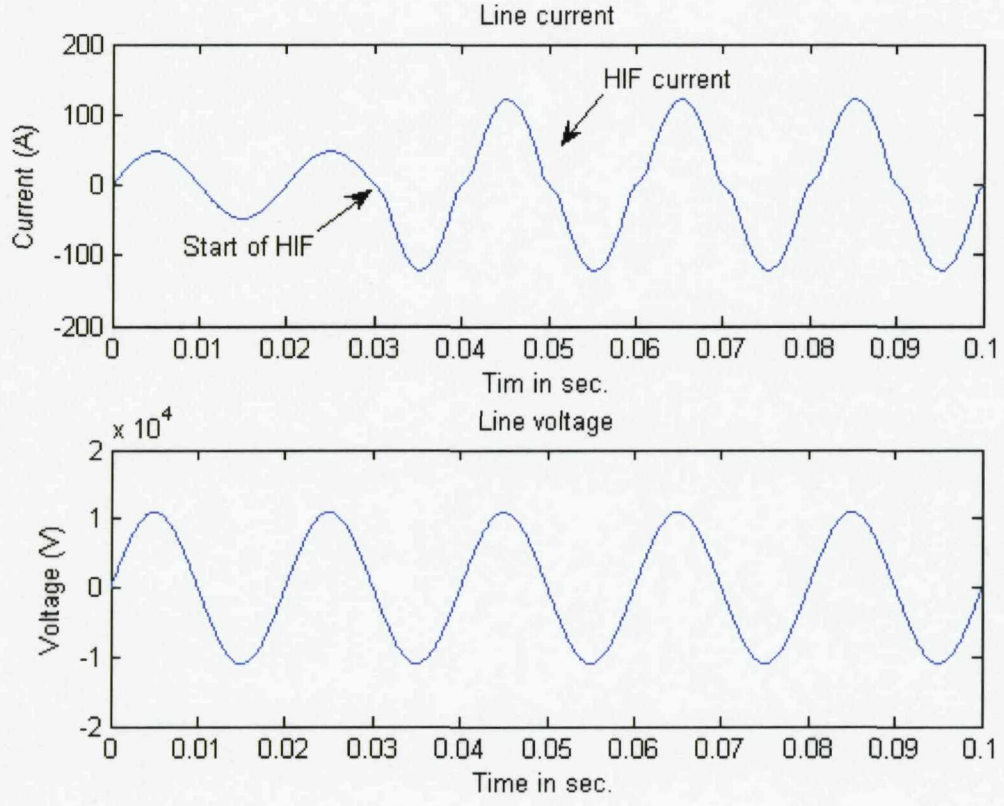

Figure 3.29D high impedance fault line current and voltage

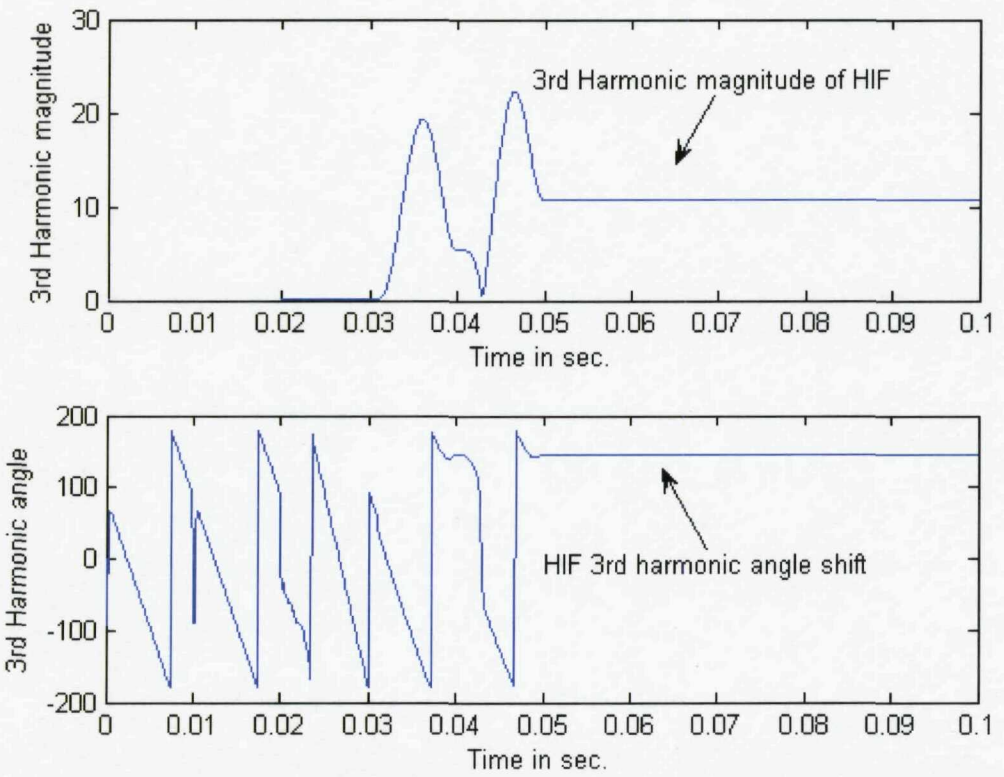

Figure 3.29E High impedance fault 3rd harmonic magnitude and phase angle

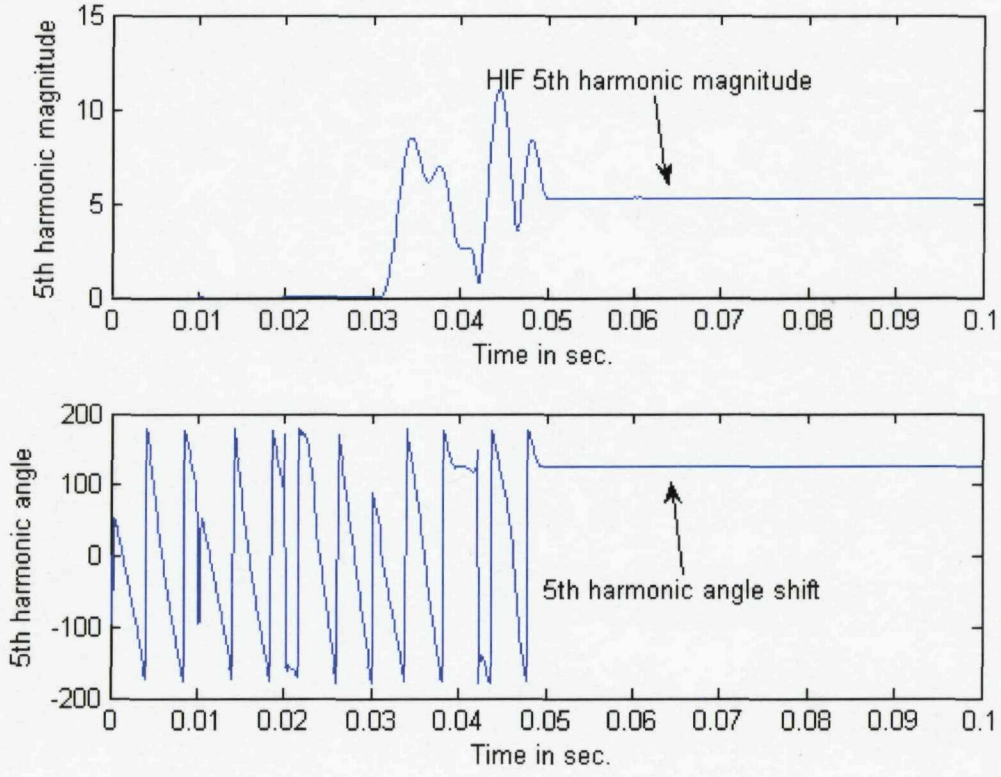

Figure 3.29F High impedance fault 5th harmonic magnitude and phase angle

3.7.4 High impedance fault with load switching

In the case of switching the high impedance fault together with the load, during the cycle before switching on the load and HIF, there are no harmonics as shown in Figure 3.30A. During the cycle when the load is switched on and the fault happens 0.005s later, there is a noticeable change in the magnitudes of the 2nd to the 7th harmonics as seen in Figure 3.30B. Moreover, an increase in the line current is observed and the HIF's asymmetrical curve is detected as seen in Figure 3.30D. In the third cycle after the event has happened the existence of the odd harmonics is noticed as shown in Figure 3.30C and the existence of the asymmetry in the fundamental current as shown in Figure 3.30.C and D. It has been observed that a phase shifts for the 3rd and the 5th harmonics of the current with, respect to fundamental current, have occurred as shown in Figures 3.30E and F.

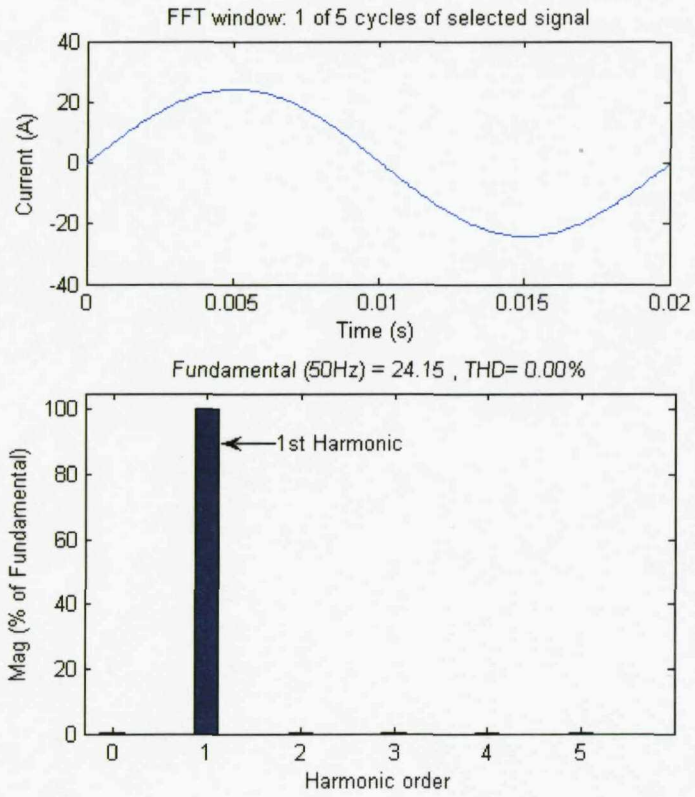

Figure 3.30A Line harmonics and current before HIF and load switching

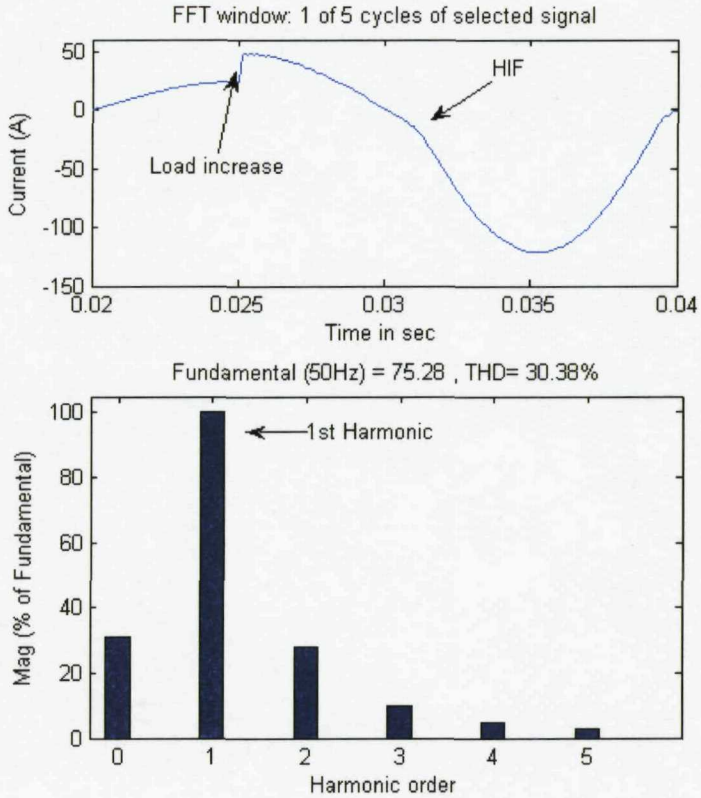

Figure 3.30B Line harmonics and current during HIF and load switching

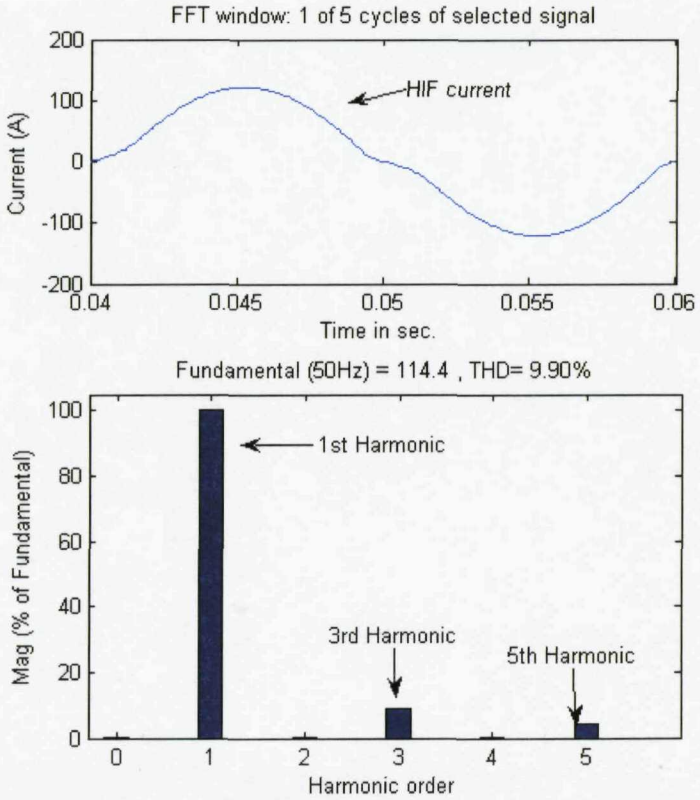

Figure 3.30C Line harmonics and current after HIF and load switching

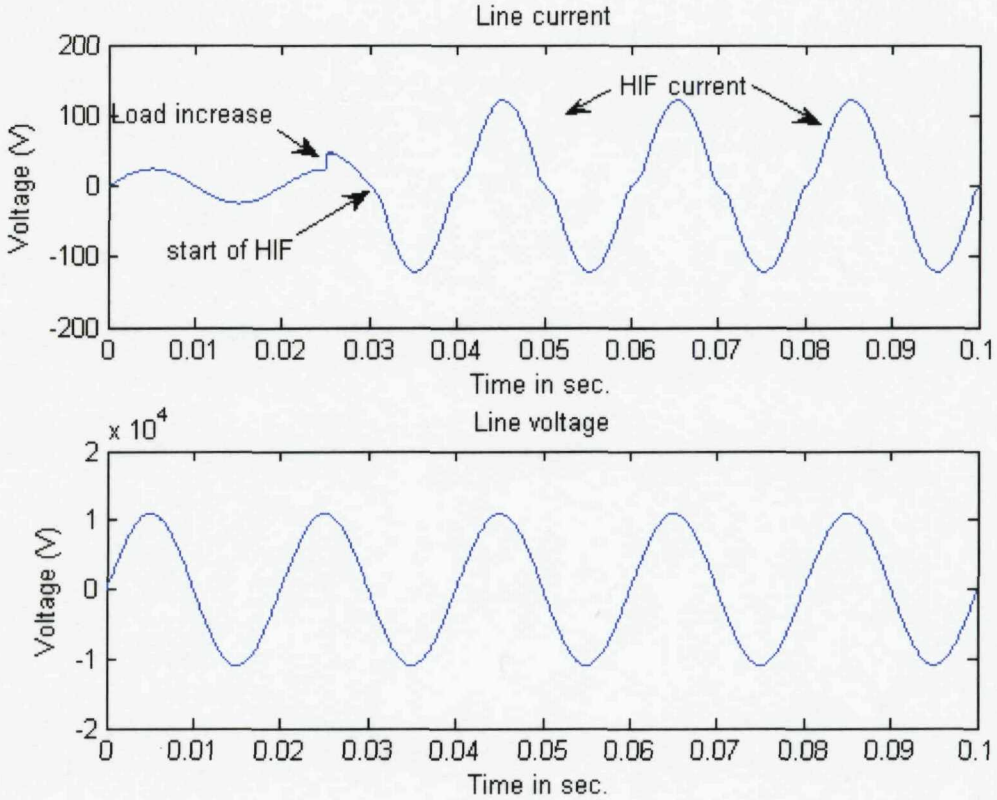

Figure 3.30D Voltage and current for HIF with load switching

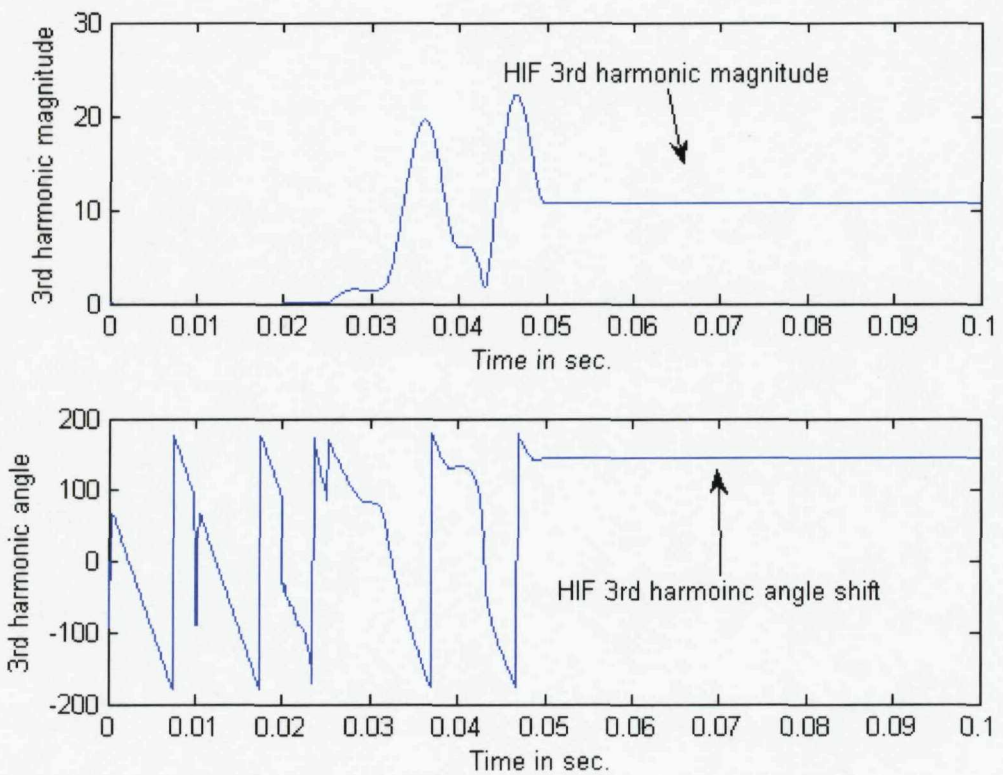

Figure 3.30E 3rd harmonic magnitude and phase angle for HIF with load switching

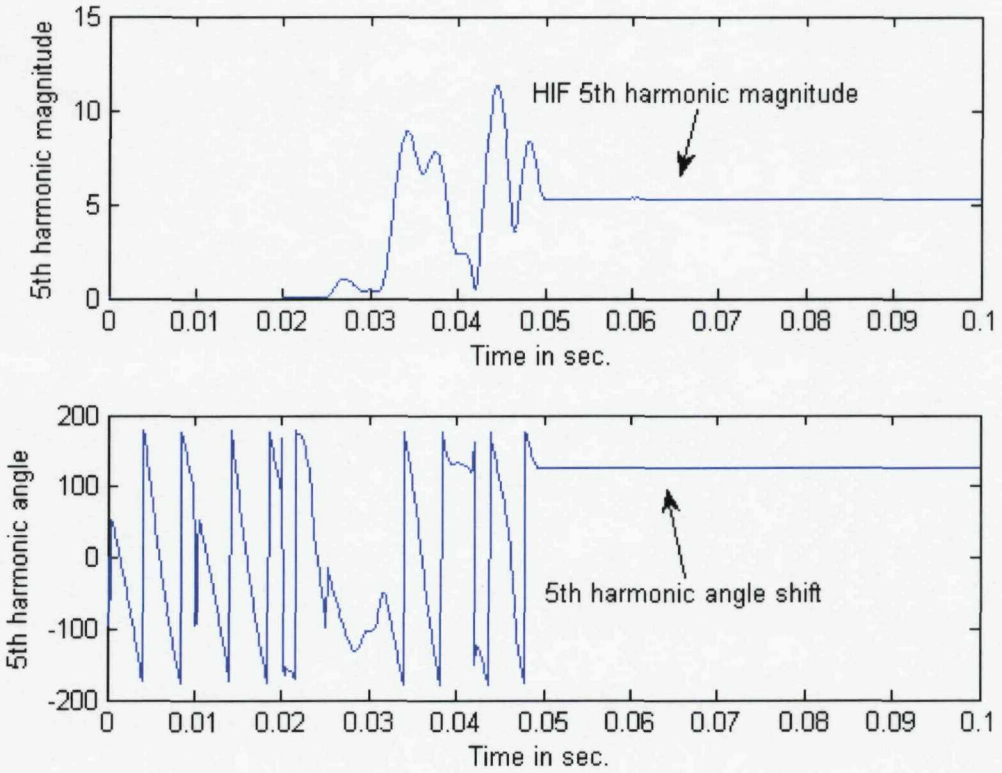

Figure 3.30F 5th harmonic magnitude and phase angle for HIF with load switching

3.7.5 High impedance fault with load and capacitor switching

In the case of simultaneous switching on the high impedance fault with a load and a capacitor, during the cycle before the switching, there are no harmonics except for the fundamental current as shown in Figure 3.31A. During the cycle when the load is switched on, with a high impedance fault switched 0.005s after the load, and the capacitor switched on 0.005s after HIF (see Figure 3.31D), there is a noticeable change in the magnitudes of the 2nd to the 7th harmonics as seen in Figure 3.31B due to the transient of the capacitor and the increase in the line current due to the increase in the load as seen in Figure 3.31D. In the cycle after the event has happened it can be noticed the existence of the odd harmonics, and the existence of the asymmetry in the fundamental current as seen in Figures 3.31C and 3.31D. It has also been observed that phase shifts for the 3rd and the 5th harmonics with respect to fundamental current take place as shown in Figure 3.31E and F.

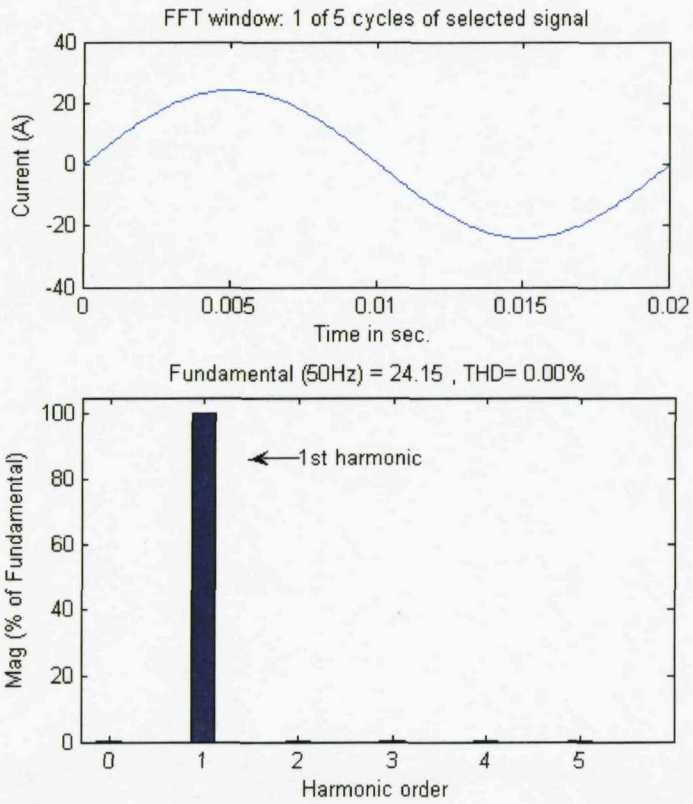

Figure 3.31A Line harmonics and current before HIF, load, and capacitor switching

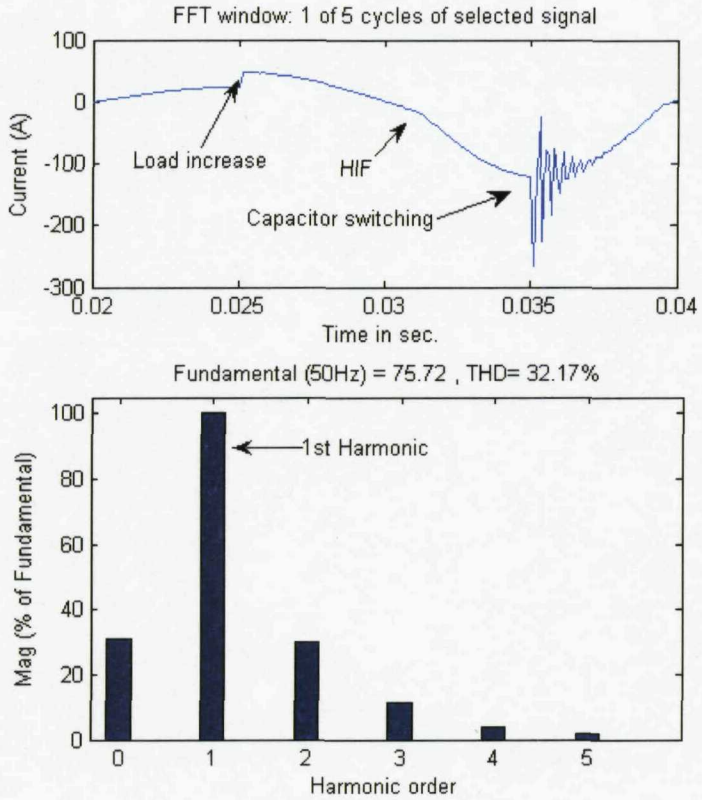

Figure 3.31B Line harmonics and current during HIF, load, and capacitor switching

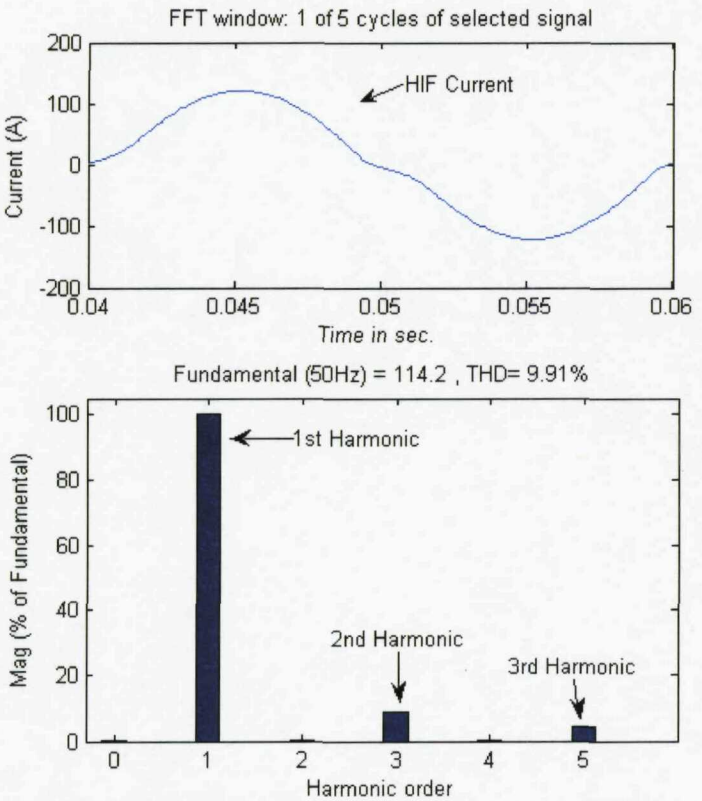

Figure 3.31C Line harmonics and current after HIF, load, and capacitor switching

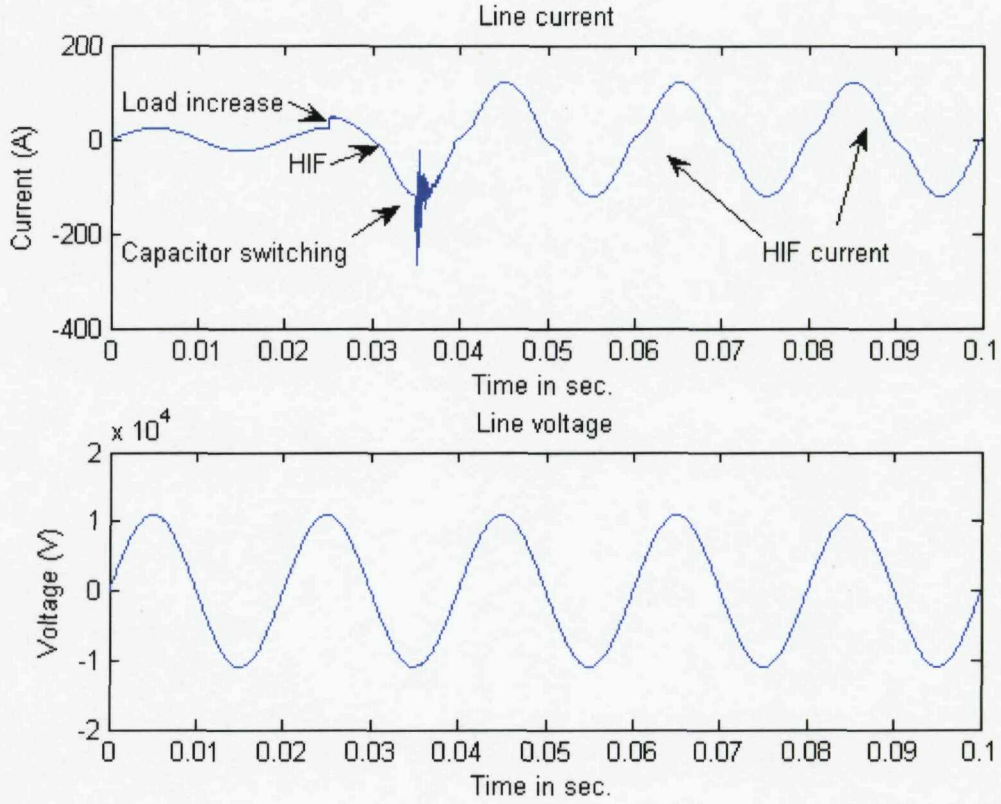

Figure 3.31D Voltage and current for high impedance fault with load and capacitor switching

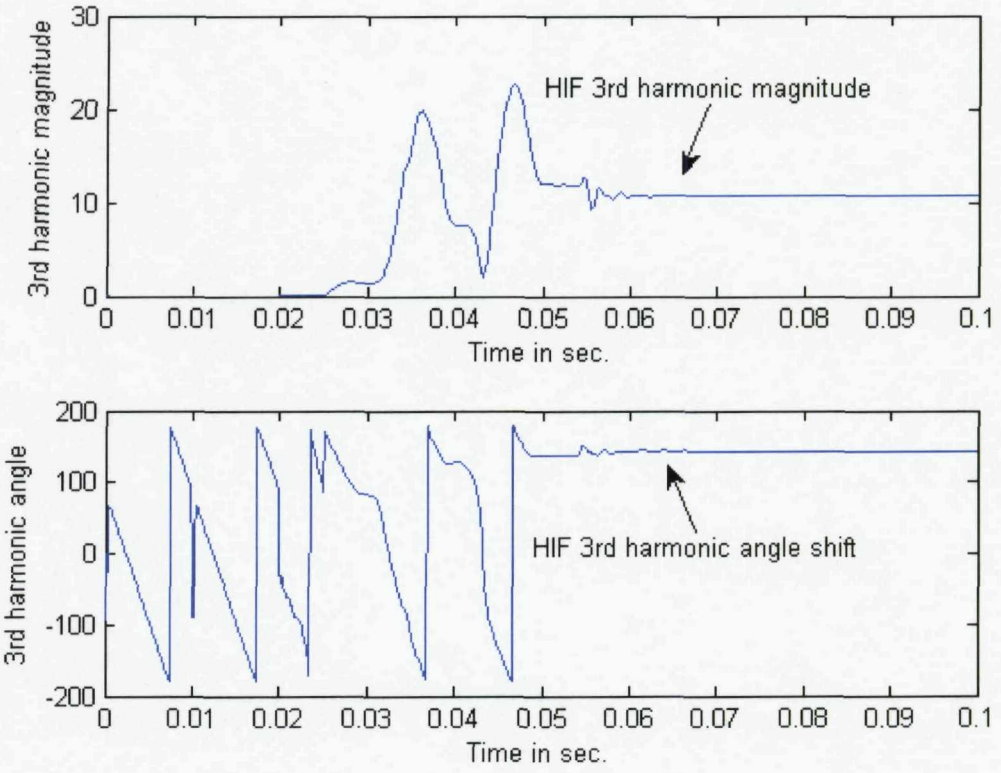

Figure 3.31E 3rd harmonic magnitude and angle for impedance fault with load and capacitor switching

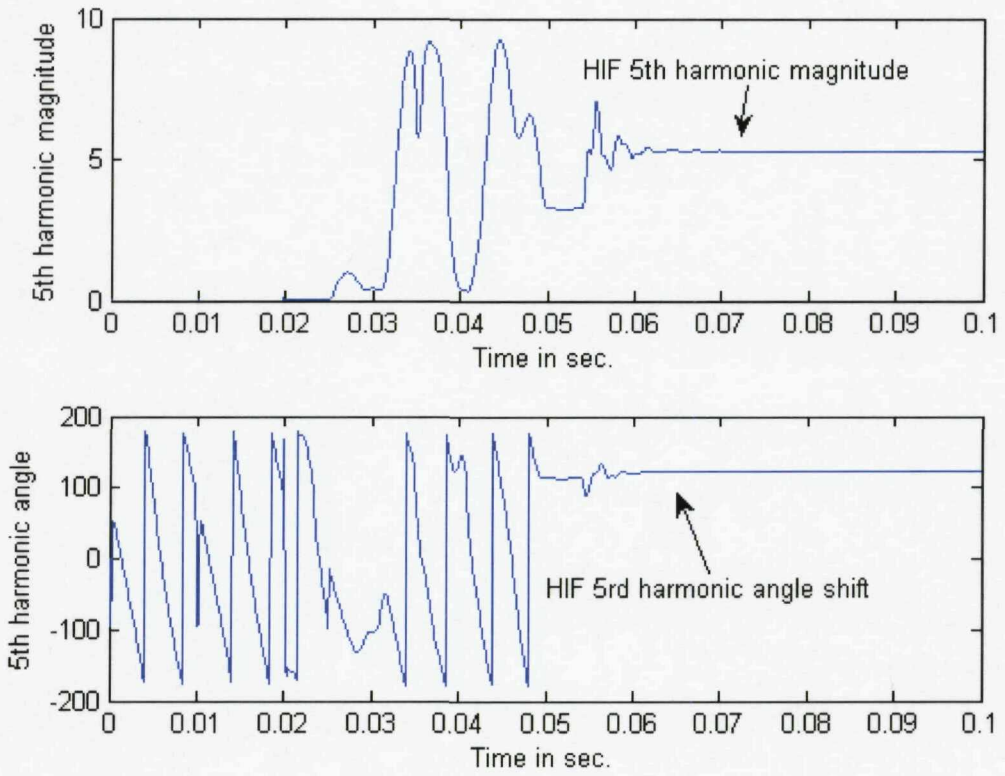

Figure 3.31F 5th harmonic magnitude and angle for impedance fault with load and capacitor switching

The conclusion from the cases reported above is that the most distinctive properties of the high impedance fault are the current asymmetry, the increase in the odd harmonics (Figures 3.29C, 3.30C, 3.31C), and the shift in the phase angle for the 3rd and 5th harmonics with respect to the fundamental current (Figures 3.29E and F, 3.30E and F, 3.31E and F).

3.8 Conclusion

The aim of this chapter was to develop a model that represents and predicts all important HIF characteristics including nonlinearity, asymmetry, harmonic content and phase shift of the 3rd and 5th harmonic. The physical processes occurring in an arc result in a unique signature. Practical data is extracted from HIF collected and experimental data curves and used to validate the proposed model. Accordingly, a new model for a HIF has been proposed and tested, containing active as well as passive elements (voltage sources, diodes, resistances and inductances), giving a very satisfactory representation of the arc characteristics. The new model preserves the unique shape of the HIF voltage and current, and it also has the harmonics content, as well as the angle shift of the 3rd and 5th harmonics, consistent with experimentally observed behaviour. Thus the proposed model can be considered an appropriate and physically well justified representation of HIF characteristics and can be harnessed to generate various data necessary for developing more reliable HIF detecting algorithms.

Chapter 4

A Brief Introduction to GA Concepts

4.1 History

Genetic algorithms (GAs) are inspired by Darwin's theory of evolution. The solution to a problem solved by genetic algorithms uses an evolutionary process. The idea behind GAs is to extract optimization strategies used successfully in the theory known as Darwinian Evolution, and transform them for application in mathematical optimization theory to find the global optimum in a defined search space.

Evolutionary computing was introduced in the 1960s by I. Rechenberg in his work "Evolution strategies". His idea was then developed by other researchers. Genetic Algorithms (GAs) were invented by John Holland and developed by him, his students and colleagues. This led to Holland's book "Adoption in Natural and Artificial Systems" published in 1975 [71]. John Holland was the pioneering founder of much of today's work in genetic algorithms, which has moved on from a purely theoretical subject (though based on computer modelling) to provide methods which can be used to actually solve some difficult practical problems.

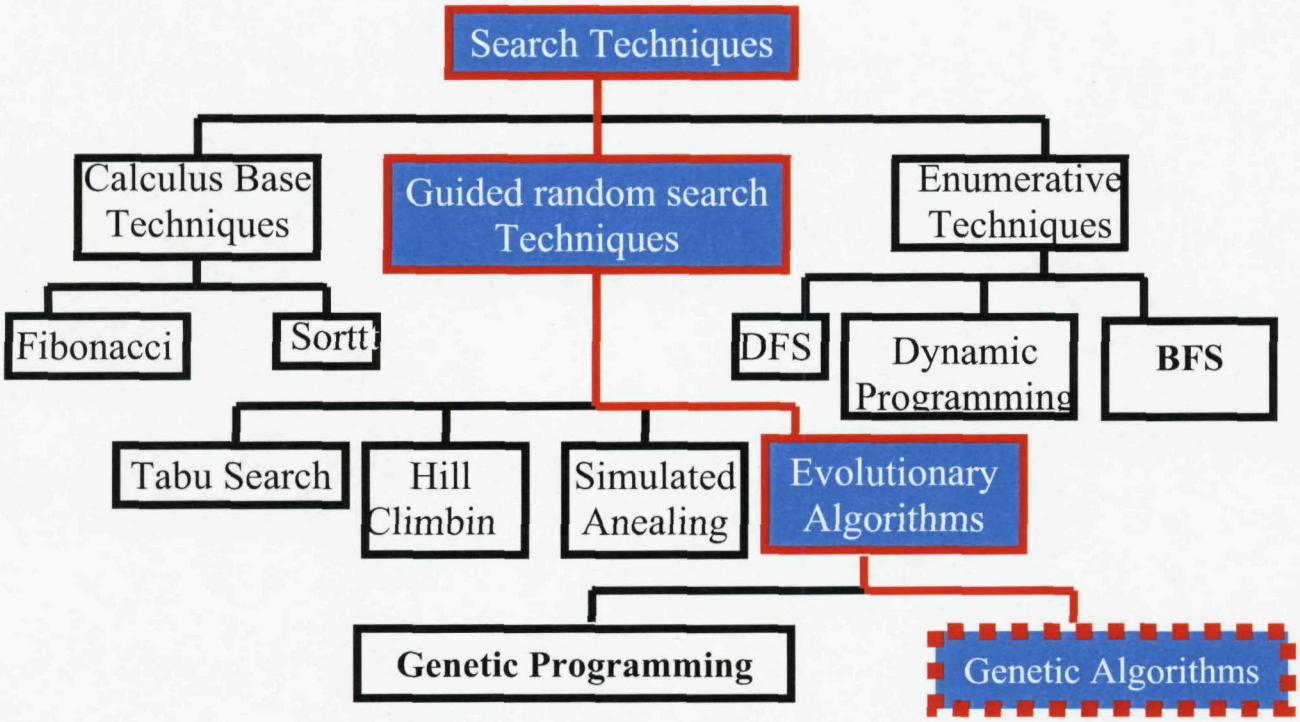

Figure 4.1 Classes of Search Techniques [72]

4.2 The Genetic Algorithms

Genetic Algorithms are adaptive search procedures for optimization and learning. As such they represent an intelligent exploitation of a random search used to solve optimization problems. They use an evolutionary metaphor to evolve populations of potential solutions in parallel. Genetic algorithms are well suited for solving adaptive problems because they have the capacity to evolve and adjust to changing environments. An obvious application of genetic algorithms is biological simulation. For example, competing evolutionary models can be explored and compared. Optimization problems, particularly those with large-dimensional search-spaces, are another common application since genetic algorithms are efficient at reducing error.

The concepts of the algorithms are based on natural selection and natural population genetics. They involve survival of the fittest among string structures. In every generation, a new set of strings are generated using bits and pieces of the fittest previous strings. They efficiently exploit historical information to speculate on new search points with expected improved performance [73]. GAs are different from other conventional optimization techniques in many ways. They use the objective function itself and not the gradient, they search from a population of strings not single a point and they work with a coding of the parameter set, not with the parameters themselves. With these reasons, and others, GAs are considered as an attractive alternative optimization technique.

GA is a simple algorithm, starts with random generation of a population. A population consists of a set of strings. Usually, the string size ranges between 50-1000. The population may be of any size according to the accuracy required. The population size remains constant throughout the whole process. Each string in GAs may be divided into a number of sub-strings. The number of sub-strings usually equals to the number of the problem variables. The problem variables are coded using suitable coding systems. In this study real coding systems were used. In addition to coding and fitness evaluation, the simple GA is composed of another three basic operations; Reproduction, Crossover and Mutation. Each string of the old population goes through these three steps before a new population is generated. In the traditional GA, all the variables of interest must first be encoded as binary digits (genes) forming a string (chromosome). To minimize a function $f(x_1,x_2,.....,x_k)$ using GA, each x_i is coded as a binary or floating-point string of length m where:

$x_1 = [10001...01001]$

$x_2 = [00101...11110]$

.....

$x_k = [11110...01011]$

where $\{x_1, x_2, ..., x_k\}$ is called a chromosome and x_i are genes.

Then three standard genetic operations, i.e., reproduction, crossover, and mutation are performed to produce a new generation [73-75]. Such procedures are repeated until the pre-specified number of generations is reached, or the required accuracy is achieved.

4.3 Characteristics of genetic algorithms

The formal structure of a GA has three components: the environment and its elements (search space), a selection based on a measurement of performance (fitness of the solution) and an adaptive plan (evolutionary operators). An initial population (possible solutions) of random individuals is usually generated. In the course of the evolutionary process, this population is evaluated: each individual is given a score reflecting its ability to adapt to a particular environment. In each generation an evolutionary behaviour is observed through two basic characteristics: competition and cooperation, where the principles of selection and reproduction are applied.

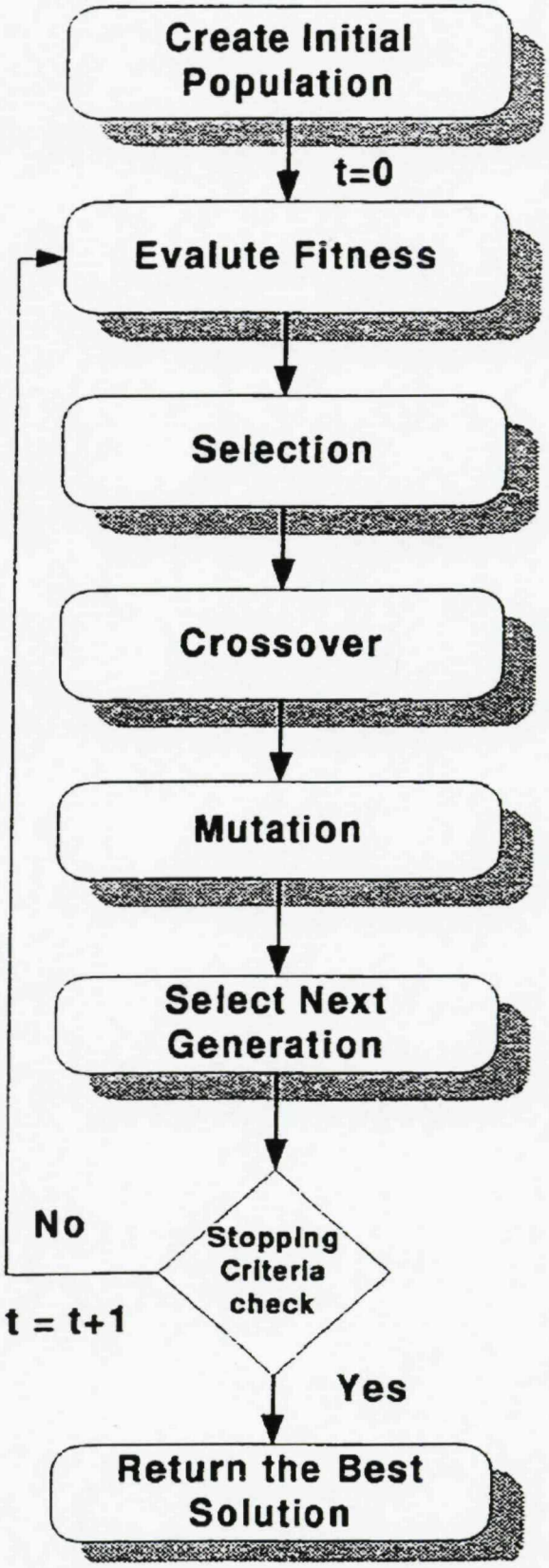

Figure 4.2 Outline of a Genetic Algorithm

4.3.1 Outline of the Basic Genetic Algorithm

1. **{Start}** Generate random population of *n* chromosomes (suitable solutions for the problem)
2. **{Fitness}** Evaluate the fitness *f(x)* of each chromosome *x* in the population
3. **{New population}** Create a new population by repeating the following steps until the new population is complete
    1. **{Selection}** Select two parent chromosomes from a population according to their fitness (the better fitness, the bigger chance to be selected)
    2. **{Crossover}** With a crossover probability cross over the parents to form a new offspring (children). If no crossover was performed, offspring is an exact copy of parents.
    3. **{Mutation}** With a mutation probability mutate new offspring at each locus (position in chromosome).
    4. **{Accepting}** Place new offspring in a new population
4. **{Replace}** Use new generated population for a further run of algorithm
5. **{Test}** If the end condition is satisfied, **stop**, and return the best solution in current population
6. **{Loop}** Go to step **2**

4.3.2 Fitness Function

The Fitness Function (FF) is one of the key elements of GAs as it determines whether a given potential solution will contribute its elements to future generations through the reproduction process. The FF should be able to provide a good measure of the quality of the solution and should differentiate between the performance of different strings. In this thesis two fitness functions (FF) are used. The first (FF1) is the 'average root error square' fitness function which is set to minimize the maximum individual error. The second fitness function (FF2) is set to minimize the 'maximum individual absolute error'. The evaluation function is the function responsible for the determination of the fitness of each individual.

4.3.3 Selection

The selection, or competition, is a stochastic process in which the chance of an individual surviving is proportional to its adaptation level. The adaptation is measured by the phenotype evolution, that is, the characteristics presented by an individual in the problem environment. The GA, through selection, determines which individuals will go to the reproduction phase. In the literature there are several selection methods where the fittest individuals from each generation are preferentially chosen for reproduction [73]. The mechanisms that give an adaptive behavior to the GAs are the selective pressure and genetic inheritance. The selection imposes pressure on the population; promoting the best individuals' survival that, subsequently, produce the potential best offspring, converging to an optimal or approximately optimal solution. This evolution occurs by means of the reproduction and manipulation of the initial population, observing equilibrium between stability and adaptability, social organization and between cooperation and competition. The selection process causes an increase in the adaptation

of the population of chromosomes, so only the individuals with the best fitness values will be selected. This will guide the search for the chromosomes using fitness value above the average. The members maintained by selection can go through changes in their fundamental characteristics through the genetic operators of mutation and crossover, generating offspring for the next generation. This process is known as reproduction, and is repeated until a satisfactory solution set is found.

4.3.4 Crossover

Crossover is a genetic step in which the members of the population obtained after the reproduction process are randomly mated according to pre-specified probability. Each pair mutually interchanges a portion of bits. The position at which the interchange starts is selected randomly. In this way, new strings are generated to form the new population. Crossover can occur at a single position or at a number of different positions [73].

4.3.5 Mutation

After crossover, the population passes through another genetic process called mutation. In this process, randomly selected bits of randomly selected strings are changed from 0 to 1 and vice versa. This process occurs according to pre-specified probability; usually less than 5% of bits are changed in this process. The mutation process is used to escape from probable local optimum [73].

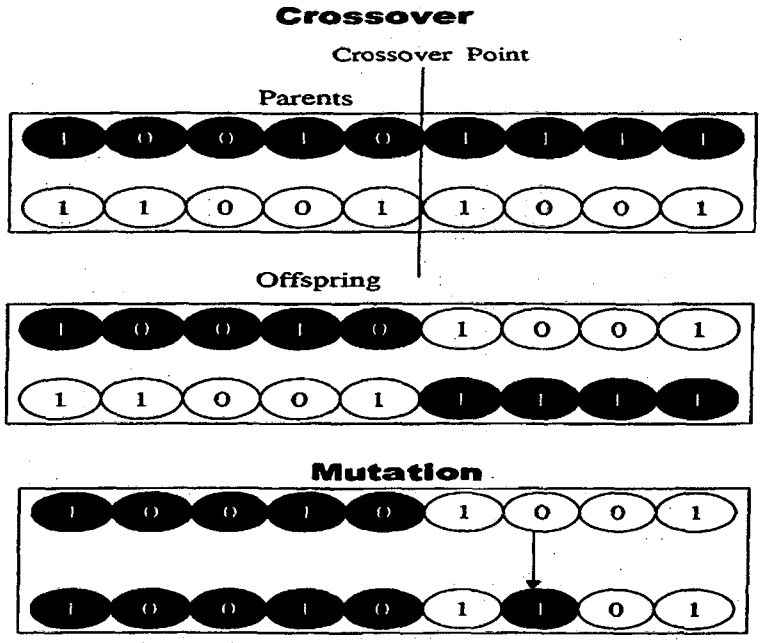

Figure 4.3 A Simple Crossover and Mutation

4.4 Real coded Genetic Algorithms

GAs are inspired by the study of genetics [73, 76, 77]. They are conceptually based on natural evolution mechanisms working on populations of solutions. An interesting feature of GAs is that they do not require any prior knowledge of the solution and they tend to exhibit reliable performance on the majority of the problems [77].

Initially, GAs were designed to operate using binary representations of the problem parameters (or unknowns). In recent studies however, the superiority of higher cardinality alphabet GAs (floating point or integer) has been demonstrated with respect to their applications to various problems. A brief description of a real-coded GA is given next.

In a real-coded genetic algorithm (RCGA), all decision variables (unknowns) are expressed as real numbers. Explicit conversion to binary does not take place. A reduction of computational effort is an obvious advantage of a real-coded GA. Another

advantage is that an absolute precision is now attainable by making it possible to overcome the crucial decision of how many bits are needed to represent potential solutions.

As in a conventional GA, an initial population of chromosomes (potential solutions) is randomly created. The best size of this population is subject to experimentation with the problem at hand. Having created a population of chromosomes, it is possible to assess the performance, or fitness, of individual members of a population. This is done through an objective function that characterizes an individual's performance in the problem domain. Then a method known as *ranking* [78] is used to rank individuals according to their objective values. Based on that ranking (i.e. fitness) of each chromosome in the initial population, a selection scheme is carried out to pick the best individuals as members of the new generation.

The selection scheme used is known as *Stochastic Universal Sampling* [79]. This scheme probabilistically selects individuals for reproduction according to their fitness. That is simply implemented by finding the cumulative sum of fitness of each chromosome in the population and generating equally spaced numbers between 0 and that sum. Therefore, only one random number is generated, all the others used being equally spaced from that point. The index of the chromosome selected is determined by comparing the generated numbers with the cumulative sum. The probability of an individual being selected is then given by

$$F(x_i) = \frac{f(x_i)}{\sum_{i=1}^{N_{ind}} f(x_i)} \qquad (4.1)$$

where $f(x_i)$ is the fitness of individual x_i and $F(x_i)$ is the probability of that individual being selected.

A discrete recombination method (equivalent to crossover) is employed for mating individuals and breeding of offsprings. Discrete recombination exchanges variable values between the individuals. A method known as simple crossover [77, 80] is implemented. To be specific, let us assume that $C_1 = (c_1^1 ... c_n^1)$ and $C_2 = (c_1^2 .. c_n^2)$ are two chromosomes that are being subjected to crossover. A position $i \in (1,2,3,.....,n-1)$ is randomly assigned. The two new chromosomes are made as follows:

$$C_{1,new} = (c_1^1, c_2^1, ..., c_i^1, c_{i+1}^2, ... c_n^2) \qquad (4.2)$$

$$C_{2,new} = (c_1^2, c_2^2, ..., c_i^2, c_{i+1}^1, ... c_n^1) \qquad (4.3)$$

Mutation of real-valued population is accomplished with the breeder genetic algorithm in [81]. Each variable is mutated with a probability, by addition of small random values (size of the mutation step). The mutation step can be reduced as the algorithm evolves. The proposed algorithm uses a generation gap and fitness-based reinsertion to implement an *elitist* strategy whereby the most fit individuals always propagate through to successive generations. For example, if G-gap = 90%, then population_size ×G-gap new individuals are produced at each generation. And then population_size ×(G-gap -1) best chromosomes are copied intact from the parent generation to the new generation to complete the population size (i.e. fill the gap). According to [73], a better average fitness is attained with the adoption of elitist strategy.

4.5 GAs versus Traditional Methods

It can be seen that the GA differs substantially from more traditional search and optimization methods. The four most significant differences are:

- GAs search a population of points in parallel, not a single point.
- GAs do not require derivative information or other auxiliary knowledge; only the objective function and corresponding fitness levels influence the directions of search.

• GAs use probabilistic transition rules, not deterministic ones.

• GAs work on an encoding of the parameter set rather than the parameter set itself (except in where real-valued individuals are used).

In cases where a particular problem does not have one individual solution, as is the case in multiobjective optimization and scheduling problems, then the GA is potentially useful for identifying these alternative solutions simultaneously.

4.6 Applications

To give an idea of the kinds of problems that GAs have been applied to successfully, here is an overview of some applications:

- Aircraft wing design (optimizing parameters that determine the shape of a wing)
- Optimal pipeline flow (optimizing, e.g., the flow of oil through a network of pipelines to satisfy customer demand)
- Scheduling problems (job-shop scheduling, etc.)
- Routing problems (TSP, network routing)
- VLSI technology, chip design (minimizing connections and communications)
- Telecommunications networks (optimal location of access points, etc.)
- Coding methods for data transmission (optimizing coding methods and their parameters)
- Robotics (evolution of robot controllers)
- Stock market prediction .

Chapter 5

A digital technique for online identification and tracking of power system harmonics based on Real Coded Genetic Algorithm

Current and voltage waveforms of a distribution or a transmission system are not pure sinusoids. There are distortions in these waveforms that consist of a combination of the fundamental frequency, harmonics and high frequency transients. This chapter presents an enhanced measurement scheme for identification and tracking of harmonics in power system. The proposed technique is not limited to stationary waveforms, but can also estimate harmonics in waveforms with time-varying amplitudes. This chapter presents a new method based on Real Coded Genetic Algorithm described in Chapter 4. The algorithm was tested using several practical cases. The effects of fitness functions as well as the effects of sampling rate and sampling window size (number of cycles) have been studied. Results are reported and discussed.

5.1 Introduction

Voltage and current waveforms of a distribution or a transmission system are distorted and consist of a combination of the fundamental frequency, harmonics and high frequency transients. In an ideal electrical power system, energy is supplied at a constant frequency with specified voltage levels. However, none of these conditions are fulfilled in practice because voltage and current waveforms are rarely pure sinusoids. Distortions can be associated, for instance, with the operation of nonlinear loads such as inverters, rectifiers, AC/DC converters and a countless number of power electronic devices that can add harmonics to the sinusoidal signal. Nowadays, it is well known that harmonics have adverse effects on the whole power system [20, 82].

Various digital signal processing techniques based on static and dynamic estimation have been suggested to evaluate power system harmonics. Some examples of static estimation included the Least-Squared Method (LSM), one of the oldest techniques used to fine tune state variables. It is based on the minimization of the mean square error between the estimated and the measured values for the voltage and current amplitudes and phase angles. For a nonlinear power system model, this technique results in reasonable parameter estimation [83]. In the Least Absolute Value estimation (LAV) technique the error to be minimized is the absolute error. Discrete Fourier Transform (DFT) is based on orthogonal functions. According to DFT, the waveform consists of a fundamental component accompanied by an infinite number of harmonics. The computational cost of this algorithm is low, but its performance can be badly affected by the DC component present in the signal [84]. The Fast Fourier Transform (FFT) algorithm is a speed-optimized DFT version. However, the application of the FFT may lead to imprecise results especially due to pitfalls such as aliasing, leakage and picket fence effect [85, 86]. On the other hand, the Kalman Filter is an example of

dynamic estimation of the signal and has the ability to identify, analyze and locate the harmonic content in a non-stationary three phase signal. Despite yielding accurate results, prior statistical analysis of the signal is necessary.

Artificial Intelligence (AI) has also been applied to power system harmonic evaluation. Expert system algorithms are based on the rule base of human expertise to diagnose the harmonics caused problems. The goal is to accomplish the analysis with less experienced engineers [87]. Artificial Neural Networks (ANNs) have been used as an online digital system to read and update harmonic parameters of electrical signals [88]. Others have used the wavelet transforms for decomposing electrical current and voltage, but the disadvantages of both methods mentioned in Chapter 2 encourages researchers to try different methods and tools especially with the availability of fast computing.

Genetic Algorithms (GA) have attracted attention as a robust algorithm for stochastic search applied to optimization problems and it has been used to solve several problems in electric power systems with good results. The following work presents a new method based on Real Coded Genetic Algorithm (RCGA) for the analysis of harmonic distortion in a power system.

5.2 Harmonic model

A signal can be defined as a function that carries information, usually about a state or a procedure of a physical system. However, signals can be represented in several ways. Mathematically, a periodic and distorted signal can be suitably represented in terms of its fundamental frequency and harmonic components, expressed as a sum of sinusoidal waveforms referred to as the Fourier series. Each frequency is an integer multiple of the fundamental system frequency. In order to obtain an approximation of such waves, mathematical models are employed.

Consider a voltage waveform with harmonic components, written as Equation (5.1) [21, 89]

$$v(t)=\frac{V_o}{2}+\sum_{i=1}^{N}V_i(t)\sin(i\omega t)+\sum_{i=1}^{N}V_i'(t)\cos(i\omega t) \qquad (5.1)$$

where $V_i(t)$ and $V_i'(t)$ are the amplitudes of the ith harmonic at time t, ω is the fundamental angular frequency and N is the number of harmonics present in the voltage waveform. Assuming that the voltage waveform is sampled at a predefined sampling rate at equal time intervals Δt, one will have a set of m samples, $v(t_1),v(t_2),...v(t_m)$, obtained for $t_1,t_2,...t_m$, where t_1 is an arbitrary time reference. One can write the following discrete system of equations in the state space form, as shown in Equation (5.2)

$$\begin{bmatrix} v(t_1)=\frac{V_o}{2}+V_1(t_1)\sin(\omega t_1)+V_i'(t_1)\cos(\omega t_1)+.....+V_N(t_1)\sin(N\omega t_1) \\ ..... \\ ..... \\ v(t_m)=\frac{V_o}{2}+V_1(t_m)\sin(\omega t_m)+V_i'(t_m)\cos(\omega t_m)+.....+V_N(t_m)\sin(N\omega t_m) \end{bmatrix} \qquad (5.2)$$

In the matrix form, Equation (5.2) can be rewritten as:

$$V = f(x) + e \qquad (5.3)$$

where:

V is the voltage sample vector m x 1;

$f(x)$ is the ideal connection vector m x 1;

x is the state vector to be estimated, i. e. the voltage amplitudes;

e is the noise m x 1 vector to be minimized.

Now the problem is to find the optimum values of the state vector x that minimize the noise vector using GA.

5.3 Fitness Function

The Fitness Function (FF) is one of the key elements of GAs as it determines whether a given potential solution will contribute its elements to future generations through the reproduction process. The FF should be able to provide a good measure of the quality of the solution and should differentiate between the performances of different strings. Two different functions are used in this work to evaluate the quality of the solution. Each function will be used and the solution obtained using both of them will be evaluated.

The evaluation function is the function responsible for the determination of the fitness of each individual. In the first Fitness Function (FF1) the Sum of Square Errors Fitness Function is used. The objective is to evaluate the estimation error (e). The coded parameters are substituted on the right of Equation (5.2) and they are compared to the measured values in each time step $V(t)$ to calculate the average error (e). We use the evaluation function as the function of the sum of quadratic errors. In this study the fitness function is set to minimize the maximum individual error. Equation (5.3) can be written in the form of:

$$V_i - F_i(x) = e_i \quad \text{For} \quad i = 1,2,.....m \qquad (5.4)$$

By squaring the individual errors and adding them together, we will end up with the following equation: (5.5)

$$F_{sum} = \sqrt{\frac{\sum_{i=1}^{m} e_i^2}{m}} \qquad (5.5)$$

Since the objective of GAs is to maximize the objective function, it is necessary to map the error square function (F_{sum}) into minimization fitness function (FF1)

$$FF1 = \frac{1}{F_{sum} + \Delta} \qquad (5.6)$$

where Δ is a small constant to avoid overflow problems if F_{sum} goes to zero.

For the second fitness function (FF2), the fitness function is set to minimize the maximum individual error. Thus the second fitness function FF2can be write as:

$$FF2 = \frac{1}{|e_{max}| + \Delta} \qquad (5.7)$$

where e_{max} is the maximum individual error in each generation.

5.4 Testing and analysis of the algorithm

5.4.1 Case study 1

Equations (5.8) and (5.9) represent a transmission line fault situation. In this case study testing is carried out on waveforms with known Fourier coefficients as seen in [90]. A single phase to ground fault is used since it is the most common type and the fault is applied at a voltage peak. With a pre-selected sampling rate and specified window size, the actual analogue signal is converted to discrete digital samples. A/D converters are used to generate the measurement vector [V]. The fitness function proposed earlier is used to evaluate the RCGA solution. A data window size of one cycle is used with different sampling frequencies. Tables 5.1 and 5.2 show the results obtained using the first fitness function FF1 with different sampling frequencies. It is very clear from the results that the estimated results for both voltage and current are very accurate for the first chosen sampling frequency, while further increase of the sampling frequency gives the same accuracy but at longer calculation times.

$$V(t)=0.0388\exp(-0.4t)+0.4994\cos(\omega t)+0.3230\sin(\omega t)+0.0708\cos(2\omega t)+0.0224\sin(2\omega t)+0.0154\cos(3\omega t)+0.0165\cos(4\omega t)+0.0219\sin(4\omega t)+0.0176\cos(5\omega t)+0.0119\sin(5\omega t)+0.0120\cos(6\omega t)+0.0289\sin(6\omega t)+0.0084\cos(7\omega t)+0.0084\sin(7\omega t) \quad (5.8)$$

$$I(t)=0.0454\exp(-0.4t)+0.4662\cos(\omega t)+0.0817\sin(\omega t)+0.0519\cos(2\omega t)+0.0543\sin(2\omega t)+0.0305\cos(3\omega t)+0.0218\cos(4\omega t)+0.0313\sin(4\omega t)+0.0178\cos(5\omega t)+0.0244\sin(5\omega t)+0.0159\cos(6\omega t)+0.0196\sin(6\omega t)+0.0157\cos(7\omega t)+0.0168\sin(7\omega t) \quad (5.9)$$

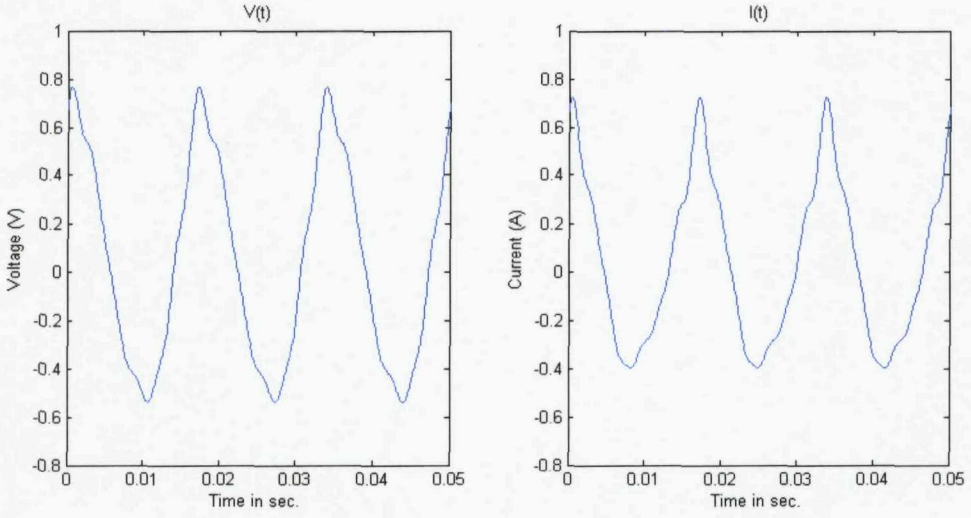

Figure 5.1 Plot of *V(t)* and *I(t)* of equations 5.8 and 5.9

Equations (5.8) and (5.9) are plotted in Figure 5.1. As may be clearly seen, the voltage and current signals are badly corrupted by harmonic noise and an exponentially decaying transient. Thus a signal of this type could be considered a good test for any algorithm aimed at harmonics identification, and rather than 'inventing' an artificial waveform to test the RCGA (which has also been done but is not reported here) it was felt that taking a practical situation - in this case a single phase to ground fault - would be more appropriate. Although these test signals do not exhibit HIF characteristics (this will be explored in Section 5.4.2), they are nevertheless typical in power systems and thus a well performing algorithm would be expected to provide high levels of accuracy. This testing should also provide useful information regarding required sampling rates. Once the RCGA has been demonstrated to work well for typical signals encountered in power systems (and the signals used here, taken from literature [90], are representative

of many other similar waveforms tested although not reported), it will be tried on a HIF signal later in this Chapter.

Table 5.1 Estimated harmonic magnitudes for *V(t)* using GA with different sampling time FF1

		GA		GA		GA	
Harmonic order	**Harmonics Magnitudes of V(t)**	**Δt=0.001s**	**%Error**	**Δt=0.0005s**	**%Error**	**Δt=0.00001s**	**%Error**
DC	0.0388	0.0388	0	0.0388	0	0.0388	0
1st	0.4994	0.4994	0	0.4994	0	0.4994	0
	0.323	0.323	0	0.323	0	0.323	0
2nd	0.0708	0.0708	0	0.0708	0	0.0708	0
	0.0224	0.0224	0	0.0224	0	0.0224	0
3rd	0.0154	0.0154	0	0.0154	0	0.0154	0
4th	0.0165	0.0165	0	0.0165	0	0.0165	0
	0.0219	0.0219	0	0.0219	0	0.0218	-0.46
5th	0.0176	0.0176	0	0.0176	0	0.0176	0
	0.0119	0.0119	0	0.0119	0	0.0119	0
6th	0.012	0.012	0	0.012	0	0.012	0
	0.0289	0.0289	0	0.0289	0	0.0289	0
7th	0.0084	0.0084	0	0.0084	0	0.0084	0
	0.0084	0.0084	0	0.0084	0	0.0084	0
	% absolute average error		**0**		**0**	**0**	**0.033**

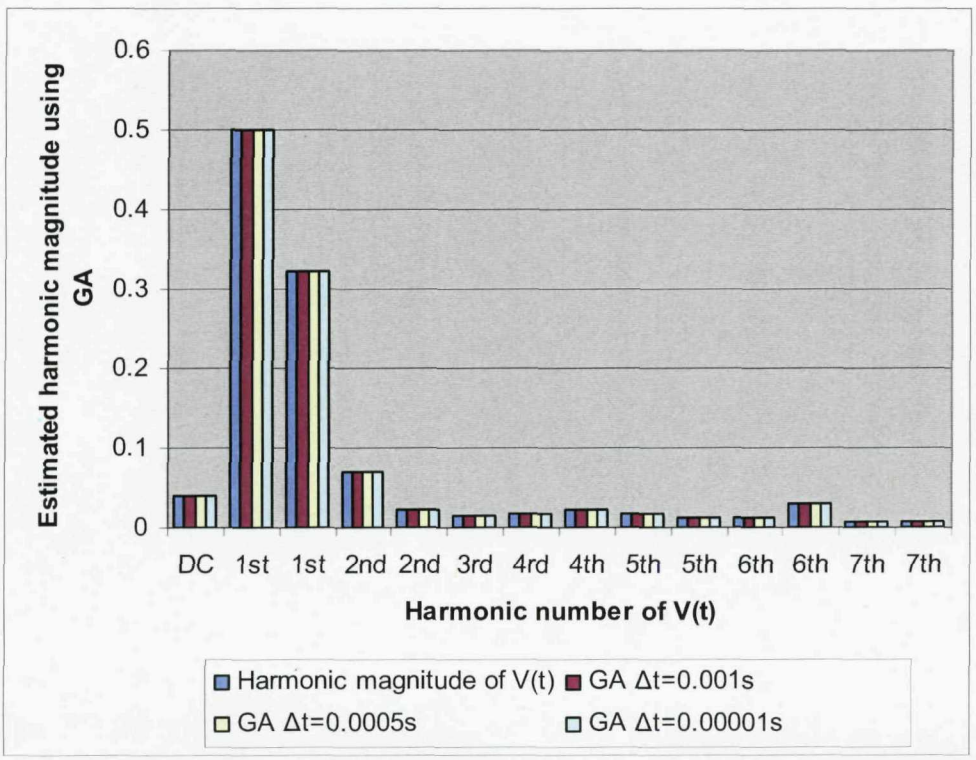

Figure 5.2 Estimated harmonic amplitude for *V(t)* using GA with different sampling time

Table 5.2 Estimated harmonic magnitudes for *I(t)* using GA with different sampling time using FF1

		GA		GA		GA	
Harmonic order	**Harmonics Magnitudes of I(t)**	**Δt=0.001s**	**%Error**	**Δt=0.0005 s**	**%Error**	**Δt=0.00001s**	**%Error**
DC	0.0454	0.0454	0	0.0454	0	0.0454	0
1st	0.4662	0.4662	0	0.4662	0	0.4663	0.022
	0.0817	0.0817	0	0.0817	0	0.0816	-0.123
2nd	0.0519	0.0519	0	0.0519	0	0.0519	0
	0.0543	0.0543	0	0.0543	0	0.0543	0
3rd	0.0305	0.0305	0	0.0305	0	0.0305	0
4th	0.0218	0.0217	-0.46	0.0219	0.46	0.0218	0
	0.0313	0.0313	0	0.0313	0	0.0313	0
5th	0.0178	0.0178	0	0.0178	0	0.0178	0
	0.0244	0.0244	0	0.0243	-0.41	0.0244	0
6th	0.0159	0.0159	0	0.0159	0	0.0159	0
	0.0196	0.0197	0.51	0.0196	0	0.0196	0
7th	0.0157	0.0157	0	0.0157	0	0.0157	0
	0.0168	0.0168	0	0.0168	0	0.0168	0
	% Absolute average error		**0.07**		**0.06**		**0.011**

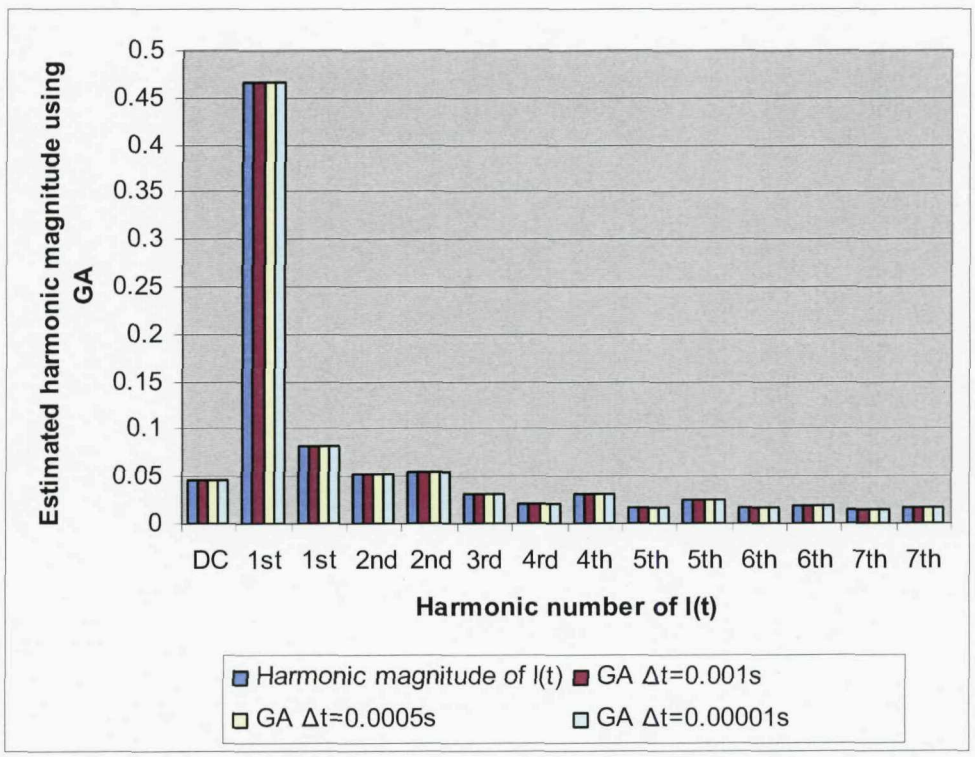

Figure 5.3 Estimated harmonic amplitude for *I(t)* using GA with different sampling time

In Table 5.3 and 5.4 the second fitness function (FF2) was tested using Case 1 to see which of the fitness functions gives a better estimation of the value of the voltage and current. FF2 was tested using different sampling frequencies and the results show that the values obtained from FF1 have much smaller average error than FF2, and thus a conclusion is that FF1 is a better fitness function in terms of accuracy.

Table 5.3 Estimated harmonic magnitudes for *V(t)* using GA with different sampling time using FF2

		GA		GA		GA	
Harmonic order	**Harmonics Magnitudes of V(t)**	**Δt=0.001s**	**%Error**	**Δt=0.0005s**	**%Error**	**Δt=0.00001s**	**%Error**
DC	0.0388	0.0387	0.26	0.0389	0.26	0.0387	0.26
1st	0.4994	0.4995	0.02	0.4992	0.04	0.4993	0.02
	0.323	0.3231	0.03	0.3224	0.19	0.3234	0.12
2nd	0.0708	0.0707	0.14	0.0706	0.28	0.0712	0.56
	0.0224	0.0225	0.45	0.0229	2.23	0.0227	1.34
3rd	0.0154	0.0154	0.00	0.0155	0.65	0.0156	1.30
4th	0.0165	0.0166	0.61	0.0164	0.61	0.0166	0.61
	0.0219	0.022	0.46	0.0211	3.65	0.0216	1.37
5th	0.0176	0.0176	0.00	0.0173	1.70	0.0174	1.14
	0.0119	0.0118	0.84	0.0121	1.68	0.0119	0.00
6th	0.012	0.0121	0.83	0.0122	1.67	0.0118	1.67
	0.0289	0.0288	0.35	0.0289	0.00	0.0292	1.04
7th	0.0084	0.0083	1.19	0.0086	2.38	0.0087	3.57
	0.0084	0.0083	1.19	0.0082	2.38	0.0083	1.19
	% Absolute average error		**0.45**		**1.27**		**1.01**

Table 5.4 Estimated harmonic magnitudes for *I(t)* using GA with different sampling time using FF2

		GA		GA		GA	
Harmonic order	**Harmonics Magnitudes of I(t)**	**Δt=0.001s**	**%Error**	**Δt=0.0005s**	**%Error**	**Δt=0.00001s**	**%Error**
DC	0.0454	0.0454	0.00	0.0453	0.22	0.0455	0.22
1st	0.4662	0.4699	0.79	0.4664	0.04	0.4663	0.02
	0.0817	0.0822	0.61	0.0818	0.12	0.0818	0.12
2nd	0.0519	0.0529	1.93	0.0515	0.77	0.052	0.19
	0.0543	0.059	8.66	0.0539	0.74	0.0545	0.37
3rd	0.0305	0.0237	22.30	0.0312	2.30	0.0305	0.00
4th	0.0218	0.0221	1.38	0.0213	2.29	0.0217	0.46
	0.0313	0.0301	3.83	0.0317	1.28	0.0315	0.64
5th	0.0178	0.0153	14.04	0.0177	0.56	0.0178	0.00
	0.0244	0.0247	1.23	0.0234	4.10	0.0245	0.41
6th	0.0159	0.0158	0.63	0.0164	3.14	0.0158	0.63
	0.0196	0.0148	24.49	0.0202	3.06	0.0196	0.00
7th	0.0157	0.02	27.39	0.0154	1.91	0.0156	0.64
	0.0168	0.0171	1.79	0.0167	0.60	0.0168	0.00
	% Absolute average error		**7.79**		**1.51**		**0.26**

5.4.1.1 RCGA approach compared with the binary approach

The binary representation in a genetic algorithm is the usual approach in encoding the parameters. However, the performance of this representation deteriorates as the number of parameters increases. Problems with several parameters end up with a very long bit string, which makes the convergence process slow.

The representation of the parameters in RCGA optimizes the encoding because individuals are directly coded as real numbers and the strings are smaller. Comparative studies have shown that RCGA is more efficient and performs better than binary GA [91-93].

In order to assess the performance of the RCGA against the Binary Coded Genetic Algorithm (BCGA) in obtaining the magnitude of the signals shown by equations 5.8 and 5.9, the results from reference [90] (which represent the BCGA solution) are compared with the solution obtained by RCGA and the results are shown in the tables below.

From the tables below by comparing the results obtained by RCGA and BCGA in term of accuracy, it is apparent that RCGA produces much better results than BCGA. For example, as shown in Table 5.5 the percentage error of obtaining the DC signal magnitude in the *V(t)* using BCGA was more than 20% while the RCGA gave the exact magnitude. For the current signal *I(t)* as shown in table 5.6, the RCGA was able to analyze all harmonic components with great accuracy while BCGA was giving up to 21% error. Moreover, the percentage of the absolute error of RCGA is much smaller than BCGA.

Table 5.5 RCGA vs BCGA in finding the magnitude of the DC component, fundamental component as well as harmonics of the voltage signal represented by equation 5.8

Harmonics Magnitudes of V(t)	RCGA	% Error	Binary GA	% Error
0.0388	0.0388	0.00	0.0308	-20.62
0.4994	0.4994	0.00	0.4995	0.02
0.323	0.323	0.00	0.3123	-3.31
0.0708	0.0708	0.00	0.0709	0.14
0.0224	0.0224	0.00	0.0225	0.45
0.0154	0.0154	0.00	0.0152	-1.30
0.0165	0.0165	0.00	0.0152	-7.88
0.0219	0.0218	-0.46	0.0235	7.31
0.0176	0.0176	0.00	0.0176	0.00
0.0119	0.0119	0.00	0.0112	-5.88
0.012	0.012	0.00	0.0112	-6.67
0.0289	0.0289	0.00	0.0293	1.38
0.0084	0.0084	0.00	0.0083	-1.19
0.0084	0.0084	0.00	0.0083	-1.19
%Absolute average error		0.03		4.10

Table 5.6 RCGA vs BCGA in finding the magnitude of the DC component, fundamental component as well as harmonics of the current signal represented by equation 5.9

Harmonics Magnitudes of I(t)	RCGA	% Error	Binary GA	% Error
0.0454	0.0454	0.00	0.0469	3.20
0.4662	0.4663	0.02	0.4692	0.64
0.0817	0.0816	-0.12	0.0821	0.49
0.0519	0.0519	0.00	0.0518	-0.19
0.0543	0.0543	0.00	0.0625	13.12
0.0305	0.0305	0.00	0.0312	2.24
0.0218	0.0218	0.00	0.0219	0.46
0.0313	0.0313	0.00	0.0312	-0.32
0.0178	0.0178	0.00	0.0176	-1.14
0.0244	0.0244	0.00	0.0312	21.79
0.0159	0.0159	0.00	0.0161	1.24
0.0196	0.0196	0.00	0.0195	-0.51
0.0157	0.0157	0.00	0.0156	-0.64
0.0168	0.0168	0.00	0.0166	-1.20
Absolute average error		0.01		3.38

5.4.2 Case study 2

Figure 5.4 below represents the HIF current and line voltage. The current signal has been built based on the HIF harmonic characteristics using Matlab. As shown from the extracted data in Section 3.4, a typical HIF contains 3rd and 5th harmonics current of certain percentages with respect to the fundamental current. The angles of the 3rd and the 5th harmonics are shifted with respect to fundamental current as shown in Section 3.7.

Based on these findings, the HIF current equation has been built and plotted and shown in Figure 5.4. The 3rd and 5th harmonics are assumed to be 10% and 5% , respectively, with respect to the fundamental current. The angle shifts of the 3rd and 5th harmonics are selected as 2.88 rad (165 degrees) and 2.76 rad (158 degrees). The magnitudes of the harmonics and angle shifts are consistent with the findings in section 3.7. In practice, the magnitudes of the harmonics depend on many factors including the surrounding environment and the intensity of the arc.

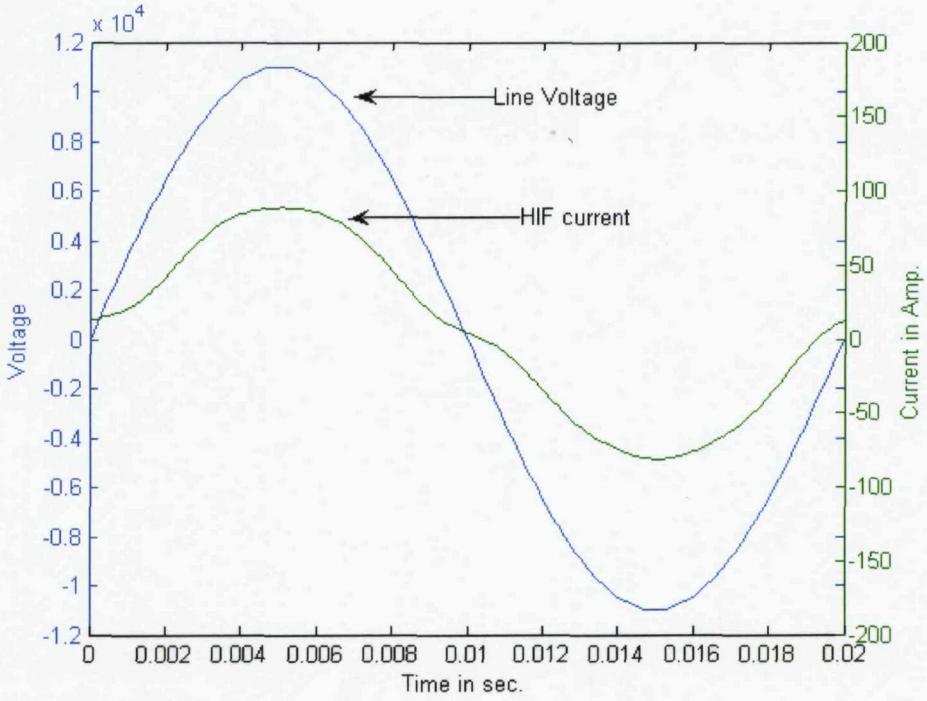

Figure 5.4 High Impedance Fault line voltage and current

$$I_{HIF} = 5 + 80\sin(\omega t) + 1\cos(2\omega t) + 8\sin(3\omega t + 2.88) + 1\cos(4\omega t) + 4\sin(5\omega t + 2.76) + 1\cos(6\omega t) + 1\sin(7\omega t + 2.62)$$

Since FF1 was found to be a better fitness function in terms of accuracy, it was used to analyse the signal in Figure 5.4 which represents a typical HIF current. The magnitudes of the signal and the phase angles are evaluated using the real coded genetic algorithm. The effect of the data window size (number of cycles) has also been studied. Table 5.7 summarizes the results of this case. The data window size is varied between 1 and 10 cycles in steps of one cycle at a sampling rate of 1000 Hz, and the corresponding number of samples is also. It is clear that the results obtained using RCGA are very accurate in estimating the magnitudes and phase angles of the HIF current. The results also show that increasing the number of cycles has little effect on the results and one cycle is enough to achieve accurate results.

Table 5.7 Estimated harmonic magnitudes for I_{HIF} using GA with different window size (cycles) and sampling rate of 1000 Hz using FF1

		DC transient	1^{st}	$\Theta 1$	2^{nd}	$\Theta 2$	3^{rd}	$\Theta 3$	4^{th}	$\Theta 4$	5^{th}	$\Theta 5$	6^{th}	$\Theta 6$	7^{th}	$\Theta 7$
	target	5	80	0	1	0	8	2.88	1	0	4	2.76	1	0	1	2.62
# of samples	window size															
21	1	5.0102	80.0086	0	1.0616	0.0004	8.012	2.8725	1.0607	0	4.0238	2.7487	0.999	0	0.9989	2.622
41	2	5.0005	79.9997	0	1.0016	0	8.0009	2.8799	0.9996	0	3.9999	2.7602	1.0001	0	1.003	2.6185
61	3	5.0003	79.9998	0	0.9996	0	7.9995	2.8798	1.0004	0	3.9992	2.7599	1.0008	0	1.0003	2.62
81	4	5.0002	79.9985	0	1.0001	0	8	2.8802	1.0006	0	4.0002	2.7598	1.0001	0	0.9996	2.6199
101	5	5.0005	80.0001	0	1.002	0	7.9982	2.88	1.0001	0	4.0001	2.7595	0.9987	0.0002	1.001	2.6204
141	7	5.0005	80.0003	0	1	0	8.0019	2.8788	0.9965	0	3.9977	2.7564	0.9976	0	1.0029	2.6221
201	10	5.0003	80.0004	0	0.9993	0	8.0008	2.8801	0.9996	0	4.0001	2.7599	1.0007	0	0.9999	2.6215

In the second case study, one window (one cycle) is used with different sampling rates. Sampling rates started from 1000 Hz and ended-up at 10000 Hz in steps of 1000 Hz. Extensive computation has confirmed that the window size of 1 (1 cycle) gives is sufficient with FF1. A sample of the results is given in Table 5.8 (window size =1 cycle only). It appears that FF1 gives accurate results using the first chosen sample range (1000 Hz) with no effect when increasing the sample rate (except increasing the time of calculation). Results from Tables 5.7 and 5.8 provide high levels of confidence that the use of RCGA to estimate the harmonic magnitude and phase angle associated with high impedance fault signal will result in accurate solutions.

Table 5.8 Estimated harmonic magnitudes for IHIF using GA with one window size (1 cycle) and different sampling rate using FF1

		DC transient	1st	Θ1	2nd	Θ2	3rd	Θ3	4th	Θ4	5th	Θ5	6th	Θ6	7th	Θ7
	target	5	80	0	1	0	8	2.88	1	0	4	2.76	1	0	1	2.62
# of samples	sample rate															
21	1000	5.0102	80.0086	0	1.0616	0.0004	8.012	2.8725	1.0607	0	4.0238	2.7487	0.999	0	0.9989	2.62
41	2000	4.9989	79.9997	0	1.0017	0	8	2.8799	1.0002	0	4.0004	2.76	1.0001	0	0.9998	2.622
61	3000	5.0019	79.9997	0	1.0006	0	8.002	2.8801	1.0005	0	3.9997	2.7601	1.0009	0	1.004	2.6198
81	4000	4.9999	79.9991	0	1.0001	0	8.0005	2.8802	1.0011	0	3.9986	2.76	1.0001	0	0.9993	2.6202
101	5000	5.0001	80.0006	0	1	0	8.0005	2.88	0.9996	0	3.9992	2.7602	1.0002	0	1.0001	2.6207
141	7000	4.9999	79.9986	0	1.0013	0	7.9987	2.8802	0.9988	0	4.0026	2.7605	1.0012	0	1.004	2.6216
201	10000	4.9995	79.9994	0	0.9993	0	8.0027	2.8798	0.9997	0	4.0004	2.76	1.0004	0	1.0018	2.6199

5.5 Conclusion

A new method for on-line tracking of power system harmonics was proposed. A Real Coded Genetic Algorithm (RCGA) has been used to solve this formulated optimization problem. This method, based on RCGA, was successfully tested using different fitness functions. The effect of window size and different sampling frequencies of the voltage and current waveform were studied. The very accurate results obtained show that the proposed method can be used as a reliable on line harmonic estimator especially for signals with time varying magnitudes.

Chapter 6

Real Coded Genetic Algorithm compared to the classical method of Fast Fourier Transform in harmonic analysis

Harmonics in voltages and currents come from various equipment used in homes, industrial facilities and offices. Any device with non-linear characteristics may be injecting harmful harmonic currents and voltages into the electrical system. Power quality has become a factor in our lives and harmonics may degrade the quality of supply. In order to design harmonic filters to maintain power quality, the evaluation of waveform distortion is needed to provide an accurate measure of power system harmonics and exact characteristics of the voltage and current waveforms. This chapter presents an enhanced analysis scheme for identification and tracking of harmonics in power systems. The proposed technique is not limited to stationary waveforms, but can also estimate harmonics in waveforms with time-varying amplitudes. The results obtained from the proposed Real Coded Genetic Algorithm (RCGA) are compared with the results obtained using the classical Fast Fourier Transform technique. The algorithm has been tested using simulated data and the effects of sampling rate have been studied. Results are reported and discussed.

6.1 Introduction

The difficulty in tracking and measuring harmonics arises due to the fact that harmonic generating sources are dynamic in nature. As power semiconductors are switched on and off at different points on each cycle, damped transients are generated. When a fault happens on a transmission line, radical changes occur in the current and voltage waveforms. The magnitudes and phases of the fundamental frequency current and voltage signals are badly corrupted by noise, in the form of a DC offset as well as frequencies above fundamental frequency [20].

The classical Fourier transform is the mechanism by which we decompose the signal to find its harmonic content. We use the Fast Fourier Transform (FFT) to obtain voltage and current frequency spectra from discrete time samples. However, misapplication of the FFT algorithm may lead to incorrect results. Although the FFT algorithm has been applied successfully in power system harmonic measurements and analysis, there are several basic assumptions embodied in the application of FFT for harmonic analysis. These assumptions are [84, 94]:

- The signal is stationary (constant in magnitude) and periodic.
- The sampling frequency is greater than twice the highest frequency to be evaluated.
- The number of periods sampled needs to be an integer.
- Only integer multiples of the fundamental frequency are taken into account in the harmonic survey. Therefore, the waveform must not contain frequencies that are not integer multiples of the fundamental frequency.

In fact, the fundamental frequency is the line frequency of the power system and the frequency resolution is the reciprocal of the sampling length of time. The sampling frequency (f_s) is equal to the number of samples multiplied by the frequency resolution defined in the application. When the above mentioned assumptions are satisfied, the results

of the FFT are accurate. There are three major pitfalls in the application of FFT, namely aliasing, leakage, and the picket-fence effect [84, 94]. "Aliasing" is the phenomenon which causes high frequency components of time function translate into low frequencies if the sampling rate is too low. The term "leakage" refers to the apparent spreading of energy from one frequency into adjacent ones. For the FFT algorithm to be applied, the third assumption (the number of periods sampled needs to be an integer) must be satisfied to avoid "leakage". However, the fundamental frequencies of the current and the voltage in a power system may not be exactly their nominal values. Moreover, there is always uncertainty in determining the actual fundamental frequency. The sampling rate of data acquisition and the sampling data are usually set at fixed numbers. If the truncation interval is not an integer multiple of the period of the fundamental, the so-called "spectral leakage" will occur since the sampled sequence will not be truncated exactly at the end of a cycle [85, 95]. In this case, the FFT algorithm will lead to incorrect results. The window techniques can be applied to the sampling data for reducing the spectral "leakage" in the FFT of such a sampled waveform [95]. Finally the "picket-fence effect" occurs if the analyzed waveform includes a frequency which is not one of the discrete harmonics of the fundamental. Since the FFT is discrete, only the amplitudes of frequencies that fall exactly on these discrete points in the frequency domain are calculated exactly. Therefore, transients caused by dynamic loads can affect the accuracy of the magnitudes of each harmonic.

In this chapter the Real Coded Genetic Algorithm (RCGA), described in Chapter 4, is used for tracking harmonics on power systems and compared with the FFT.

6.2 Fourier Transform

The Fourier transform is used in many fields of science as a versatile mathematical tool to alter a problem to one that can be solved more easily. The Fourier transform decomposes a signal or a function into a sum of sines and cosines of different frequencies

which sum up to the original signal or function. The main advantage of the Fourier transform lies in its ability to transfer the signal from its time domain to the frequency domain which usually contains more information [96].

For a continuous function $f(t)$, the Fourier transform $F(f)$ is defined as:

$$F(f) = \int_{-\infty}^{\infty} f(t) * e^{-j2\pi ft} dt \qquad (6.1)$$

And the inverse transform is given as follows:

$$f(t) = \int_{-\infty}^{\infty} F(t) * e^{j2\pi ft} dt \qquad (6.2)$$

6.2.1 Discrete Fourier Transform DFT

Introducing computers and microprocessors in power numerical calculations of the Fourier transform requires discrete sample values of $f(t)$ which will be denoted $f(t_k)$.

Letting $f_k = f(t_k)$, where $k = 0, 1, 2, \ldots\ldots\ldots, N-1$, leads to the discrete Fourier transform as:

$$F_n = \sum_{k=0}^{N-1} f_k * e^{-j2\pi nk/N} \qquad (6.3)$$

The inverse transform is given as follows:

$$f_k = \frac{1}{N} \sum_{k=0}^{N-1} F_n * e^{j2\pi nk/N} \qquad (6.4)$$

The Discrete Fourier Transform (DFT) yields frequency coefficients of a signal representing the projection of an orthogonal sine and cosine basis functions. This is an adequate method of analysis if a signal is predominantly sinusoidal, periodic and stationary. As power system disturbances are subject to transient and non-periodic components, the DFT alone may fail to provide an accurate signal analysis. If a signal is altered in localized time instant, the entire frequency spectrum can be affected.

6.2.2 Fast Fourier Transform FFT

Theoretically the DFT can be applied to any series of values but, in practice, for a large series, it takes considerable time to perform the required computations, the time taken being proportional to the square of the number of points in the series. A much faster algorithm was developed around 1965 called the Fast Fourier Transform (FFT). The only restriction on the use of FFT is the number of points in the series which ideally should be a power of 2. The computation time for FFT is proportional to $N\log_2(N)$, where N is the number of points in the series [96]. The basic idea is to break up a transform of length N into two transforms of length $N/2$ using the identity of:

$$\sum_{n=0}^{N-1} a_n * e^{-j2\pi nk/N} = \sum_{n=0}^{N/2-1} a_{2n} * e^{-j2\pi(2n)k/N} + \sum_{n=0}^{N/2-1} a_{2n+1} * e^{-j2\pi(2n+1)k/N} \qquad (6.5)$$

6.3 The harmonic model

Mathematically, signals can be represented in several ways. A periodic and distorted signal can be suitably represented in terms of its DC component, fundamental frequency and harmonic components; the last two expressed as a sum of sinusoidal waveforms referred to as the Fourier series. Each harmonic component has its own amplitude and phase angle, as well as a frequency that is an integer multiple of the fundamental system frequency. Consider a voltage waveform with harmonic components, written as equation (6.6) [97]

$$V(t) = V_0 e^{-\lambda t} + \sum_{i=1}^{N} A_{ci}\cos(i\omega_0 t + \phi_{ci}) + A_{si}\sin(i\omega_0 t + \phi_{si}) \qquad (6.6)$$

where V_0 is the constant component of $V(t)$ and λ is its time constant; $A_{ci}, A_{si}, \theta_{ci}, \theta_{si}$ are the cosine and sine amplitudes and phase angles of the ith harmonics respectively; ω_0 is the fundamental frequency and N is the number of harmonics used to represents $V(t)$.

In order to obtain the waveform parameters, mathematical algorithms are employed. Assuming the signal $V(t)$ is sampled at a predefined time interval Δt, there will be a set of m samples, $v(t_1), v(t_2), \ldots v(t_m)$, obtained for $t_1, t_2, \ldots, t_m$, where t_1 is an arbitrary time reference. A system of equations can be written as shown in 6.7 were $e_{tm}, m = 1, \ldots, m$ is the estimation error at time t_m. The problem is to find the values for V_0, A_{ci}, A_{si}.

$$\begin{bmatrix} V(t_1) \\ \cdot \\ \cdot \\ \cdot \\ V(t_m) \end{bmatrix} = \begin{bmatrix} e^{\lambda t_1} + \cos(\omega_0 t_1 + \theta_{c1}) + \sin(\omega_0 t_1 + \theta_{s1}) + \ldots + \cos(N\omega_0 t_1 + \theta_{cN}) + \sin(N\omega_0 t_1 + \theta_{sN}) \\ \ldots\ldots\ldots\ldots\ldots\ldots\ldots\ldots\ldots\ldots\ldots\ldots\ldots\ldots\ldots\ldots\ldots\ldots\ldots\ldots \\ \ldots\ldots\ldots\ldots\ldots\ldots\ldots\ldots\ldots\ldots\ldots\ldots\ldots\ldots\ldots\ldots\ldots\ldots\ldots\ldots \\ e^{\lambda t_m} + \cos(\omega_0 t_m + \theta_{c1}) + \sin(\omega_0 t_m + \theta_{s1}) + \ldots + \cos(N\omega_0 t_m + \theta_{cN}) + \sin(N\omega_0 t_m + \theta_{sN}) \end{bmatrix} \begin{bmatrix} V_0 \\ A_{c1} \\ A_{s1} \\ \cdot \\ \cdot \\ A_{cN} \\ A_{sN} \end{bmatrix} + \begin{bmatrix} e(t_1) \\ e(t_2) \\ \cdot \\ \cdot \\ e(t_m) \end{bmatrix} \qquad (6.7)$$

6.4 Fitness Function

In order to apply an evolutionary algorithm to a given problem, we need a way of evaluating candidate solutions. This is done with a fitness function. A fitness function is a function that takes an input as a representation, translates this into the corresponding candidate solution, tests this candidate solution on the given problem and then returns a number that indicates how good this solution is, i.e., its fitness. A fitness function is usually constructed in such a way that a higher fitness value is assigned to better solutions. The fitness function for a given problem (whether it is a minimization or maximization problem) can always be written in the appropriate form. In this study the fitness function is set to minimize the maximum individual error. The evaluation function is the function responsible for the determination of the fitness of each individual. Its objective is to evaluate the estimation error. The coded parameters are compared to the measured value in each time step to calculate the average error. The fitness function of Section 5.3 is used in calculations.

6.5 Testing of Algorithm

The testing is undertaken using some typical signals encountered in power systems (with data taken from literature, Section 6.5.1) and also those representative of HIF waveforms (Section 6.5.3) with direct comparisons of results between the proposed new RCGA technique and the classical FFT. It is appreciated that the presence of an exponential term may make the FFT perform poorly (at least for a smaller number of sampling points) and this is discussed further in Section 6.5.2 (where comparisons of FFT performance are also made before and after the exponential term has been removed). It will be argued that the RCGA offers an advantage of not needing an exponential term filtered out before the harmonic analysis.

6.5.1 Case 1

In this case a single phase to ground fault is used as described by equations 6.8 and 6.9 and plotted in Figure 6.1 (it is a transmission line fault case presented in [97]). The fault is applied at a voltage peak. With a pre-selected sampling rate and specified window size, the actual analogue signal is converted to discrete digital samples. A/D converters are used to generate the measurement vector [*V*]. The fitness function proposed earlier (FF1) is used to evaluate the RCGA solution and compare it with the solution of the FFT. A data window size of one cycle is used with fixed sampling frequency ($\Delta t = 0.001s$). Tables 6.1 and 6.2 show the results obtained using RCGA and FFT. The results from the tables are plotted in Figures 6.2 and 6.3 in terms of accuracy (percentage error). The obtained results appear to suggest that the numbers generated by the RCGA yield a much better estimation when compared to the traditional FFT method. In Table 6.3 the sampling time of current *I(t)* has been decreased to see at what stage FFT would give a result close to RCGA. As may be seen, in order for FFT to achieve a very small percentage error to match the RCGA's accuracy, it needs many more samples per cycle than RCGA (RCGA only needs 20 samples per cycle). Finally, Figure 6.4 compares RCGA with FFT in terms of accuracy. As shown, FFT needs more processing power and more computing time to match RCGA's accuracy.

In the following tables and figures, it should be noted that the harmonics are shown separately for the *cos* and *sin* terms, in accordance with the equations 6.8 and 6.9.

$$V(t)=0.0550\exp(-0.4t)+0.9829\cos(\omega t)+0.1842\sin(\omega t)+0.0141\cos(2\omega t)+0.02454\sin(2\omega t)+0.0077\cos(3\omega t)+0.0197\sin(3\omega t)+0.0050\cos(4\omega t)+0.0168\sin(4\omega t)+0.0039\cos(5\omega t)+0.0154\sin(5\omega t)+0.0033\cos(6\omega t)+0.0161\sin(6\omega t)+0.0033\cos(7\omega t)+0.0230\sin(7\omega t) \quad (6.8)$$

$$I(t)=0.2491\exp(-0.4t)+0.9587\cos(\omega t)+0.2841\sin(\omega t)+0.0619\cos(2\omega t)+0.1054\sin(2\omega t)+0.0329\cos(3\omega t)+0.0811\sin(3\omega t)+0.0206\cos(4\omega t)+0.0643\sin(4\omega t)+0.0146\cos(5\omega t)+0.0528\sin(5\omega t)+0.0116\cos(6\omega t)+0.0448\sin(6\omega t)+0.0052\cos(7\omega t)+0.0401\sin(7\omega t) \quad (6.9)$$

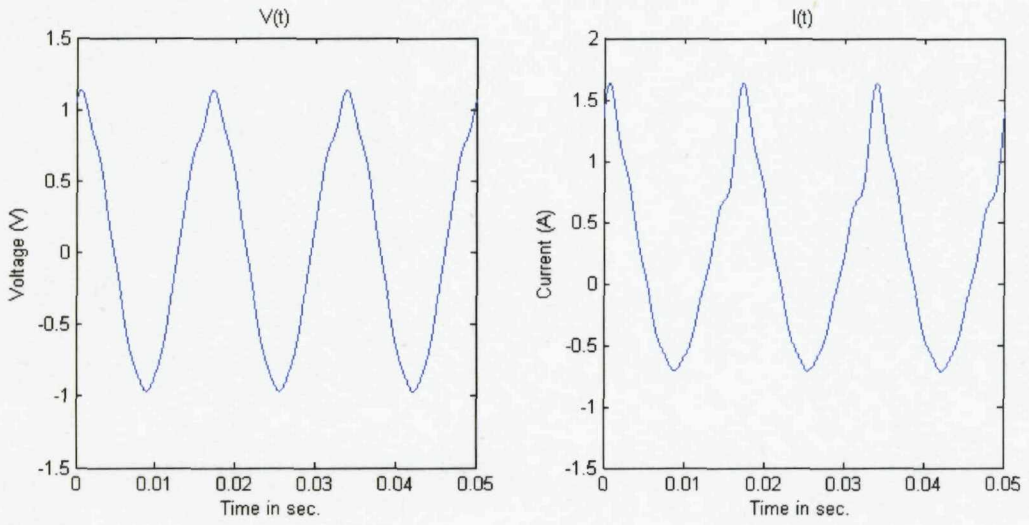

Figure 6.1 Plot of *V(t)* and *I(t)* of equations 6.8 and 6.9

Table 6.1 Estimated harmonics magnitudes for *V(t)* using GA and FFT at Δt =0.001s

		Fourier		**GA**	
Harmonic order	**Harmonics Magnitudes of *V(t)***	**Δt=0.001s**	**%Error**	**Δt=0.001s**	**%Error**
		Calculation time 0.0156s		Calculation time 1.86s	
DC	0.0550	0.1034	88.00	0.055	0
1st	0.9829	1.0231	4.09	0.9829	0
	0.1842	0.0298	-83.82	0.1842	0
2nd	0.0141	0.0128	-9.22	0.0141	0
	0.0245	0.0194	-20.82	0.0245	0
3rd	0.0077	0.0019	-75.32	0.0077	0
	0.0197	0.013	-34.01	0.0197	0
4th	0.0050	0.0039	-22.00	0.005	0
	0.0168	0.0082	-51.19	0.0168	0
5th	0.0039	0.0036	-7.69	0.0039	0
	0.0154	0.0047	-69.48	0.0154	0
6th	0.0033	0.0025	-24.24	0.0033	0
	0.0161	0.0025	-84.47	0.0161	0
7th	0.0033	0.0009	-72.73	0.0033	0
	0.0230	0.0012	-94.78	0.0230	0
	%Absolute average Error		49.46		0

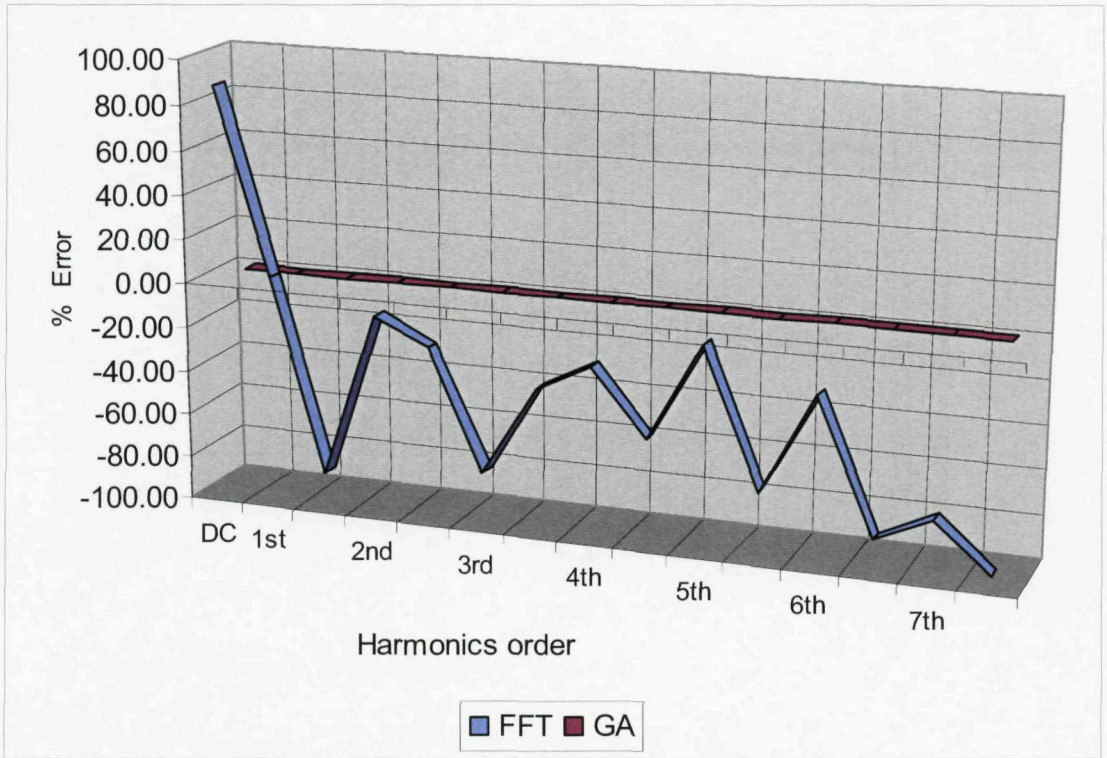

Figure 6.2 Estimated harmonics magnitudes for *V(t)* using GA and FFT

Table 6.2 Estimated harmonics magnitudes for *I(t)* using GA and FFT at Δt =0.001s

		Fourier		GA	
Harmonic order	**Harmonics Magnitudes of *I(t)***	**Δt=0.001s**	**%Error**	**Δt=0.001s**	**%Error**
		Calculation time 0.0156s		Calculation time 1.86s	
DC	0.2491	0.3007	20.71	0.2491	0
1st	0.9587	1.0265	7.07	0.9587	0
	0.2841	0.1366	-51.92	0.2841	0
2nd	0.0619	0.0659	6.46	0.0619	0
	0.1054	0.0803	-23.81	0.1055	0.095
3rd	0.0329	0.049	48.94	0.0329	0
	0.0811	0.0494	-39.09	0.0811	0
4th	0.0206	0.0327	58.74	0.0206	0
	0.0643	0.0262	-59.25	0.0643	0
5th	0.0146	0.0176	20.55	0.0146	0
	0.0528	0.0097	-81.63	0.0528	0
6th	0.0116	0.0023	-80.17	0.0116	0
	0.0448	0.0011	-97.54	0.0448	0
7th	0.0052	0.0164	215.38	0.0052	0
	0.0401	0.0048	-88.03	0.0401	0
	%Absolute average Error		59.95		0.006

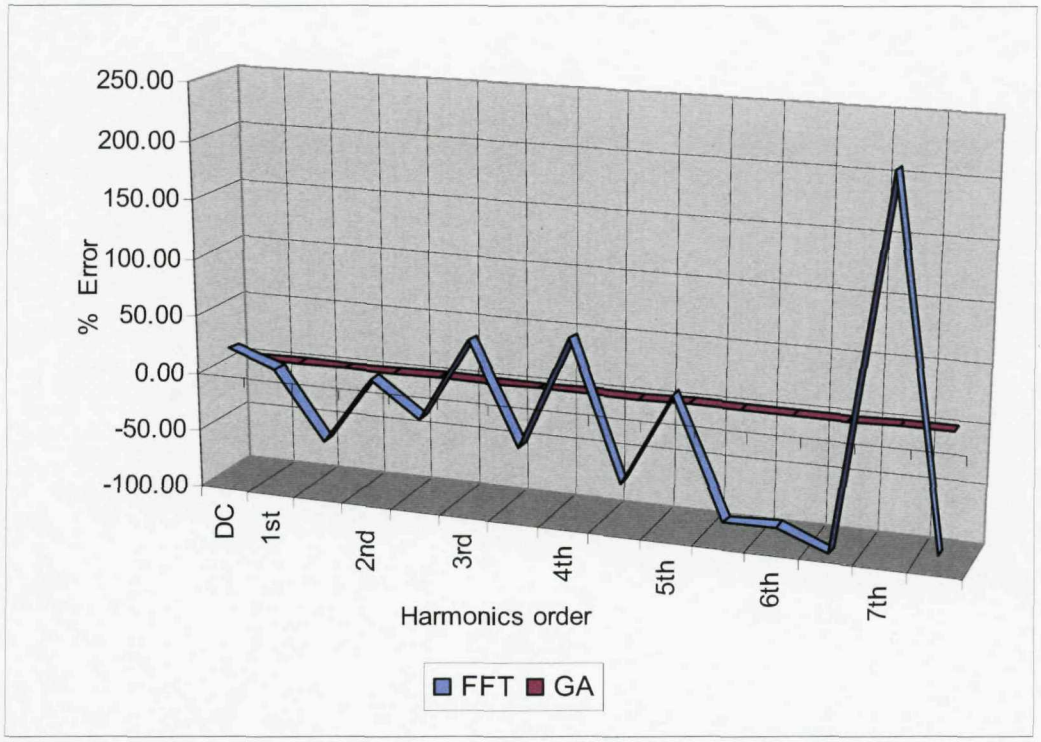

Figure 6.3 Estimated harmonics magnitudes for *I(t)* using GA and FFT

Table 6.3 RCGA and FFT yielding similar accuracy for *I(t)*

		Fourier		**GA**	
Harmonic order	**Harmonics Magnitudes of *I(t)***	**Δt=0.0000001s**	**%Error**	**Δt=0.001s**	**%Error**
		Calculation time 6.5s		Calculation time 1.86s	
DC	0.2491	0.2481	-0.40	0.2491	0
1st	0.9587	0.9587	0.00	0.9587	0
	0.2841	0.2847	0.21	0.2841	0
2nd	0.0619	0.0619	0.00	0.0619	0
	0.1054	0.1057	0.28	0.1055	0.095
3rd	0.0329	0.0329	0.00	0.0329	0
	0.0811	0.0813	0.25	0.0811	0
4th	0.0206	0.0206	0.00	0.0206	0
	0.0643	0.0645	0.31	0.0643	0
5th	0.0146	0.0146	0.00	0.0146	0
	0.0528	0.0529	0.19	0.0528	0
6th	0.0116	0.0116	0.00	0.0116	0
	0.0448	0.0449	0.22	0.0448	0
7th	0.0052	0.0052	0.00	0.0052	0
	0.0401	0.0402	0.25	0.0401	0
	%absolute average Error		0.14		0.006

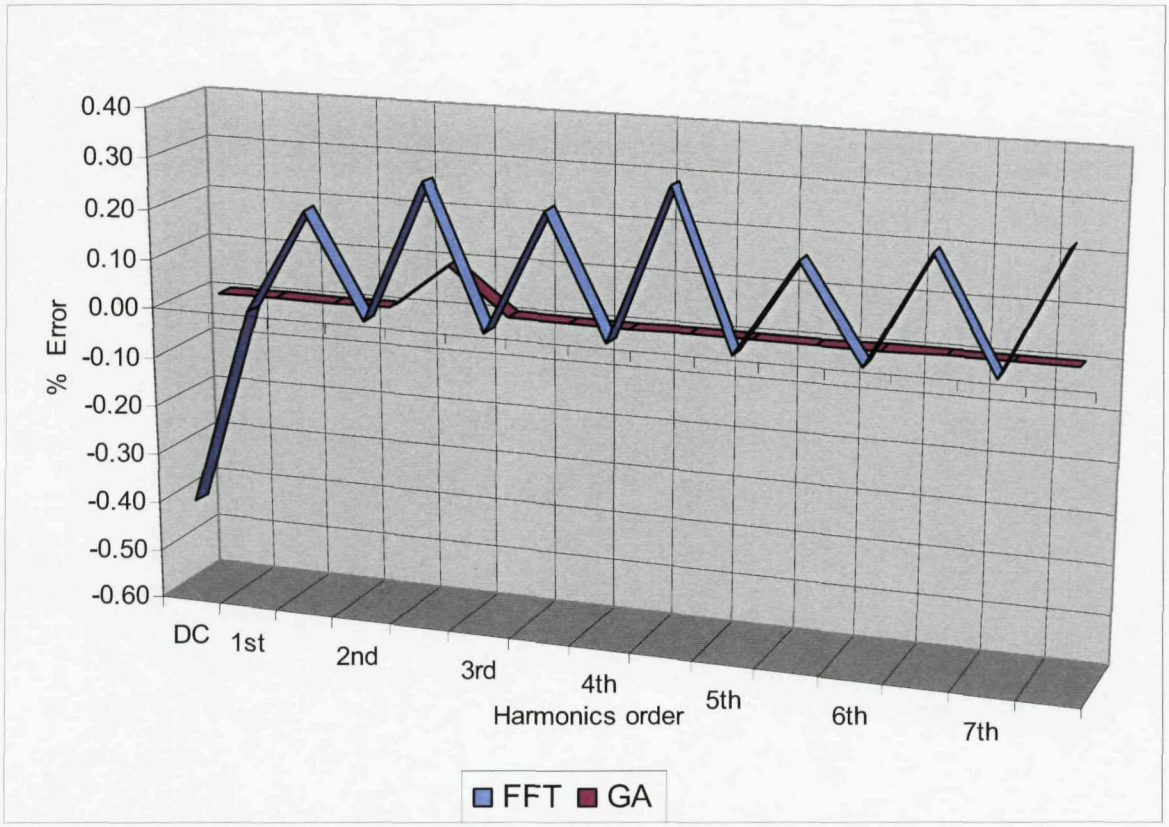

Figure 6.4 Details of errors of RCGA and FFT for Table 6.3.

In addition to other comparisons, the overall computing times (using the same processor) for the different RCGA and FFT analyses have been shown in Tables 6.1 to 6.3. As expected, for the same sampling time (e.g. Δt=0.001s in Table 6.1) the FFT is much faster (two orders of magnitude). However, the accuracy of the FFT result is very poor and thus a much smaller sampling time needs to be used for the FFT to achieve similar levels of accuracy to the RCGA, as demonstrated by Table 6.3. Then it turns out that the total computing time using FFT is actually higher (by a factor of nearly four) than the time the RCGA needs to achieve the same accuracy (at much higher sampling time). Thus the comparison of computing times needs to be made in the context of accuracy, and under the conditions of similar accuracy the RCGA performs faster.

6.5.2 The effect of the exponential term in the FFT analysis

It has been recognised (e.g. [84]) that FFT may incorrectly analyse the harmonic content if an exponential (or constant) term is present in the signal. However, in this work it has been found that the FFT may actually achieve the desired accuracy providing much shorter sampling times are used (as already observed in the previous Section 6.5.1). To investigate this further, the signals of equations 6.8 and 6.9 have been analysed again using FFT and various sampling times (shorter than those used for RCGA) as shown in Tables 6.4 and 6.5. It can be seen that by reducing the sampling time from Δt=0.001s (the value found to be sufficient for accurate performance of RCGA) the average error can now be reduced to acceptable levels (although still worse than the error of the RCGA computation with a larger sampling time). This seems to suggest that FFT could be used directly when analysing the HIF signals but the process would be much more expensive (in terms of computing times) and thus more challenging for the design of an identification system.

The alternative would be to first filter out any constant or exponential terms from the signal. This should make the task easier for the FFT as indeed demonstrated by Tables 6.6 and 6.7. However, using the same sampling times as for the RCGA, even with no DC signal, the accuracy is still poor and it is only after a significant increase of the number of sampling points that the error becomes appreciably smaller (when comparing with similar results using a signal containing an exponential terms). Thus the benefit of applying filtering before using FFT is not necessarily as strong as might have been expected. Moreover, filtering would add to the cost and complexity of the identification circuitry, not to mention the fact that normally at least a few cycles would be required to accurately remove the non-periodic component.

Overall, it can be argued that although an individual FFT analysis of a given signal may be much faster than the equivalent RCGA computation (in the example of Section 6.5.1

by a factor of 100), the overall computing times to achieve the same average accuracy favour the RCGA computation (unless a lower lever of accuracy is accepted, in which case the FFT will perform faster). Moreover, RCGA does not require filtering (to remove the non-harmonic components) and performs well even when relatively large sampling times are used.

It is therefore concluded that the RCGA offers a good alternative to the classical FFT as a tool for analysing current and voltage waveforms in power systems and, in the case of signals typical to high impedance faults, appears to be a better choice as it copes well with signals containing non-harmonic terms and does not require filtering.

Table 6.4 Estimated harmonics magnitudes for *V(t)* using FFT with different sampling times

Harmonic order	**Magnitude of harmonics for *V(t)***	**Fourier Δt=0.001s**	**%Error**	**Fourier Δt=0.0001s**	**%Error**	**Fourier Δt=0.00001s**	**%Error**
		Calculation time 0.0156s		Calculation time 0.0313s		Calculation time 0.0469s	
DC	0.055	0.1034	88.00	0.06	9.09	0.0553	0.55
1st	0.9829	1.0231	4.09	0.989	0.62	0.9835	0.06
	0.1842	0.0298	-83.82	0.16	-13.14	0.182	-1.19
2nd	0.0141	0.0128	-9.22	0.0119	-15.60	0.0139	-1.42
	0.0245	0.0194	-20.82	0.023	-6.12	0.024	-2.04
3rd	0.0077	0.0019	-75.32	0.0087	12.99	0.0079	2.60
	0.0197	0.013	-34.01	0.018	-8.63	0.0194	-1.52
4th	0.005	0.0039	-22.00	0.006	20.00	0.0051	2.00
	0.0168	0.0082	-51.19	0.0157	-6.55	0.0166	-1.19
5th	0.0039	0.0036	-7.69	0.0047	20.51	0.0041	5.13
	0.0154	0.0047	-69.48	0.0143	-7.14	0.0153	-0.65
6th	0.0033	0.0025	-24.24	0.0044	33.33	0.0035	6.06
	0.0161	0.0025	-84.47	0.015	-6.83	0.0159	-1.24
7th	0.0033	0.0009	-72.73	0.0056	69.70	0.0035	6.06
	0.023	0.0012	-94.78	0.02	-13.04	0.0225	-2.17
	%Absolute average error		**49.46**		**16.22**		**2.26**

Table 6.5 Estimated harmonics magnitudes for *I(t)* using FFT with different sampling time

Harmonic order	Magnitude of harmonics for *I(t)*	Fourier Δt=0.001s	%Error	Fourier Δt=0.0001s	%Error	Fourier Δt=0.00001s	%Error
		Calculation time 0.0156s		Calculation time 0.0313s		Calculation time 0.0469s	
DC	0.2491	0.3007	20.71	0.26	4.38	0.2487	-0.16
1st	0.9587	1.0265	7.07	0.9671	0.88	0.9596	0.09
	0.2841	0.1366	-51.92	0.25	-12.00	0.273	-3.91
2nd	0.0619	0.0659	6.46	0.064	3.39	0.06	-3.07
	0.1054	0.0803	-23.81	0.102	-3.23	0.1055	0.09
3rd	0.0329	0.049	48.94	0.037	12.46	0.0342	3.95
	0.0811	0.0494	-39.09	0.072	-11.22	0.081	-0.12
4th	0.0206	0.0327	58.74	0.025	21.36	0.022	6.80
	0.0643	0.0262	-59.25	0.057	-11.35	0.064	-0.47
5th	0.0146	0.0176	20.55	0.018	23.29	0.0155	6.16
	0.0528	0.0097	-81.63	0.045	-14.77	0.0526	-0.38
6th	0.0116	0.0023	-80.17	0.0147	26.72	0.012	3.45
	0.0448	0.0011	-97.54	0.04	-10.71	0.0445	-0.67
7th	0.0052	0.0164	215.38	0.0084	61.54	0.0055	5.77
	0.0401	0.0048	-88.03	0.032	-20.20	0.039	-2.74
	% Absolute average error		**59.95**		**15.83**		**2.52**

Table 6.6 Estimated harmonics magnitudes for *V(t)* with no exponential function using FFT with different sampling time

Harmonic order	Harmonics magnitude of *V(t)*	Fourier Δt=0.001s	%Error	Fourier Δt=0.0001s	%Error	Fourier Δt=0.00001s	%Error
		Calculation time 0.0156s		Calculation time 0.0313s		Calculation time 0.0469s	
DC	**No DC**	**No DC**		**No DC**		**No DC**	
1st	0.9829	1.0231	4.09	0.9875	0.47	0.9835	0.06
	0.1842	0.0297	-83.88	0.1687	-8.41	0.1826	-0.87
2nd	0.0141	0.0128	-9.22	0.0148	4.96	0.0139	-1.42
	0.0245	0.0194	-20.82	0.0241	-1.63	0.0244	-0.41
3rd	0.0077	0.0019	-75.32	0.0075	-2.60	0.0077	0.00
	0.0197	0.013	-34.01	0.0193	-2.03	0.0196	-0.51
4th	0.005	0.0039	-22.00	0.0052	4.00	0.005	0.00
	0.0168	0.0082	-51.19	0.0164	-2.38	0.0167	-0.60
5th	0.0039	0.0036	-7.69	0.0045	15.38	0.004	2.56
	0.0154	0.0047	-69.48	0.015	-2.60	0.0153	-0.65
6th	0.0033	0.0025	-24.24	0.0044	33.33	0.0034	3.03
	0.0161	0.0025	-84.47	0.0156	-3.11	0.016	-0.62
7th	0.0033	0.0009	-72.73	0.0052	57.58	0.0035	6.06
	0.023	0.0012	-94.78	0.0224	-2.61	0.0228	-0.87
	% Absolute average error		**46.71**		**10.08**		**1.26**

Table 6.7 Estimated harmonics magnitudes for *I(t)* with no exponential function using FFT with *different sampling time*

Harmonic order	Harmonics magnitude of *I(t)*	Fourier Δt=0.001s	%Error	Fourier Δt=0.0001s	%Error	Fourier Δt=0.00001s	%Error
		Calculation time 0.0156s		Calculation time 0.0313s		Calculation time 0.0469s	
DC	**No DC**	**No DC**		**No DC**		**No DC**	
1st	0.9587	1.0265	7.07	0.9671	0.88	0.9596	0.09
	0.2841	0.137	-51.78	0.2697	-5.07	0.2827	-0.49
2nd	0.0619	0.065	5.01	0.0633	2.26	0.062	0.16
	0.1054	0.081	-23.15	0.1032	-2.09	0.1052	-0.19
3rd	0.0329	0.049	48.94	0.0359	9.12	0.0332	0.91
	0.0811	0.05	-38.35	0.079	-2.59	0.0809	-0.25
4th	0.0206	0.0327	58.74	0.0239	16.02	0.0209	1.46
	0.0643	0.0262	-59.25	0.0619	-3.73	0.0641	-0.31
5th	0.0146	0.0176	20.55	0.015	2.74	0.015	2.74
	0.0528	0.0097	-81.63	0.0498	-5.68	0.0525	-0.57
6th	0.0116	0.0023	-80.17	0.014	20.69	0.0119	2.59
	0.0448	0.0011	-97.54	0.041	-8.48	0.0444	-0.89
7th	0.0052	0.0164	215.38	0.008	53.85	0.0055	5.77
	0.0401	0.0048	-88.03	0.0353	-11.97	0.0396	-1.25
	% Absolute average error		**62.54**		**10.37**		**1.26**

6.5.3 Case 2

In case 1 only the magnitudes of the harmonics were estimated using FFT and GA. In case 2 both the magnitudes of the harmonics and the phase angles are analysed and compared. This time a signal representative of a HIF has been used with the fault current I_{HIF} described in Figure 5.4. The results obtained using the window sizes of one cycle with different sampling times are displayed in Table 6.8, which clearly shows that GA has performed much better than FFT in estimating the magnitude of the harmonics and the phase angle of each harmonic. In order for FFT to get a good result, many more samples per cycle would be needed. As in Case 1, although an individual FFT calculation is much faster compared to RCGA (using the same sampling times), in order to achieve the same level of accuracy the FFT needs much shorter sampling times leading to overall longer computing times.

Table 6.8 RCGA and FFT in terms of Δt and accuracy for I_{HIF} magnitude and phase angle

		GA		FFT		FFT
	Harmonics Magnitudes of IHIF	**Δt =0.001**		**Δt =0.001**		**Δt =0.0000001**
		Calculation time 1.15s		Calculation time 0.0156s		Calculation time 1.97s
DC transient	5	5.0009		5.336		5
1st	80	80.0013		76.4214		79.9999
Θ1	0	0		0.1591		0.0373
2nd	1	1.0003		0.1997		1
Θ2	0	0		1.6007		0.0002
3rd	8	7.9988		10.6703		7.728
Θ3	2.88	2.88		3.3565		2.88
4th	1	0.9993		0.2101		1
Θ4	0	0		1.4524		0.0001
5th	4	4.001		4.104		3.7124
Θ5	2.76	2.7601		3.5822		2.76
6th	1	0.9989		0.381		1
Θ6	0	0		0.6814		0.0001
7th	1	0.9999		0.3815		0.8671
Θ7	2.62	2.62		4.315		2.62

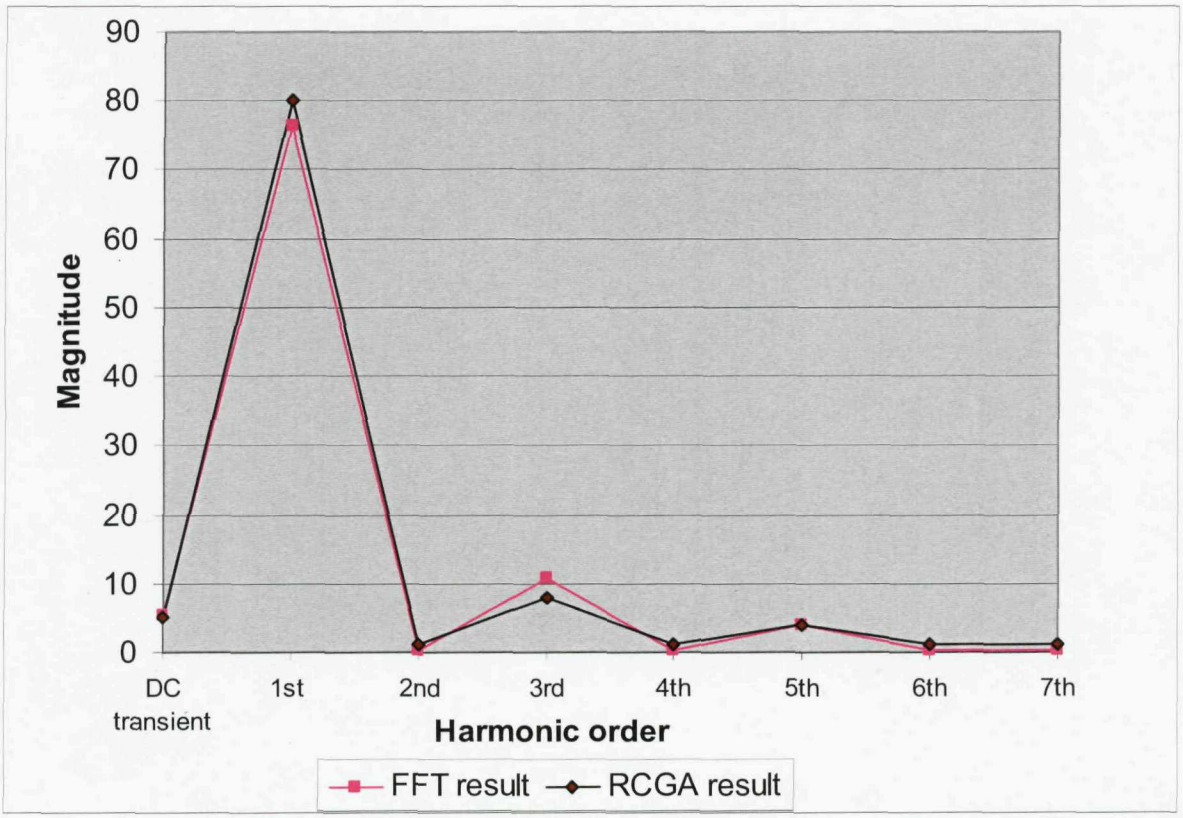

Figure 6.5 Signal magnitudes using RCGA and FFT for Table 6.8

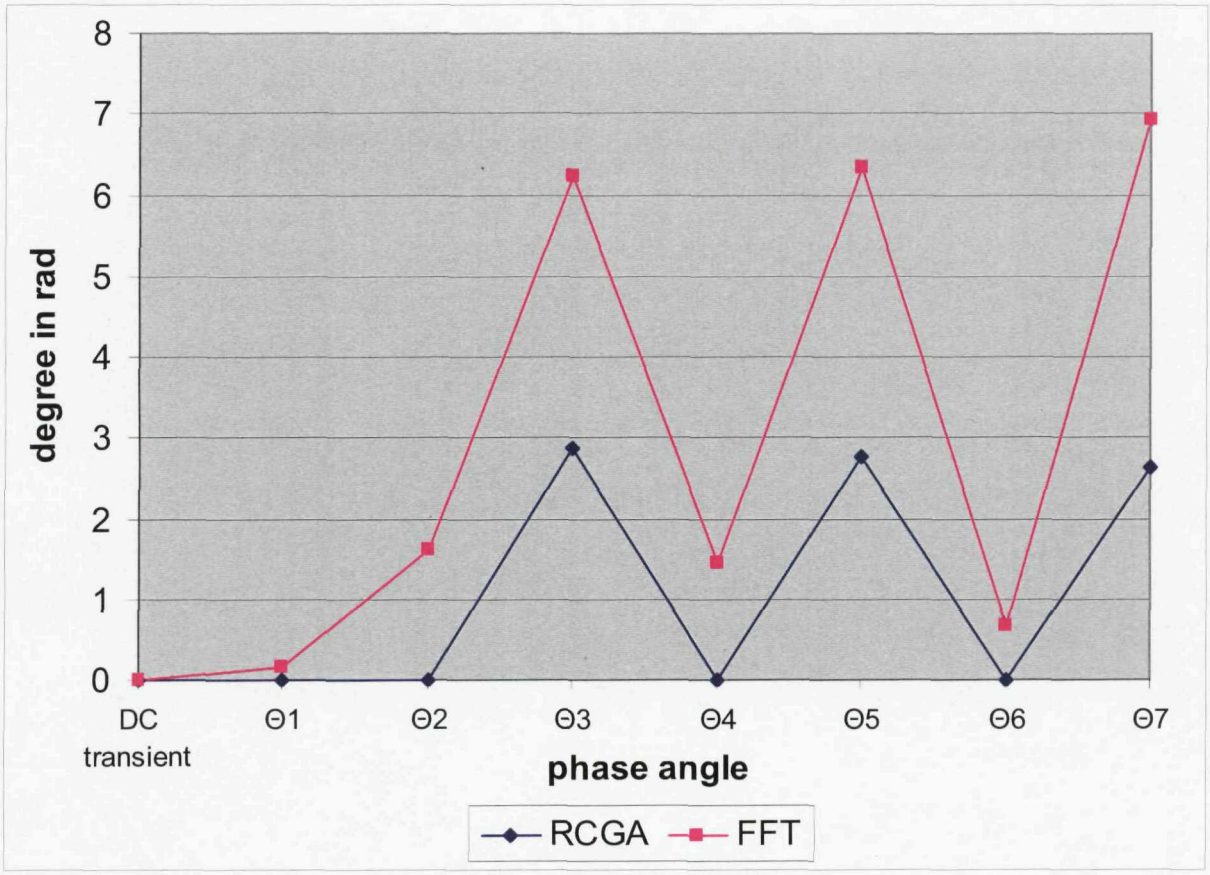

Figure 6.6 Estimation of phase angles using RCGA and FFT for Table 6.8

Figures 6.5 and 6.6 have been plotted based on the results in Table 6.8. It is clear that RCGA performs better in estimating the magnitudes and the angles of the signal.

6.7 Conclusion

It has been shown that the new algorithm based on RCGA performs well, in comparison with the classical FFT, for identification of harmonics in signals typically encountered in power systems and in particular in waveforms representative of High Impedance Faults. If there is no DC offset or exponential term, then the FFT is overall very efficient (at least in terms of the total computing times, though still requires more sampling points than the RCGA) and the RCGA may not offer significant advantages (except for the fact that it needs fewer sampling points for the same accuracy). On the other hand, in

practical situations the exponential term or a DC offset are likely to be present (which is certainly the case for HIFs) and then the RCGA works better. To make the FFT work effectively either the DC component has to be filtered out (which may require some cycles of the waveform to be done accurately) or a large number of sampling points needs to be introduced; in either case the RCGA - which does not require filtering and works well with a small number of sampling points irrespective of the presence or absence of the DC term - appears to offer a better alternative. It has also been demonstrated that both the magnitude and the phase angle of the relevant harmonics are estimated very accurately and thus the RCGA may be argued to be particularly appropriate in the context of HIF identification.

Chapter 7

Arcing High Impedance Fault detection using Real Coded Genetic Algorithm

Faults on primary distribution feeders can be divided into two major classes, namely Low Impedance Faults (LIFs) and High Impedance Faults (HIFs). While it is easy to detect and clear LIFs by conventional protection devices, such as reclosers, fuses, overcurrent relays and circuit breakers, it is difficult to detect HIFs using such devices. This is due to the fact that currents passing through HIFs normally fall within the unprotected region of conventional overcurrent protection schemes (Figure 7.1). High Impedance Faults on electric power distribution feeders are of great concern to electric power utilities. HIFs often exhibit arcing and flashing at the point of contact. They are also characterized by the presence of high frequency components. Power companies have long searched for means to reliably detect and clear HIFs on distribution feeders. While some progress has been made, a definitive solution to the problem remains to be found. The improvement of HIF detection is not only a technical issue but involves several complex operational, legal, and economic aspects as well [15]. The legal issues arise when a downed undetected conductor results in electrocution accidents or property damage which may leads the injured parties to sue the utility; the economic issue might be indirect such as reducing the liability.

This chapter presents a new method for detecting High Impedance Faults in distribution systems using Real Coded Genetic algorithm (RCGA) to analyse the harmonics and phase angles of the fault current signals. The method is used to discriminate HIFs by identifying specific events that happen when a HIF occurs.

7.1 Introduction

To date, no technique has been found that could detect all HIFs and achieve a high degree of security or dependability for distinguishing them from HIF-like events, such as load or capacitor switching. This is practically impossible because of the probabilistic nature of HIF detection [98]. Unlike conventional protection, which works with predefined decisions based on measured parameters, one cannot tell that a fault is present with complete confidence when HIF detectors are used. Furthermore, the operator will not be able to tell whether the detected fault is really hazardous to the public or not [9]. Some HIFs may be detected by conventional overcurrent protection but the threshold of overcurrent relays must be set at a relatively high current level to prevent tripping by inrush currents thereby causing unnecessary service interruption. Most detection schemes involve the adjustment of the existing overcurrent protection to be more sensitive by lowering its setting. Such schemes have failed to operate in 32% of high impedance faults and led to several unexpected service interruptions [1]. However, most HIFs need special techniques to detect and distinguish them from other normal system events.

As mentioned earlier, the primary motivator for HIF detection is to ensure safety to public and properties, and to avoid legal implications. In the absence of practical and reliable HIF detectors, some HIFs may remain undetected until they are discovered while doing some preventive maintenance or reported by the public when they notice a downed conductor or experience a disconnection of power supply.

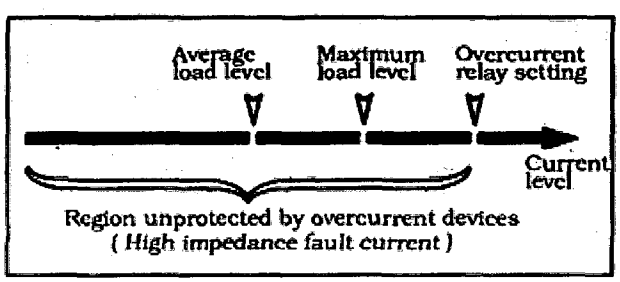

Figure 7.1 Relation of high impedance fault current to overcurrent device settings

In the past two decades many techniques have been proposed to improve the detection of HIFs in power distribution systems and they have been reviewed in Chapter 2.6.

Recently the utilities have intensified research programs searching for more efficient protection against this type of a fault. As utilities start to apply HIF detectors to their overhead distribution feeders, a number of issues have to be considered: control action (trip vs alarm), economics and legal liability. The most difficult decision to be made after HIF detectors are installed is what action should be taken after a HIF is detected. This is because HIFs rarely result in damage to electric system secondary equipment [98] and they typically do not exhibit any hazard to the distribution system stability or integrity as the amount of current that flows in HIFs is small when compared to normal load current. Each utility may have different strategy on whether to trip or only initiate an alarm when a HIF is detected based on thorough evaluation of all possible consequences. If a feeder is not tripped or patrolled for downed conductor events, consequences may include personal injury, legal liability and property damage. On the other hand, when a feeder is unnecessarily tripped, it may result in traffic accidents, thefts, medical emergencies and customer inconvenience. One possible strategy for HIF detection is presented in Table 7.1 [4, 5, 9] . For example, according to the table an alarm should be initiated when there is a load loss with no overcurrent or arcing. But the feeder should be tripped if there is arcing and overcurrent event when there is no load loss. On the other hand, utilities also have to evaluate the advantages of installing HIF detectors against the cost of the installation. The only economic advantage of HIF detection is the reduced legal liability. This may not be enough justification for some utilities to install HIF detectors. What makes this decision really complicated are the unknown consequences on public safety from downed conductors. The cost impact for installing HIF detectors can be reduced if the detectors are integrated with distribution automation or load management systems [15].

Table 7.1 Down conductor and fault detector scheme logic

Arcing	Load loss	Overcurrent	Decision
N	N	N	Normal
N	N	Y	Overcurrent*
N	Y	N	Alarm
N	Y	Y	Alarm,overcurrent*
Y	N	N	Alarm- arcing
Y	N	Y	Trip- down wire
Y	Y	N	Trip- down wire
Y	Y	Y	Trip- down wire

*Trip by conventional protection

HIFs have been studied since the early 1970s to find such characteristics in the current and voltage waveforms which would make HIF detection possible and practical [5]. Most of the research has focused on developing more sensitive detectors [9]. The main difficulty associated with this approach is to maintain the delicate balance between the sensitivity of the detector (overcurrent protection) and the selectivity of the protection scheme. In other words, if the overcurrent relays are set to pick-up for small changes in current, such as HIF currents, there will be many unwanted trippings due to normal system operations, like load switching. Many HIF detection techniques have been developed by researchers including waveform detectors which are the cheapest to install [12] and they are based on the analysis of the voltage and current waveforms. They have been developed over the last two decades and one such detector is presently being manufactured by General Electric (GE) [98].

Though some detection techniques have shown a good capability of detecting HIFs, the challenge is to make these techniques insensitive to other disturbances similar to HIFs. This chapter describes a novel digital technique suitable for detecting high impedance faults. A Real Coded Genetic Algorithm (RCGA) has been employed to analyse the harmonics and phase angles of high impedance fault current signals. The method is used to discriminate HIFs based on specific events that happen during the occurrence of a HIF.

7.2 Arc current characteristics

An arc is defined as a luminous electrical discharge flowing through a gas between two electrodes. In the case of an arcing HIF, when an energized conductor touches the ground, the electric contact is not solid. Due to the existence of air between the ground and the conductor, the high potential difference across a short distance excites the appearance of an arc.

Many authors have worked on the theory and dynamics of voltages and currents in an electric arc, most such studies are experimentally based. In [66] and later in [67] a model explaining the phenomenon using a spark gap was proposed. This air gap will not conduct till the applied voltage reaches the breakdown point. Then the current flows and reaches a maximum when the applied voltage equals the arc voltage. After that, the arc current decreases and becomes zero, i.e. the arc is extinguished. When extinction occurs, the arc requires a potential, known as restrike voltage, to reignite. This reignition will have the opposite polarity. This explains the typical voltage-current waveform of an arc shown in Figure 5.3 Many electric models have been proposed describing arc behavior as reviewed by [68].

In the context of downed conductors, Russell [99] conducted staged HIF tests studying dependencies of arc current magnitude on potential difference, gap distance, features of the grounding surface and environmental conditions of the grounding point. A high degree of random behaviour was observed due to impurities (wet soil, dry soil or sandy soil) near the grounding point, heat from the arc that is intense enough to fuse substances and the evolution of different paths for current flow on surfaces.

In this chapter, a more dynamic and random HIF model is applied. It combines most of the advantages of the previous models proposed while remaining simple and universal; it was first put forward by the authors in [100] and it was presented in this thesis in Chapter 3.

7.3 Field visit

This research was initially encouraged by the Ministry of Electricity and Water in Kuwait due to the ongoing problems with high impedance fault due to the very dry environment. Most of the primary distribution circuits in the rural areas in Kuwait consist of overhead lines. For instance, all primary distribution circuits in the rural areas in the system of the Ministry of Electricity and Water (MEW) are 11kV (wooden poles) overhead lines. A survey conducted by the Electric Power Research Institute (EPRI) on primary distribution feeders (35 kV and below) found that around 95 % of all faults occurred on overhead lines [101], thus their protection is of particular importance.

According to the engineers at MEW, high impedance faults are a long lasting and existing problem on the electrical system in the rural areas due to the very dry environment and there are no statistics on the number of high impedance fault cases. The most common HIF cases investigated by this research in Kuwait were due to a distribution line falling on very dry sand because of the very dry environment or by the growing trees that the line runs adjacent to. In general one of the major causes of power outages are trees. Specially on distribution systems the outages related to trees account for 20% to 50% of all unplanned outages [102]. For example, the US black out in 2003 was generated by many events and one of them was a tripped line due to a tree flashover [1]. Utilities in North America spend an estimated of $2 to $10 billion to manage the vegetation around the transmission lines to prevent service disruptions and safety hazards associated with trees touching conductors [102].

During the course of this research many visits have been made to several locations in Kuwait where high impedance faults occurred. Some of the cases were photographed with the assistance of MEW staff (see Figure 7.2).

In one particular overhead line, as seen in Figure 7.3, a fatal accident had happened where the line was on the ground and energized. Even though the line was on the ground for

some time, the relay in the substation did not trip and two teenagers passing by were tampering with the line which resulted in their electrocution. One was instantly killed and the other was badly hurt and severely burned. This specific overhead line has a history of many accidents because it runs alongside a populated area.

A

B

C

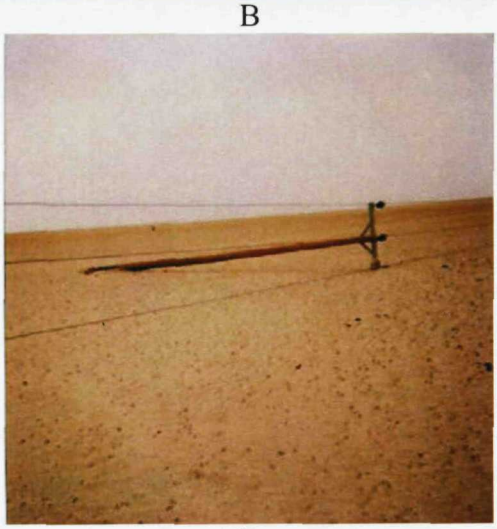

D

E

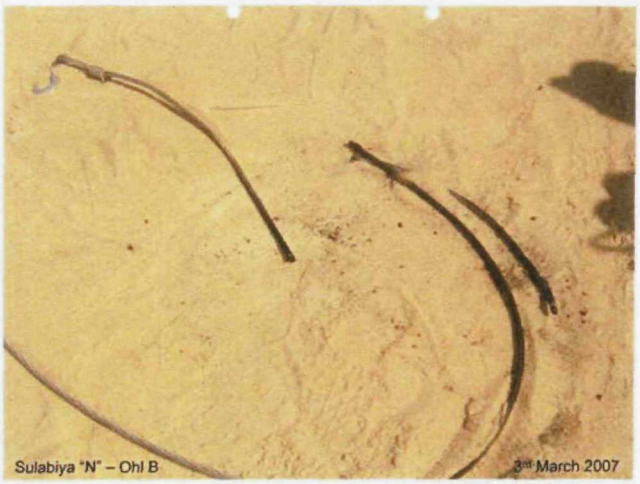

F

G

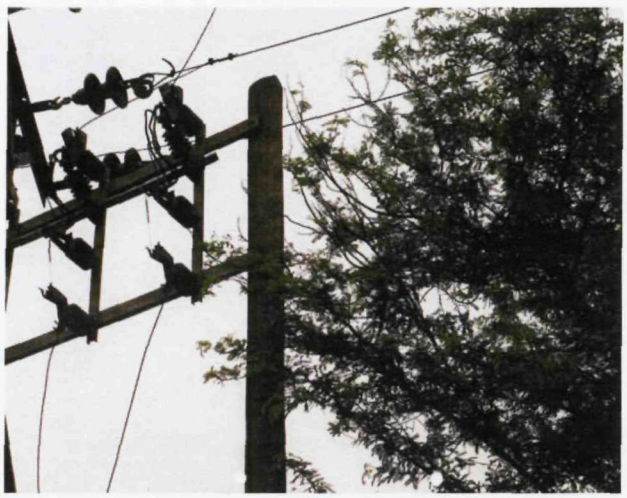

H

Figure 7.2 High Impedance Fault cases in Kuwait
A, B, C, E, H- 11kV overhead line touching trees
D, G – Fallen energized overhead line
F – Black spots in the sand around the line due to arcing

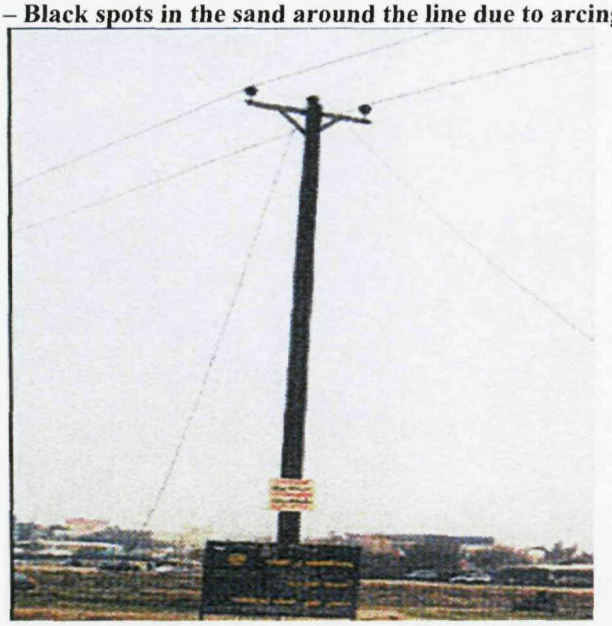

Figure 7.3 The fatal High Impedance Fault case

7.4 Testing the algorithm

In this test a practical power system case that represents a section of the overhead line circuit in Figure 7.3 was simulated to demonstrate the ability of the Real Coded Genetic Algorithm to track harmonics during normal and abnormal conditions in a power system. The section of this overhead line was chosen where the fatal accident, mentioned before, had happened. The system was simulated using Simulink and Sim Power Systems block set. The simulated system is shown in Figure 7.4. A three-phase, 50 Hz, 11kV power system transmits power from a substation to an equivalent network through a 2.5 km transmission line. The voltage source is simulated with a Simplified Sim Power Systems three phase voltage source block. Universal transformer blocks are used to model the transformers. The transmission line is modelled in sections, as shown in Figure 7.4, from Section 1 to Section 5, where it is split in four places along the lines connected between buses. A three-phase resistive load is located at each end of the section through a 1000 kVA 11/0.433 kV transformer, while load 1= 100kW, load 2= 750 kW, load 3= 750 kW and load 4= 500kW .The load may be varied to simulate either balanced or unbalanced loading conditions but for this case all loads are distributed evenly across the three phases (an idealised and balanced load) no harmonics are assumed to be present. Voltages and currents are measured in block B1. In order to verify the proposed algorithm and assess its transient performance, a high impedance fault was applied to the system at many locations on the line, although only one location is shown in Figure 7.4. The HIF box shown contains the HIF model already presented in Chapter 3. Other locations are shown in an Appendix 5.

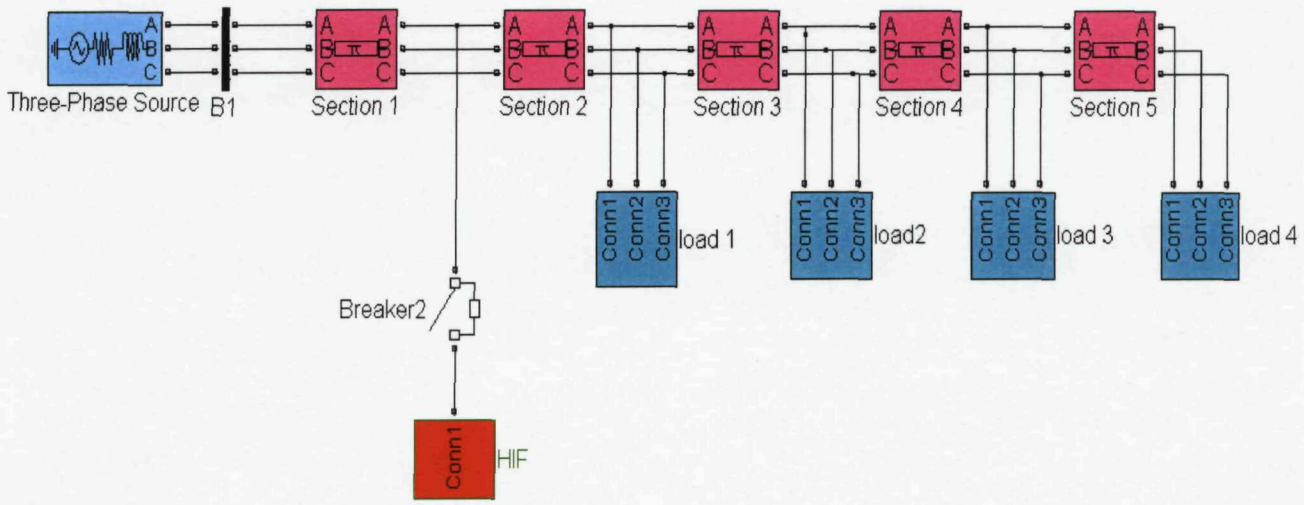

Figure 7.4 System of study

7.5 Detection criteria

To achieve the objective of this chapter a Real Coded Genetic Algorithm was used to analyze the harmonics of the current waveform. The methods presented in Chapter 5 and 6 have been used to analyze the current signal generated by a HIF. The fitness function used in this case had been represented in [103-105] and was referred to in Chapter 5 as FF1.

Figure 7.5 shows the relationship between the percentage of the 3rd harmonic fault current and the total fault current. The data used to plot Figure 7.5 was collected from several simulated HIF cases using the HIF model presented in Chapter 3. The result agrees with the HIF 3rd harmonic prediction by [64] and also matches the 3rd harmonic HIF testing curve in [106]. Figure 7.5 shows that the percentage value of the 3rd harmonic current increases rapidly below the fault current of about 100A and the higher the fault current the smaller the percentage of the 3rd harmonic. Based on this observation, a detection criterion has been put forward in [106] for the 3rd harmonics by stipulating that if the value for a given fault current exceeds the red line, then this will indicate the occurrence of a HIF. For example, according to the graph in Figure 7.5, a HIF current of a 100A should have a 3rd harmonic of about 5% or more while a HIF current of 50A should have a 3rd harmonic of

about 10% or more; these values may then be used as a threshold for a HIF detection. The 3rd harmonic threshold criterion is simple but not reliable [17]. Tests have demonstrated that an incorrect identification may easily occur, especially if the actual harmonic value is close to the threshold (on either side of the curve). Moreover, the 3rd harmonic may have been produced by an event not related to HIF and the criterion is not capable of discriminating between different sources of harmonics.

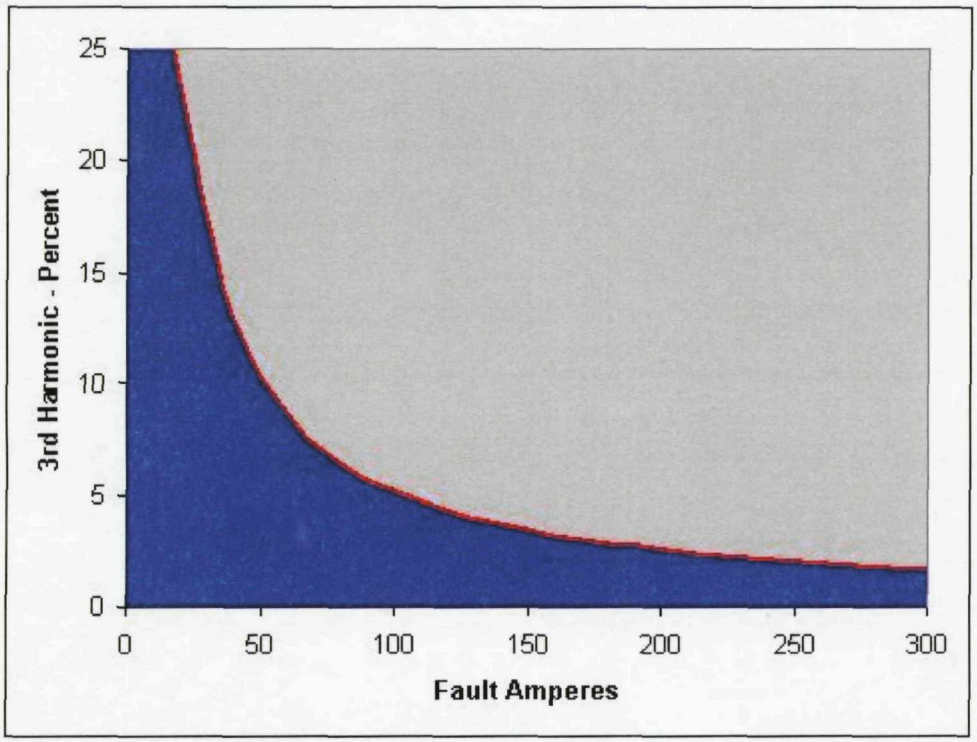

Figure 7.5 3rd harmonic fault current vs the percentage of 3rd harmonic current

In this thesis a new set of criteria is proposed based on not just the 3rd harmonic magnitude but on magnitudes and phase angles of both the 3rd and the 5th harmonics (effectively a combination of four criteria). After many simulation tests a threshold was specified for the harmonics and the angle shift to determine a HIF. Table 7.2 shows the threshold in order to declare a HIF. All criteria indicated in the table must be exceeded in order to indicate an existence of a HIF.

Table 7.2 HIF decision detection criteria

Decision	3rd harmonic	Angle of 3rd harmonic	5th harmonic	Angle of 5th harmonic
Trip - HIF	Exceeds 1% of fundamental current	Exceeds 100 degree with respect to fundamental current	Exceeds 0.5% of fundamental current	Exceeds 100 degree with respect to fundamental current

In other words, if a signal has a 3rd and 5th harmonics that exceed 1% and 0.5%, respectively, and it has angle shifts for the 3rd and 5th harmonics that exceed 100 degree (both taken with respect to the fundamental current) this will be declared as a HIF current signal. Extensive testing has shown this set of criteria to be much more reliable and less sensitive to other non-HIF harmonics generating events.

7.6 Testing and results

As may be seen in Table 7.3, before the HIF occurs, the load current is normal with no change in the phase angle and no harmonic currents. After the HIF has been applied there was a noticeable, but not large, increase in the line current; this can be interpreted by the protection relay as a load increase instead of a fault, simply because the HIF does not draw sufficient current for the relay to act. In a normal fault, the current in the fault would be much greater than the relay setting, therefore the relay would react to the fault; in the HIF case this will not happen because the setting in the relay is much less than the HIF current (see Figure 7.1). During the existence of the HIF there is a noticeable change in the circuit harmonics.

From Table 7.3 in column A, when the line is under normal operation, the line current is about 187A and no harmonics or phase change in the harmonics are detected. In column B, when HIF existed 0.5 km away from the substation where the detection relay that implements RCGA in analysing the transmission line current is located, the method has recorded that 3rd harmonic is 3.4% of the fundamental current and 5th harmonic has increased by 1.28% of the fundamental current. There was an increase of load current from 187A to

223A (36A increase which might appear to a normal relay as a load increase only). By looking at the angle shifts of the third and fifth harmonics with respect to fundamental current, the 3rd harmonic had a shift in angle of 2.44rad (140 degree), while the 5th harmonic had a 2.1rad (120 degree). According to the detection criteria the designed relay will give a flag to confirm the existence of HIF.

In other cases, as seen in Table 7.3, columns C, D and E, where the HIF existed at 1.1, 1.75, and 2.3 km away from the relay, the 3rd and 5th harmonics were about 2% and 1.13% of the fundamental current, respectively. The line current increases by about 19.5A and the angle shifts were about 2.6rad (149 degree) for the 3rd harmonic and 2.3rad (132 degree) for the 5th harmonic. Again, since these are the peculiar characteristics of a HIF and since the values analyzed by the relay exceed the detection criteria, then a flag is given to confirm the existence of HIF.

Table 7.3 Current harmonics and phase angles before and after high impedance fault
Column A: line current and phase angle under normal operation
Column B: line current and phase angle after HIF 0.5km from the substation
Column C: line current and phase angle after HIF 1.1km from the substation
Column D: line current and phase angle after HIF 1.75km from the substation
Column E: line current and phase angle after HIF 2.3km from the substation

Distance from substation	A 0.0km	B 0.5 km	C 1.1 km	D 1.75 km	E 2.3 km
	Before HIF	After HIF	After HIF	After HIF	After HIF
1st	187.19 A	223.21 A	206.79 A	206.73 A	206.72 A
Θ1	0 rad	0 rad	0 rad	0 rad	0 rad
3rd	0 A	7.77 A	4.17A	4.22 A	4.19 A
Θ3	0 rad	2.44 rad	2.64 rad	2.62 rad	2.61 rad
5th	0 A	2.85 A	1.51 A	1.57 A	1.53 A
Θ5	0 rad	2.1 rad	2.36 rad	2.35 rad	2.334rad

In the second test a HIF and load switching on the transmission line was simulated. The current has been sampled and analyzed by the proposed method to see whether the algorithm would distinguish between load switching and HIF.

A load of 750kW was switched on the line 0.04 sec. before HIF. Samples of the line current are displayed in Table 7.4. During normal operation, the line is carrying a 123A and no harmonics and phase angles have been recorded by the algorithm (Column A). During the load switching cycle (Column B) an increase in the line current is noticed (about 64A) and due to the load transient a 3rd and 5th harmonics are recorded and they represents 0.87% and 0.7% of the fundamental current respectively. An angle shift of the 3rd and 5th harmonics is noticed and they were 1.3rad (74 degree) for the 3rd harmonic and 1.2rad (71 degree) for the 5th harmonics. The switching load transient did not pass the algorithm detection criteria specified for detecting HIF and no flag is therefore given. After the load switching the line is back to normal operation with a line current of 187A (Column C) with no harmonics or phase angle shift. During HIF (Column D) the algorithm is giving a flag of the existence of HIF due to the fact that it has detected an increase in the line current of the amount of about 19.6A and a 3rd and 5th harmonics in the value of 2.01% and 0.73% respectively with respect to the fundamental current and an angle shift of 2.64rad (151 degree) for the 3rd harmonic and 2.36rad (135 degree) for the 5th harmonic.

Table 7.4 Current harmonics and phase angles before, during and after high impedance fault and load switching
Column A: line current and phase angles under normal operation
Column B: line current and phase angles during the cycle of load switching
Column C: line current and phase angles a after the load switching
Column D: line current and phase angles under HIF

	A	B	C	D
1st	123 A	187.34 A	187.2 A	206.79 A
Θ1	0 rad	0 rad	0 rad	0 rad
3rd	0 A	1.64 A	0 A	4.17 A
Θ3	0 rad	1.30 rad	0 rad	2.64 rad
5th	0 A	1.36 A	0 A	1.50A
Θ5	0 rad	1.24 rad	0 rad	2.36 rad

7.7 Conclusions

A new method for high impedance fault detection is proposed. The problem is formulated as an estimation task and a Real Coded Genetic Algorithm is used to solve this optimization problem. The method was put to the test on a particular overhead line which was simulated using Matlab. The simulated overhead line represents a line in operation which has a history of many high impedance faults and several incidents; a recent HIF case was fatal. The method was successfully tested on tracking the harmonics and current angles associated with the HIF. The results obtained show that the proposed approach can be used as a promising method of identifying high impedance faults.

Chapter 8

Summary and Conclusions

8.1 Summary and Conclusions

One of the challenges that face electricity utilities is the detection of HIFs on electric power distribution feeders. Most HIFs draw little current, which makes them difficult to detect by conventional overcurrent relays. If HIFs are not detected, they create a public hazard and threaten the lives of the public. It is the desire to improve public safety which has been the primary motivator for the development of HIF detectors.

Many HIF detection techniques have been developed over the last three decades. However, till the present there is no technique that can detect all HIFs with sufficient degree of consistency or reliability. In other words, it is relatively easy to develop a HIF detector, but it is extremely difficult to make this detector able to distinguish HIFs from HIF-like events, such as normal load switching. Another difficulty that faces the researchers in HIF detection field is the scarcity of data about HIF events due to the legal implications associated with injuries or damages that might result from an undetected HIF.

Some of the HIF detection techniques which have been developed based on expert systems are already available but there are no reports about their field performance. On the other hand, there are no commercially available genetic algorithm-based detectors so far. This fact, among other reasons, such as the advantages of genetic algorithms over conventional systems, has motivated this work. This work was also motivated by the fact that most of the rural areas connected to 11kV distribution circuits in the system of Ministry of Electricity and Water in Kuwait are overhead lines, and many accidents have happened due to faults occurring on such lines.

The objective of this work was to develop a high impedance fault model that can give us most of HIFs characteristics including harmonics content of HIF and voltage-current signatures. Another objective was to develop a genetic algorithm-based HIF diagnosis system that can reliably detect the HIF and distinguish it from HIF-like normal system operating conditions, such as load or capacitor switching, and finally identify the fault.

These objectives have been achieved through performing the following activities:
In Chapter 2 the problems of detecting HIFs and the previous research efforts are described. In Chapter 3 the physical aspects of the phenomenon of arcing are explained and a new model that represents HIFs is presented, tested and analyzed to demonstrate that it contains the unique characteristics, including the signature waveform, the harmonics and angles. This was achieved by simulation of a typical 11kV overhead distribution feeder using Matlab. Five cases were simulated:

A. Normal load switching. (0.035 s)
B. Normal load and capacitor switching. (0.025 s- 0.035 s)
C. High impedance fault. (0.03 s)
D. High impedance fault with load switching. (0.03 s – 0.025 s)
E. High impedance fault with load and capacitor switching. (0.03 s – 0.025 s – 0.035 s)

The proposed model succeeded in representing and predicting all important high impedance fault characteristics and may be considered as an appropriate and physically well justified representation of HIFs. It can be used to generate various data necessary for developing more reliable HIF detecting algorithms.

In Chapter 5 a novel method of using Real Coded Genetic Algorithm (RCGA) was described to track power system harmonics and phase angles. The use of different fitness functions, as well as the effects of sampling rate and sampling window size (number of cycles), were tested with different study cases. The first case was to track the magnitudes of the harmonics of a line to ground fault using different fitness functions and sampling times.

The RCGA was successful in accurately finding the harmonics of the voltage and current and a particular fitness function was chosen to carry out the rest of the testing due to its good performance. In the second case, HIF-like current waveforms were used and the challenge was to track the magnitudes of different harmonics and their angles due to HIF. The effect of sampling frequency and the number of cycles were studied. The method was able to estimate the value of the harmonics and the phase angles of the current with a very high accuracy. The results obtained from the test cases show that the proposed method can be used as a reliable on-line harmonic estimator especially for signals with time varying magnitudes.

In Chapter 6 a comparative study between the proposed genetic algorithm (RCGA) and the Fourier transform (FFT) is presented. In case one, a transmission line fault situation was considered and in the second case, a HIF-like current waveform was analysed. The results obtained show that RCGA was able to estimate the magnitude and phase angle of each harmonic very accurately with only 20 samples per cycle for signals both containing or void of the DC or exponential term. On the other hand, the FFT performed very poorly with 20 samples per cycle if a DC or an exponential term were present (to achieve the same accuracy as RCGA 200000 sample per cycle were needed). The performance of FFT improves significantly if no DC or exponential term is present, but - as such terms do exist in real HIF and other power system disturbances - they would first need to be filtered out this would delay the actual harmonic analysis. Overall, as no filtering is needed when using the genetic algorithm and to avoid delays in harmonic identification in real life situation, it is argued that the RCGA is a better alternative to FFT in this application.

In Chapter 7, the use of the RCGA algorithm was put to the test by applying it to track the harmonics and phase angles resulting from arcing high impedance faults. Since this research was motivated by the fact that most of the distribution lines in the rural area operated by the Ministry of Electricity and Water in Kuwait are 11kV overhead lines with a history of high impedance faults, a particular distribution line was simulated using Matlab

using real data. The high impedance fault model, presented in Chapter 3, was used and put to the test. The method was successful in tracking harmonics and current angles associated with HIF and the results obtained increase the confidence that the proposed approach can be used to identify high impedance faults.

Finally, a new set of criteria, based on combination of magnitudes and phase angle shifts of the 3^{rd} and the 5^{th} harmonics, has been proposed and shown to be reliable, especially in comparison with the previously used simple criterion relying on the magnitude of the 3^{rd} harmonic only. The use of magnitudes and phase angles of two harmonics alleviates - at least to some extent - a possible problem of harmonics due to other causes being present and thus wrongly being identified as HIF related, since it is highly unlikely that the particular features of the HIF will be also characteristic to other system disturbances.

To summarize, in this project new principles of identifying HIFs have been established and investigated using various simulations. The particular elements of novelty include:

- Creating a more accurate and flexible circuit representation of a HIF.
- Developing a particular genetic algorithm (RCGA) for harmonic analysis of waveforms typical to power systems, shown to outperform the classical FFT if DC or exponential terms are present, as in the HIFs.
- Identifying the most important and unique features of HIFs which may be used for identification purposes.
- Creating a new set of criteria for more reliable HIF detection.

8.2 Future work

This section highlights some of the areas which in the author's view would benefit from further research.

1. Only a single line to ground HIFs is simulated in this work because the majority of faults on overhead distribution lines are of this type. It would be intersting if this work could be extended to consider other fault types.
2. One of the major difficulties that faced this researcher was the shortage or complete lack of practical data about HIF events due to the legal implications related to injuries or damages that might result from an undetected HIF, and thus the unwillingness of distribution companies to disclose such data. It would be beneficial if the method was further tested on real data of reported high impedance fault cases.
3. As concluded in EPRI's survey of faults on primary distribution systems, 95% of the faults on primary distribution feeders occur on overhead lines [101]. Around 5-20% of these faults are HIFs [5]. Though only about 5% of the faults are occurring on underground distribution cable circuits, it may be worth investigating if the proposed RCGA-based HIF diagnosis system would work adequately well for these underground faults. Despite the fact that HIFs on underground distribution cables do not result in public hazard, detecting such HIFs could be advantageous to save the power losses that are unavoidable if HIFs remain undetected.
4. More tests could be performed to study cases of unbalance loading and existence of higher harmonics.
5. This thesis only provided the principles of the new detection system. The next natural step would be to build an experimental rig to test the ideas put forward here.

Appendix

Appendix 1

Symmetrical Components

The method of symmetrical components is a very important tool for the analysis of three phase electrical systems. It provides a practical technology for understanding and analyzing electrical power system operation during unbalanced conditions. The fundamental principle of symmetrical components, as applied to three phase circuits, is that an unbalanced group of three related vectors (for example, three unsymmetrical and unbalanced vectors of voltage or current in a three phase system) can be resolved into three sets of vectors. The three vectors of each set are of equal magnitude and spared either zero or 120 degrees apart. Each set is a "symmetrical component" of the original unbalanced vectors. The same concept of resolution can be applied to rotating vectors, such as voltages or currents. This method decomposes a three phase system into three distinct sets of symmetrical components:

Positive (1), Negative (2), and Zero (0) sequence

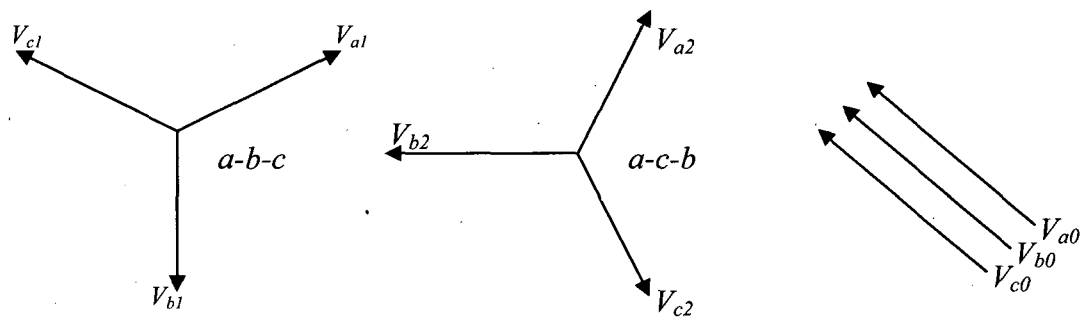

Figure 1 Three sets of balanced phasors which are the symmetrical components of three unbalanced phasors

1. Positive-sequence components consisting of three phasors equal in magnitude, displaced from each other by 120° in phase, and having the same phase sequence as the original phasors.

2. Negative-sequence components consisting of three phasors equal in magnitude, displaced from each other by 120° in phase, and having the phase sequence opposite to that of the original phasors.
3. Zero-sequence components consisting of three phasors equal in magnitude and with zero phase displacement form each other.

The phase sequence of the positive-sequence components phasers is abc, and the phase sequence of the negative-sequence components is acb. If the phasors are voltages they may be presented as V_a, V_b and V_c (the current phasor can be written with the same format) and they can be expressed in term of their components as shown:

$$V_a = V_{a1} + V_{a2} + V_{a0} \quad (2.1)$$

$$V_b = V_{b1} + V_{b2} + V_{b0} \quad (2.2)$$

$$V_c = V_{c1} + V_{c2} + V_{c0} \quad (2.3)$$

The three sets of balanced phasors that are the symmetrical components of three unbalanced phasors are shown in Figure 1. Because of the phase displacement of the symmetrical components of the voltages and current in three phase system, it is convenient to have a shorthand method of indicating the rotation of phasor trough 120°. The letter a is commonly used to designate the operator that causes a rotation of 120° in the counterclockwise direction. Such an operator is a complex number of unit magnitude with an angle of 120° and defined by the following expressions:

$$a = 1\angle 120°$$

$$a^2 = 1\angle 240°$$

$$a^3 = 1\angle 360° = 1$$

Now the expression of V_b and V_c can be presented as the product of some function of the operator a and a component of V_a. Figure1 verifies the following relations:

$$V_{b1} = a^2 V_{a1} \qquad V_{c1} = a^2 V_{a1}$$

$$V_{b2} = a V_{a2} \qquad V_{c2} = a^2 V_{a2} \qquad (2.4)$$

$$V_{b0} = V_{a0} \qquad V_{c0} = V_{a0}$$

Repeating equation 2.1 and substituting equation 2.4 in equation 2.2 and 2.3 yield:

$$V_a = V_{a1} + V_{a2} + V_{a0} \qquad (2.5)$$

$$V_b = a^2 V_{a1} + a V_{a2} + V_{a0} \qquad (2.6)$$

$$V_c = a V_{a1} + a^2 V_{a2} + V_{a0} \qquad (2.7)$$

In a matrix form:

$$\begin{bmatrix} V_a \\ V_b \\ V_c \end{bmatrix} = \begin{bmatrix} 1 & 1 & 1 \\ 1 & a^2 & a \\ 1 & a & a^2 \end{bmatrix} \begin{bmatrix} V_{a0} \\ V_{a1} \\ V_{a2} \end{bmatrix} \qquad (2.8)$$

For convenience let:

$$A = \begin{bmatrix} 1 & 1 & 1 \\ 1 & a^2 & a \\ 1 & a & a^2 \end{bmatrix} \qquad (2.9)$$

Where

$$A^{-1} = \frac{1}{3} \begin{bmatrix} 1 & 1 & 1 \\ 1 & a & a^2 \\ 1 & a^2 & a \end{bmatrix} \qquad (2.10)$$

Now multiplying both sides of equation 2.8 by A^{-1} yields:

$$\begin{bmatrix} V_{a0} \\ V_{b1} \\ V_{c2} \end{bmatrix} = \frac{1}{3} \begin{bmatrix} 1 & 1 & 1 \\ 1 & a & a^2 \\ 1 & a^2 & a \end{bmatrix} \begin{bmatrix} V_a \\ V_b \\ V_c \end{bmatrix} \qquad (2.11)$$

Equation 2.11 can be written in separate equations as following:

$$V_{a0} = \frac{1}{3}(V_a + V_b + V_c) \qquad (2.12)$$

$$V_{a1} = \frac{1}{3}(V_a + aV_b + a^2V_c)$$

$$V_{a2} = \frac{1}{3}(V_a + a^2V_b + aV_c)$$

The components $V_{b0}, V_{b1}, V_{b2}, V_{c0}, V_{c1}$ and V_{c2} can be found by equation 2.4.

Equation 2.12 shows that no zero-sequence components exist if the sum of the unbalanced phasors is zero. Since the sum of the line to line voltage phasors in three phase system is always zero, zero sequence components are never present in the line voltage, regardless of the amount of unbalance. The sum of the three line to neutral voltage phasors is not necessarily zero, and voltages to neutral may contain zero sequence components.

The preceding equations could have been written for currents instead of voltages, and they are summarized for current as shown:

$$I_a = I_{a1} + I_{a2} + I_{a0}$$

$$I_b = a^2 I_{a1} + aI_{a2} + I_{a0}$$

$$I_c = aI_{a1} + a^2 I_{a2} + I_{a0}$$

$$I_{a0} = \frac{1}{3}(I_a + I_b + I_c) \qquad (2.13)$$

$$I_{a1} = \frac{1}{3}(I_a + aI_b + a^2 I_c)$$

$$I_{a2} = \frac{1}{3}(I_a + a^2 I_b + aI_c)$$

In a three phase system the sum of the line current in the return path through the neutral is equal to In. Thus

$$I_n = I_a + I_b + I_c \qquad (2.14)$$

Comparing equation 2.13 and 2.14 gives

$$I_n = 3I_{a0}$$

In the non-existence of a path through the neutral of a three phase system, the line currents contains no zero-sequence components, and the I_n is zero.

Appendix 2

Test circuit for Chapter 3

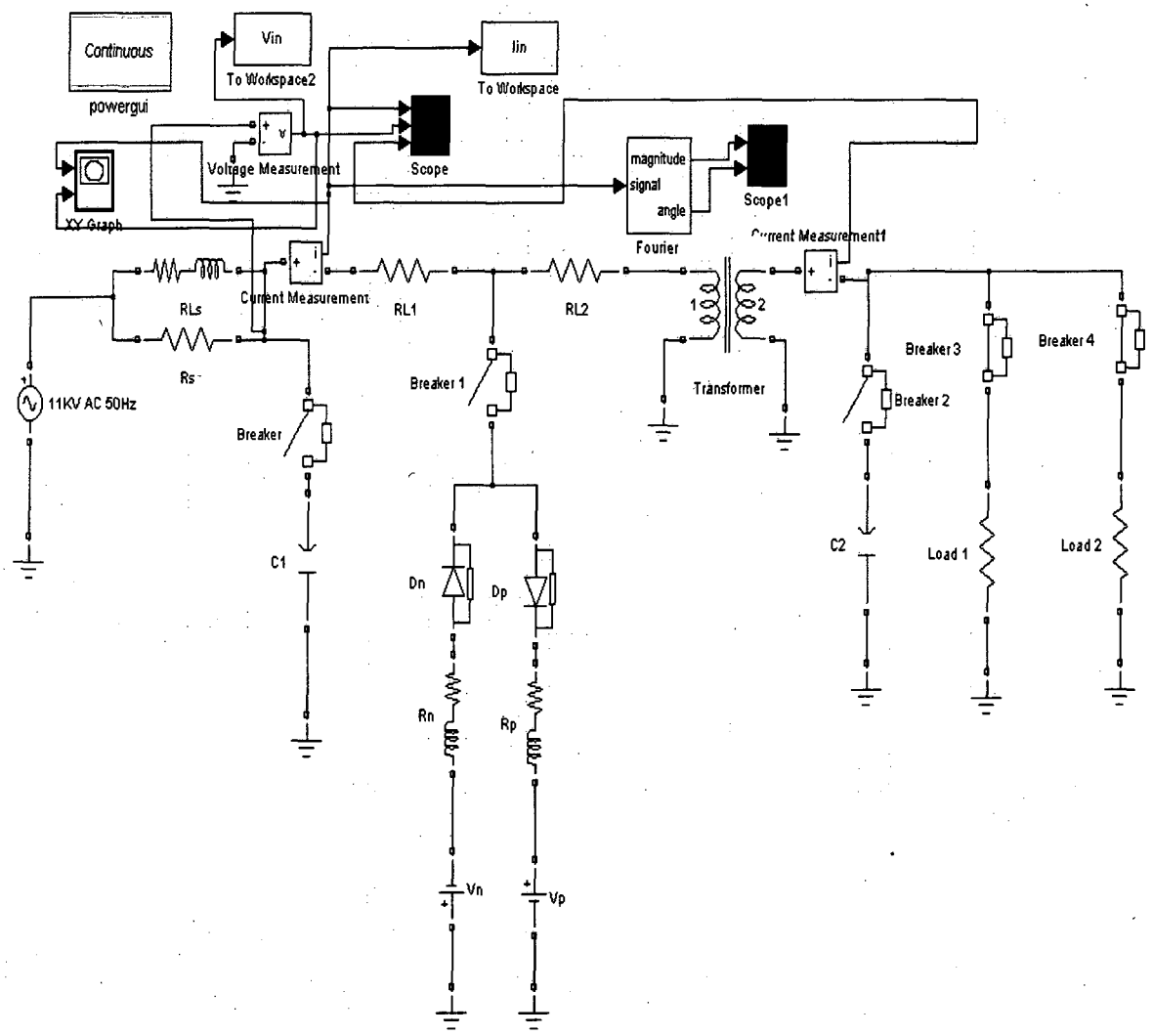

This circuit is a simplified model of a 11 kV three-phase power system. Only one phase of the transmission system is represented. The equivalent source is modeled by a voltage source in series with its internal impedance (RLs Rs)

The source feeds 11kv/0.433kV transformer through a 50 km transmission line. The line distributed parameters (R = 0.035Ω/km) and two shunt capacitances C1 and C2 are connected to the line. The load is connected to the transformer low side is load 1 and load 2 (266kW each) is modelled by an R load block.

A circuit breaker is used to switch the load at the receiving end of the transmission line.

A high impedance fault model is connected at the center of the line to simulate a HIF case and it is controlled by a circuit breaker. Current and Voltage Measurement blocks provide signals for visualization purpose.

Appendix 3

GA code for the voltage and current in case1 chapter 5 using FF1

```
function ObjVal = Va(Chrom);
w=2*pi*50;
t=0:0.001:0.02;
Vact=(0.0388*exp(-0.4*t))...
  +(0.4994*cos(ω*t))...
  +(0.3230*sin(ω*t))...
  +(0.0708*cos(2* ω*t))...
  +(0.0224*sin(2* ω*t))...
  +(0.0154*cos(3* ω*t))...
  +(0.0165*cos(4* ω*t))...
  +(0.0219*sin(4* ω*t))...
  +(0.0176*cos(5* ω*t))...
  +(0.0119*sin(5* ω*t))...
  +(0.0120*cos(6* ω*t))...
  +(0.0289*sin(6* ω*t))...
  +(0.0084*cos(7* ω*t))...
  +(0.0084*sin(7* ω*t));

[Nind,Nvar] = size(Chrom);

for i=1:Nind
    Vcal=(Chrom(i,1)*exp(-0.4*t))...
       +(Chrom(i,2)*cos(ω *t))...
       +(Chrom(i,3)*sin(ω *t))...
       +(Chrom(i,4)*cos(2* ω*t))...
       +(Chrom(i,5)*sin(2* ω*t))...
       +(Chrom(i,6)*cos(3* ω*t))...
       +(Chrom(i,7)*cos(4* ω*t))...
       +(Chrom(i,8)*sin(4* ω*t))...
       +(Chrom(i,9)*cos(5* ω*t))...
       +(Chrom(i,10)*sin(5* ω*t))...
       +(Chrom(i,11)*cos(6* ω*t))...
       +(Chrom(i,12)*sin(6* ω*t))...
       +(Chrom(i,13)*cos(7* ω*t))...
       +(Chrom(i,14)*sin(7* ω*t));

      ObjVal(i,1)=sum((Vact-Vcal).^2);
end
//
```

```
function ObjVal = Ia(Chrom);
w=2*pi*50;
t=0:0.001:0.02;
Iact=(0.0454*exp(-0.4*t))...
  +(0.4662*cos(ω*t))...
  +(0.0817*sin(ω*t))...
  +(0.0519*cos(2* ω*t))...
  +(0.0543*sin(2* ω*t))...
  +(0.0305*cos(3* ω*t))...
  +(0.0218*cos(4* ω*t))...
  +(0.0313*sin(4* ω*t))...
  +(0.0178*cos(5* ω*t))...
  +(0.0244*sin(5* ω*t))...
  +(0.0159*cos(6* ω*t))...
  +(0.0196*sin(6* ω*t))...
  +(0.0157*cos(7* ω*t))...
  +(0.0168*sin(7* ω*t));

[Nind,Nvar] = size(Chrom);

for i=1:Nind
    Ical=(Chrom(i,1)*exp(-0.4*t))...
       +(Chrom(i,2)*cos(ω*t))...
       +(Chrom(i,3)*sin(ω*t))...
       +(Chrom(i,4)*cos(2* ω*t))...
       +(Chrom(i,5)*sin(2* ω*t))...
       +(Chrom(i,6)*cos(3* ω*t))...
       +(Chrom(i,7)*cos(4* ω*t))...
       +(Chrom(i,8)*sin(4* ω*t))...
       +(Chrom(i,9)*cos(5* ω*t))...
       +(Chrom(i,10)*sin(5* ω*t))...
       +(Chrom(i,11)*cos(6* ω*t))...
       +(Chrom(i,12)*sin(6* ω*t))...
       +(Chrom(i,13)*cos(7* ω*t))...
       +(Chrom(i,14)*sin(7* ω*t));

      ObjVal(i,1)=sum((Iact-Ical).^2);
end
//
```

GA code for the voltage and current in case 1 Chapter 5 using FF2

```
function ObjVal = Va(Chrom);
w=2*pi*50;
t=0:0.001:0.02;
Vact=(0.0388*exp(-0.4*t))...
  +(0.4994*cos(ω *t))...
  +(0.3230*sin(ω *t))...
  +(0.0708*cos(2* ω*t))...
  +(0.0224*sin(2* ω*t))...
  +(0.0154*cos(3* ω*t))...
  +(0.0165*cos(4* ω*t))...
  +(0.0219*sin(4* ω*t))...
  +(0.0176*cos(5* ω*t))...
  +(0.0119*sin(5* ω*t))...
  +(0.0120*cos(6* ω*t))...
  +(0.0289*sin(6* ω*t))...
  +(0.0084*cos(7* ω*t))...
  +(0.0084*sin(7* ω*t));

[Nind,Nvar] = size(Chrom);

for i=1:Nind
    Vcal=(Chrom(i,1)*exp(-0.4*t))...
       +(Chrom(i,2)*cos(ω *t))...
       +(Chrom(i,3)*sin(ω *t))...
       +(Chrom(i,4)*cos(2* ω*t))...
       +(Chrom(i,5)*sin(2* ω*t))...
       +(Chrom(i,6)*cos(3* ω*t))...
       +(Chrom(i,7)*cos(4* ω*t))...
       +(Chrom(i,8)*sin(4* ω*t))...
       +(Chrom(i,9)*cos(5* ω*t))...
       +(Chrom(i,10)*sin(5* ω*t))...
       +(Chrom(i,11)*cos(6* ω*t))...
       +(Chrom(i,12)*sin(6* ω*t))...
       +(Chrom(i,13)*cos(7* ω*t))...
       +(Chrom(i,14)*sin(7* ω*t));

      ObjVal(i,1)=sum(abs((Vact-Vcal)));
end
//
```

```
function ObjVal = Ia(Chrom);
w=2*pi*50;
t=0:0.001:0.02;
Iact=(0.0454*exp(-0.4*t))...
  +(0.4662*cos(ω *t))...
  +(0.0817*sin(ω *t))...
  +(0.0519*cos(2* ω *t))...
  +(0.0543*sin(2* ω *t))...
  +(0.0305*cos(3* ω *t))...
  +(0.0218*cos(4* ω *t))...
  +(0.0313*sin(4* ω*t))...
  +(0.0178*cos(5* ω*t))...
  +(0.0244*sin(5* ω*t))...
  +(0.0159*cos(6* ω*t))...
  +(0.0196*sin(6* ω*t))...
  +(0.0157*cos(7* ω*t))...
  +(0.0168*sin(7* ω*t));

[Nind,Nvar] = size(Chrom);

for i=1:Nind
    Ical=(Chrom(i,1)*exp(-0.4*t))...
       +(Chrom(i,2)*cos(ω *t))...
       +(Chrom(i,3)*sin(ω *t))...
       +(Chrom(i,4)*cos(2* ω *t))...
       +(Chrom(i,5)*sin(2* ω*t))...
       +(Chrom(i,6)*cos(3* ω*t))...
       +(Chrom(i,7)*cos(4* ω*t))...
       +(Chrom(i,8)*sin(4* ω*t))...
       +(Chrom(i,9)*cos(5* ω*t))...
       +(Chrom(i,10)*sin(5* ω*t))...
       +(Chrom(i,11)*cos(6* ω*t))...
       +(Chrom(i,12)*sin(6* ω*t))...
       +(Chrom(i,13)*cos(7* ω*t))...
       +(Chrom(i,14)*sin(7* ω*t));

      ObjVal(i,1)=sum(abs((Iact-Ical)));
end
```

GA code for the generated HIF current in case 2 Chapter 5 using FF1

```
function ObjVal = Ia(Chrom);
w=2*pi*50;
cycle=1;
step=0.0001;
period=0.02;
t=0:step:cycle*period;

Iact=(5)...
  +(80*sin(ω *t))...
  +(1*cos(2* ω *t))...
  +(8*sin(3* ω *t+2.88))...
  +(1*cos(4* ω *t))...
  +(4*sin(5* ω *t+2.76))...
  +(1*cos(6* ω *t))...
  +(1*sin(7* ω *t+2.62));

[Nind,Nvar] = size(Chrom);

for i=1:Nind
    Ical=Chrom(i,1)...
        +(Chrom(i,2)*sin(ω *t+Chrom(i,3)))...
        +(Chrom(i,4)*cos(2* ω*t+Chrom(i,5)))...
        +(Chrom(i,6)*sin(3* ω*t+Chrom(i,7)))...
        +(Chrom(i,8)*cos(4* ω*t+Chrom(i,9)))...
        +(Chrom(i,10)*sin(5* ω*t+Chrom(i,11)))...
        +(Chrom(i,12)*cos(6* ω*t+Chrom(i,13)))...
        +(Chrom(i,14)*sin(7* ω*t+Chrom(i,15)));

        ObjVal(i,1)=sum((Iact-Ical).^2);

end
//
```

Appendix 4

GA code for the voltage and current in case1 chapter6 using FF1

```
function ObjVal = Va(Chrom);
w=2*pi*50;
t=0:0.001:0.02;
Vact=(0.0550*exp(-0.4*t))...
     +(0.9829*cos(ω *t))...
     +(0.1842*sin(ω *t))...
     +(0.0141*cos(2* ω*t))...
     +(0.0245*sin(2* ω*t))...
     +(0.0077*cos(3* ω*t))...
     +(0.0197*sin(3* ω*t))...
     +(0.0050*cos(4* ω*t))...
     +(0.0168*sin(4* ω*t))...
     +(0.0039*cos(5* ω*t))...
     +(0.0154*sin(5* ω*t))...
     +(0.0033*cos(6* ω*t))...
     +(0.0161*sin(6* ω*t))...
     +(0.0033*cos(7* ω*t))...
     +(0.0230111*sin(7* ω*t));

[Nind,Nvar] = size(Chrom);

for i=1:Nind
   Vcal=(Chrom(i,1)*exp(-0.4*t))...
      +(Chrom(i,2)*cos(ω*t))...
      +(Chrom(i,3)*sin(ω*t))...
      +(Chrom(i,4)*cos(2* ω*t))...
      +(Chrom(i,5)*sin(2* ω*t))...
      +(Chrom(i,6)*cos(3* ω*t))...
      +(Chrom(i,7)*sin(3* ω*t))...
      +(Chrom(i,8)*cos(4* ω*t))...
      +(Chrom(i,9)*sin(4* ω*t))...
      +(Chrom(i,10)*cos(5* ω*t))...
      +(Chrom(i,11)*sin(5* ω*t))...
      +(Chrom(i,12)*cos(6* ω*t))...
      +(Chrom(i,13)*sin(6* ω*t))...
      +(Chrom(i,14)*cos(7* ω*t))...
      +(Chrom(i,15)*sin(7* ω*t));

     ObjVal(i,1)=sum((Vact-Vcal).^2);
end
```

```
function ObjVal = Ia(Chrom);
w=2*pi*50;
t=0:0.001:0.02;
Iact=(0.2491*exp(-0.4*t))...
  +(0.9587*cos(ω*t))...
  +(0.284*sin(ω*t))...
  +(0.0619*cos(2*.ω*t))...
  +(0.1054*sin(2* ω*t))...
  +(0.0329*cos(3* ω*t))...
  +(0.0811*sin(3* ω*t))...
  +(0.0206*cos(4* ω*t))...
  +(0.0643*sin(4* ω*t))...
  +(0.0146*cos(5* ω*t))...
  +(0.0528*sin(5* ω*t))...
  +(0.0116*cos(6* ω*t))...
  +(0.0448*sin(6* ω*t))...
  +(0.0052*cos(7* ω*t))...
  +(0.0401111*sin(7* ω*t));

[Nind,Nvar] = size(Chrom);

for i=1:Nind
    Ical=(Chrom(i,1)*exp(-0.4*t))...
       +(Chrom(i,2)*cos(ω*t))...
       +(Chrom(i,3)*sin(ω*t))...
       +(Chrom(i,4)*cos(2* ω*t))...
       +(Chrom(i,5)*sin(2* ω*t))...
       +(Chrom(i,6)*cos(3* ω*t))...
       +(Chrom(i,7)*sin(3* ω*t))...
       +(Chrom(i,8)*cos(4* ω*t))...
       +(Chrom(i,9)*sin(4* ω*t))...
       +(Chrom(i,10)*cos(5* ω*t))...
       +(Chrom(i,11)*sin(5* ω*t))...
       +(Chrom(i,12)*cos(6* ω*t))...
       +(Chrom(i,13)*sin(6* ω*t))...
       +(Chrom(i,14)*cos(7* ω*t))...
       +(Chrom(i,15)*sin(7* ω*t));

      ObjVal(i,1)=sum((Iact-Ical).^2);
end
//
```

FFT code for the current in case 1 Chapter 6

```
t0=cputime;
w=2*pi*50;
c=1;
step=0.0000001;
period=0.02;
t=0:step:c*period
x=(0.2491*exp(-0.4*t))...
  +(0.9587*cos(ω*t))...
  +(0.2841*sin(ω*t))...
  +(0.0619*cos(2* ω*t))...
  +(0.1054*sin(2* ω*t))...
  +(0.0329*cos(3* ω*t))...
  +(0.0811*sin(3* ω*t))...
  +(0.0206*cos(4* ω*t))...
  +(0.0643*sin(4* ω*t))...
  +(0.0146*cos(5* ω*t))...
  +(0.0528*sin(5* ω*t))...
  +(0.0116*cos(6* ω*t))...
  +(0.0448*sin(6* ω*t))...
  +(0.0052*cos(7* ω*t))...
  +(0.0401*sin(7* ω*t));
y = fft(x)/((period*c/step+1)/2);
m = abs(y);
t=0.004 %threshold
ind=find(m>t) %indices at which positions m exceeds t
m(ind) %the values of m at these indices
%plot(m(1:(period*c/step)/2+1))
y(ind) %the values of the FFT at these indices
%ysmall=y([1:c:c*7+1]);ysmall(1)=ysmall(1)/2;ysmall
angle(y([1:c:c*7+1])) %angle of the FFT values for the harmonics
re=real(y([1:c:c*7+1]));re(1)=re(1)/2;re %cosine amplitudes
im=-imag(y([1:c:c*7+1]));im(1)=im(1)/2;im %sine amplitudes
```

GA code for the generated HIF current in case 2 Chapter 6 using FF1

```
function ObjVal = Ia(Chrom);
w=2*pi*50;
cycle=1;
step=0.0001;
period=0.02;
t=0:step:cycle*period;

Iact=(5)...
  +(80*sin(ω *t))...
  +(1*cos(2* ω *t))...
  +(8*sin(3* ω *t+2.88))...
  +(1*cos(4* ω *t))...
  +(4*sin(5* ω *t+2.76))...
  +(1*cos(6* ω *t))...
  +(1*sin(7* ω *t+2.62));

[Nind,Nvar] = size(Chrom);

for i=1:Nind
    Ical=Chrom(i,1)...
        +(Chrom(i,2)*sin(ω *t+Chrom(i,3)))...
        +(Chrom(i,4)*cos(2* ω *t+Chrom(i,5)))...
        +(Chrom(i,6)*sin(3* ω *t+Chrom(i,7)))...
        +(Chrom(i,8)*cos(4* ω *t+Chrom(i,9)))...
        +(Chrom(i,10)*sin(5* ω *t+Chrom(i,11)))...
        +(Chrom(i,12)*cos(6* ω *t+Chrom(i,13)))...
        +(Chrom(i,14)*sin(7* ω *t+Chrom(i,15)));

        ObjVal(i,1)=sum((Iact-Ical).^2);

end
//
```

FFT code for the generated HIF current in case 2 Chapter 6

```
w=2*pi*50;
c=2;
step=0.00001;
period=0.02;
t=0:step:c*period;

z= (5)...
  +(80*sin(ω *t))...
  +(1*cos(2* ω *t))...
  +(8*sin(3* ω *t+2.88))...
  +(1*cos(4* ω *t))...
  +(4*sin(5* ω *t+2.76))...
  +(1*cos(6* ω *t))...
  +(1*sin(7* ω *t+2.62));

 zz= (5)...
  +(80*cos(ω *t-pi/2))...
  +(1*cos(2* ω *t))...
  +(8*cos(3* ω *t+2.88-pi/2))...
  +(1*cos(4* ω *t))...
  +(4*cos(5* ω *t+2.76-pi/2))...
  +(1*cos(6* ω *t))...
  +(1*cos(7* ω *t+2.62-pi/2));


y = fft(z)/((period*c/step+1)/2);


ang=angle(y([1:c:c*10+1])); ang%angle of the FFT values for the harmonics
im=imag(y([1:c:c*10+1]));im(1)=im(1)/2;im %sine amplitudes
re=real(y([1:c:c*10+1]));re(1)=re(1)/2;re %cosine amplitudes
%plot(t,z)
```

Appendix 5

Three phase circuit for Chapter 7

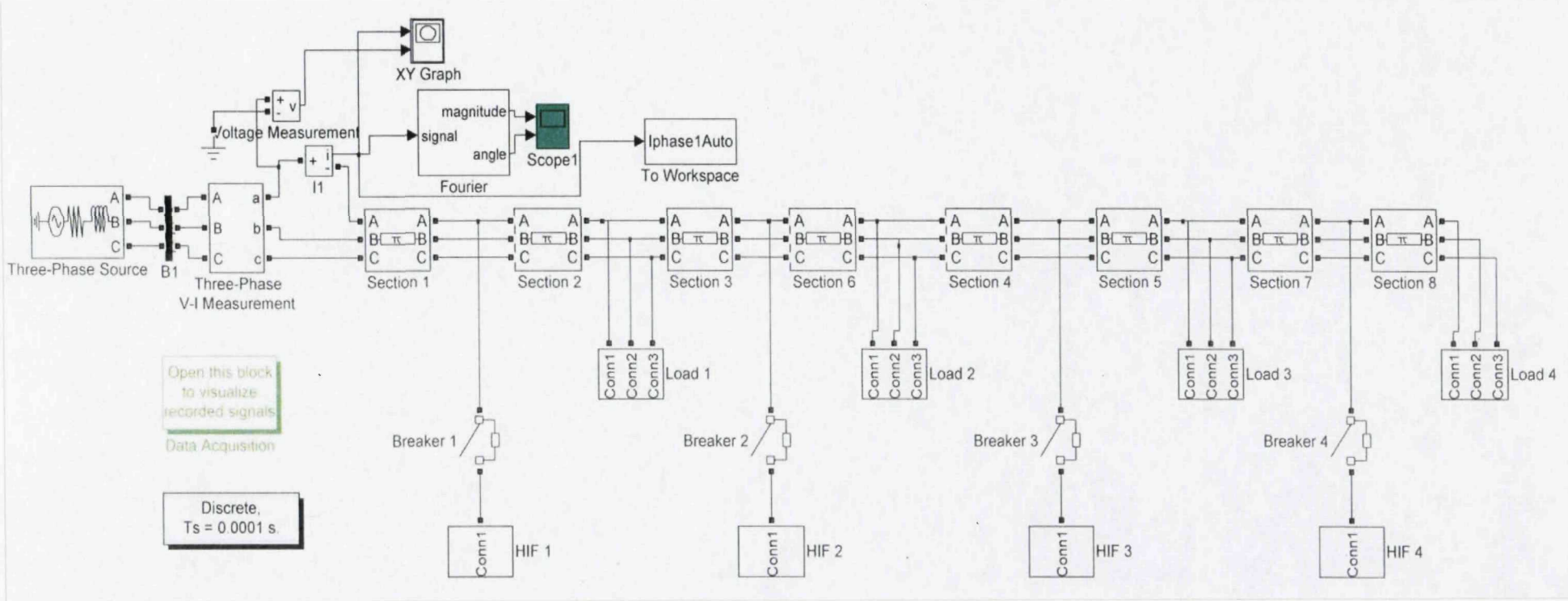

Publications

i. M.EL-Naggar and N. Zamanan, "A Digital Genetic Based Algorithms For Measurement of Earth Fault Loop Impedance," In Proceedings of The International Conference on Advanced Power System Automation and Protection APAP2004, Korea, 2004.

ii. N. Zamanan, J. Sykulski, and A. K. Al-Othman, "A digital technique for online identification and tracking of power system harmonics based on Real Coded Genetic Algorithm," In Proceedings of Sixth IASTED International Conference EUROPEAN POWER AND ENERGY SYSTEMS (521-052), pp. 144-148, Rhodes, Greece, 2006.

iii. N. Zamanan, J. K. Sykulski, and A. K. Al-Othman, "Real Coded Genetic Algorithm Compared to the Classical Method of Fast Fourier Transform in Harmonics Analysis," In Proceedings of the 41st International Universities Power Engineering Conference, Newcastle upon Tyne, UK. , 2006.

iv. N. Zamanan and J. K. Sykulski, "Modelling arcing high impedance faults in relation to the physical processes in the electric arc," *WSEAS Transactions on Power Systems*, vol. 1 (8), pp. 1507-1512, 2006.

v. N. Zamanan and J. K. Sykulski, "Modelling arcing high impedance faults in relation to the physical processes in the electric arc," presented at 6th WSEAS Int. Conf. on POWER SYSTEMS (PE '06), pp. 28-33, Lisbon, Portugal, 2006.

vi. N. Zamanan, J. K. Sykulski, and A. K. Al-Othman, (2007) "Arcing High Impedance Fault Detection Using Real Coded Genetic Algorithm". In Proceedings of Third IASTED Asian Conference Power and Energy Systems, pp. 35-39, Phuket, Thailand.

References:

[1] J. W. Bialek, "Recent blackouts in US and continental Europe: Is liberalisation to blame?," *Cambridge working papers in Economics CWPE 0407/ CMI working paper 34*, 2004.

[2] PSRC, "High impedance fault detection technology," *Report of PSRC working group D15*, 1996.

[3] R. Patterson, "Signatures and software find high impedance faults," *IEEE Computer Applications in Power*, vol. 8, pp. 12-15, 1995.

[4] L. Li and M. A. Redfern, "A review of techniques to detect downed conductors in overhead distribution systems," presented at Proceedings of 7th International Conference on Developments in Power Systems Protection (DPSP 2001), 9-12 April 2001, Amsterdam, Netherlands, 2001.

[5] C. G. Wester, "High impedance fault detection on distribution systems," presented at 1998 Rural Electric Power Conference Presented at 42nd Annual Conference, 26-28 April 1998, St. Louis, MO, USA, 1998.

[6] A. M. Sharaf, R. M. El-Sharkawy, R. Al-Fatih, and M. Al-Ketbi, "High impedance fault detection on radial distribution and utilization systems," presented at Proceedings of 1996 Canadian Conference on Electrical and Computer Engineering, 26-29 May 1996, Calgary, Alta., Canada, 1996.

[7] W. H. Kwon, G. W. Lee, Y. M. Park, M. C. Yoon, and M. H. Yoo, "High impedance fault detection utilizing incremental variance of normalized even order harmonic power," *IEEE Transactions on Power Delivery*, vol. 6, pp. 557-64, 1991.

[8] C. L. Benner and B. D. Russell, "Practical high-impedance fault detection on distribution feeders," *IEEE Transactions on Industry Applications*, vol. 33, pp. 635-40, 1997.

[9] B. M. Aucoin and R. H. Jones, "High impedance fault detection implementation issues," *IEEE Transactions on Power Delivery*, vol. 11, pp. 139-145, 1996.

[10] M. Carpenter, R. R. Hoad, T. D. Bruton, R. Das, S. A. Kunsman, and J. M. Peterson, "Staged-fault testing for high impedance fault data collection," presented at 2005 58th Annual Conference for Protective Relay Engineers, 5-7 April 2005, College Station, TX, USA, 2005.

[11] IEEE, "Downed power lines: why they can't always be detected," *IEEE Power Engineering soceity public affairs document*, 1989.

[12] J. T. Tengdin, E. E. Baker, J. J. Burke, B. D. Russell, R. H. Jones, T. E. Wiedman, and N. J. Johnson, "Application of high impedance fault detectors: a summary of the panel session held at the 1995 IEEE PES summer meeting," presented at Proceedings of 1996 Transmission and Distribution Conference and Exposition, 15-20 Sept. 1996, Los Angeles, CA, USA, 1996.

[13] PSRC, "Distribution line protection practices industry survey results," *IEEE power system relay committee report* 2002.

[14] PSRC, "Distribution line protection practices industry survey results," *IEEE power system relay committee report*, 1995.

[15] M. Aucoin, "Status of high impedance fault detection," *IEEE Transactions on Power Apparatus and Systems*, vol. PAS-104, pp. 638-644, 1985.

[16] B. M. Aucoin and B. D. Russell, "Detection of incipient and low current faults in electric distribution systems," Washington, DC, USA, 1989.

[17] S. Ebron, D. L. Lubkeman, and M. White, "Neural network approach to the detection of incipient faults on power distribution feeders," *IEEE Transactions on Power Delivery*, vol. 5, pp. 905-914, 1990.

[18] PSRC, "The Interruption of Downed Conductors on Low Voltage Distribution Systems"Data collected by Pennsylvania Power and Light Co. " 1974 and 1975 fallen 12kV overhead Distribution conductiors, Breakdown of 390 Cases"," IEEE power system relay committee report 1976.

[19] W. D. Stevenson, *Elements of power system analysis*: McGraw-Hill Inc., 1975.

[20] J. Arrillaga, D. A. Bradely, and P. S. Bondger, *Power Systems Harmonics*. New York: John Wiley & Sons, 1985.

[21] R. C. Dugan, M. F. McGranaghan, and H. W. Beaty, *Electrical Power Systems Quality*. United states: McGraw Hill, 1996.

[22] IEEE, "IEEE 512-1992 Recommended practices and requirements for harmonic control in electrical power systems."

[23] D. I. Jeerings and J. R. Linders, "Unique aspects of distribution system harmonics due to high impedance ground faults," *IEEE Transactions on Power Delivery*, vol. 5, pp. 1086-94, 1990.

[24] H. Calhoun, M. T. Bishop, C. H. Eichler, and R. E. Lee, "Development and testing of an electro-mechanical relay to detect fallen distribution conductors," *IEEE Transactions on Power Apparatus and Systems*, vol. PAS-101, pp. 1643-50, 1982.

[25] R. Patterson, W. Tyska, B. D. Russell, and B. M. Aucoin, "A microprocesor-based digital feeder monitor with high-impedance fault detection," *47th annual conference for protective relay engineers*, 1994.

[26] M. Aucoin and B. D. Russell, "Detection of distribution high impedance faults using burst noise signals near 60Hz," *IEEE Transactions on Power Delivery*, vol. PWRD-2, pp. 342-348, 1987.

[27] A. R. Sedighi, M. R. Haghifam, O. P. Malik, and M. H. Ghassemian, "High impedance fault detection based on wavelet transform and statistical pattern recognition," *IEEE Transactions on Power Delivery*, vol. 20, pp. 2414-21, 2005.

[28] A. Lazkano, J. Ruiz, E. Aramendi, and L. A. Leturiondo, "A new approach to high impedance fault detection using wavelet packet analysis," presented at Proceedings of 2000 International Conference on Harmonics and Quality of Power, 1-4 Oct. 2000, Orlando, FL, USA, 2000.

[29] K. Chul-Hwan, K. Hyun, K. Young-Hun, B. Sung-Hyun, R. K. Aggarwal, and A. T. Johns, "A novel fault-detection technique of high-impedance arcing faults in transmission lines using the wavelet transform," *IEEE Transactions on Power Delivery*, vol. 17, pp. 921-9, 2002.

[30] H. M. jaber and A. I. megahed, "a Wavelet-FIRANN technique for high impedance arcing faults detection in distribution systems.," *international conference on power systems transients*, 1995.

[31] T. M. Lai, L. A. Snider, E. Lo, and D. Sutanto, "High-impedance fault detection using discrete wavelet transform and frequency range and RMS conversion," *IEEE Transactions on Power Delivery*, vol. 20, pp. 397-407, 2005.

[32] L. A. Snider and Y. Y. Shan, "The artificial neural networks based relay algorithm for distribution system high impedance fault detection," presented at APSOM-97. International Conference on Advances in Power System Control, Operation and Management, 11-14 Nov. 1997, Hong Kong, 1997.

[33] M. Al-Dabbagh and L. Al-Dabbagh, "Neural networks based algorithm for detecting high impedance faults on power distribution lines," presented at Proceedings of International Conference on Neural Networks, 10-16 July 1999, Washington, DC, USA, 1999.

[34] H. Khorashadi-Zadeh, "A novel approach to detection high impedance faults using artificial neural network," Bristol, UK, 2004.

[35] R. Keyhani, M. Deriche, and E. Palmer, "A high impedance fault detector using a neural network and subband decomposition," presented at Proceedings of ISSPA 2001. Sixth International Symposium on Signal Processing and its Applications, 13-16 Aug. 2001, Kuala Lumpur, Malaysia, 2001.

[36] L. L. Lai, "Application of neural networks to fault classification and protection," Hong Kong, 1997.

[37] T. M. Lai, L. A. Snider, E. Lo, C. H. Cheung, and K. W. Chan, "High impedance faults detection using artificial neural network," Hong Kong, China, 2003.

[38] A. M. Sharaf, L. A. Snider, and K. Debnath, "A neural network based relaying scheme for distribution system high impedance fault detection," presented at 1993 First New Zealand International Two-Stream Conference on Artificial Neural Networks and Expert Systems, 24-26 Nov. 1993, Dunedin, New Zealand, 1993.

[39] A.-R. Sedighi, M.-R. Haghifam, and O. P. Malik, "Soft computing applications in high impedance fault detection in distribution systems," *Electric Power Systems Research*, vol. 76, pp. 136-144, 2005.

[40] H. Ching-Lien, C. Hui-Yung, and C. Ming-Tong, "Algorithm comparison for high impedance fault detection based on staged fault test," *IEEE Transactions on Power Delivery*, vol. 3, pp. 1427-35, 1988.

[41] A. M. Sharaf and S. I. Abu-Azab, "A smart relaying scheme for high impedance faults in distribution and utilization networks," Halifax, NS, Canada, 2000.

[42] A. F. Sultan, G. W. Swift, and D. J. Fedirchuk, "Detecting arcing downed-wires using fault current flicker and half-cycle asymmetry," *IEEE Transactions on Power Delivery*, vol. 9, pp. 461-70, 1994.

[43] Y. Sheng and S. M. Rovnyak, "Decision tree-based methodology for high impedance fault detection," *IEEE Transactions on Power Delivery*, vol. 19, pp. 533-536, 2004.

[44] A. Lazkano, J. Ruiz, L. A. Leturiondo, and E. Aramendi, "High impedance arcing fault detector for three-wire power distribution networks," Lemesos, Cyprus, 2000.

[45] B. D. Russell and R. P. Chinchali, "A digital signal processing algorithm for detecting arcing faults on power distribution feeders," *IEEE Transactions on Power Delivery*, vol. 4, pp. 132-40, 1989.

[46] M. El-Hami, "A distribution system fault location technique utilizing high frequency spectrum of fault current," Galway, Ireland, 1994.

[47] A. A. Girgis, W. Chang, and E. B. Makram, "Analysis of high-impedance fault generated signals using a Kalman filtering approach," *IEEE Transactions on Power Delivery*, vol. 5, pp. 1714-24, 1990.

[48] A. V. Mamishev, B. D. Russell, and C. L. Benner, "Analysis of high impedance faults using fractal techniques," *IEEE Transactions on Power Systems*, vol. 11, pp. 435-40, 1996.

[49] R. E. Lee and M. T. Bishop, "Comparison of measured high impedance fault data to digital computer modeling results," *IEEE Transactions on Power Apparatus and Systems*, vol. PAS-104, pp. 2754-2758, 1985.

[50] A. E. Emanuel, D. Cyganski, J. A. Orr, S. Shiller, and E. M. Gulachenski, "High impedance fault arcing on sandy soil in 15 kV distribution feeders: contributions to the evaluation of the low frequency spectrum," *IEEE Transactions on Power Delivery*, vol. 5, pp. 676-86, 1990.

[51] M. B. Djuric and V. V. Terzija, "New approach to the arcing faults detection for fast autoreclosure in transmission systems," *IEEE Transactions on Power Delivery*, vol. 10, pp. 1793-1798, 1995.

[52] A. T. Johns, R. K. Aggarwal, and Y. H. Song, "Improved techniques for modelling fault arcs on faulted EHV transmission systems," *IEE Proceedings Generation, Transmission and Distribution*, vol. 141, pp. 148-154, 1994.

[53] S. R. Nam, J. K. Park, Y. C. Kang, and T. H. Kim, "A modeling method of a high impedance fault in a distribution system using two series time-varying resistances in EMTP," presented at Proceedings of Power Engineering Society Summer Meeting, 15-19 July 2001, Vancouver, BC, Canada, 2001.

[54] J. A. Rees, *Electrical Breakdown in Gases*: The Macmillan Press LTD, 1973.

[55] J. S. Townsend, "The diffusion of ions into gases," *philosophical transactions of the Royal Society of London, series A, Containing papers of a mathematical or physical character*, vol. 193, pp. 129-158, 1900.

[56] J. Slepian, *A series of lectures on conduction of electricity in gases*, 1933.

[57] T. H. Lee, "Plasma physics and interruption of an electric circuit," *proc. of the IEEE*, vol. 57, pp. 307-323, 1969.

[58] J. M. Somerville, *The Electric Arc*: John Wiley & sons inc. printed in GB by Butler & Tanner Ltd, 1959.

[59] H. Edels, "Properties and theory of the electric arc," *IEE Proceedings A*, vol. 108, pp. 55-69, 1961.

[60] J. Slepian, "Extinction of an A.C. Arc," *Journal of the A.I.E.E*, October 1928.

[61] F. M. Penning, *Electrical Discharges in Gases*: Macmillan & Co. Ltd., 1965.

[62] K. G. Emeleus, *The Conduction of Electricity Through Gases*: Methuen & Co. LTD, 1951.

[63] F. Austin., R. Maxfield, and R. Benedict, *Theory of Gaseous Conduction and Electronics* McGraw-Hill Book Co.,inc., 1941.

[64] D. I. Jeerings and J. R. Linders, "Ground resistance-revisited," *IEEE Transactions on Power Delivery*, vol. 4, pp. 949-56, 1989.

[65] R. Rudenberg, *Transient performance of electric power system: phenomena in lumped networks*, First ed: MIT press, 1950.

[66] R. H. Kaulinann and J. C. Page, "Arcing fault protection for low-voltage," *power distribution systems- nature of the problem," AIEE Trans*, pp. 160-167, June 1960.

[67] J. R. Dunki-Jacobs, "The effects of arcing ground faults on low-voltage system design," *IEEE Transactions on Industry Applications*, vol. IA-8, pp. 223-30, 1972.

[68] T. Gammon and J. Matthews, "The historical evolution of arcing-fault models for low-voltage systems," Sparks, NV, USA, 1999.

[69] T. Gammon and J. Matthews, "Instantaneous arcing-fault models developed for building system analysis," *IEEE Transactions on Industry Applications*, vol. 37, pp. 197-203, 2001.

[70] P. Persephonis, K. Vlachos, C. Georgiades, and J. Parthenios, "The inductance of the discharge in a spark gap," *Journal of Applied Physics*, vol. 71, pp. 4755-62, 1992.

[71] J. Holland, *Adoption in Natural and Artificial Systems*: The MIT Press, 1975.

[72] J. Stender, *Parallel Genetic Algorithms: Theory and Applications*: IOS Press, 1993.

[73] D. E. Goldberg, *Genetic Algorithms in Search Optimization and Machine Learning.* Reading, Ma: Addison Wesely, 1989.

[74] M. Mitchell, *An introduction to Genetic Algorithms*: MIT press, 1999.

[75] D. A. Coley, *An introduction to Genetic Algorithms For Scientists and Engineers*: World scientific, 1999.

[76] E. Falkenauer, *Genetic algorithms and grouping problems*. New York: Wiley, 1997.

[77] Z. Michalewicz, *Genetic algorithms + data structures = evolution programs*: 3rd rev. and extended ed. Berlin; New York: Springer-Verlag,, 1996.

[78] D. Whitley, "The GENITOR Algorithm and Selection Pressure: Why Rank-Based Allocation of Reproductive Trials is Best," presented at Proc. ICGA 3, 1989.

[79] J. E. Baker, "Reducing bias and inefficiency in the selection algorithm," Cambridge, MA, USA, 1987.

[80] A. H. Wright, "Genetic algorithms for real parameter optimization," presented at Foundations of Genetic Algorithms,(edited by Gregory J. E. Rawlins), Morgan Kaufman, 1991.

[81] H. Mühlenbein and D. Schlierkamp-Voosen, "Predictive Models for the Breeder Genetic Algorithm: I. Continuous Parameter Optimization," *Evolutionary Computation*, vol. 1, pp. 25-49, 1993.

[82] S. B. Davan and A. Straughen, *Power Semiconductor Circuits*. New York: John Wiley & Sons, 1985.

[83] I. Kamwa and R. Grondin, "Fast adaptive schemes for tracking voltage phasor and local frequency in power transmission and distribution systems," *IEEE Transactions on Power Delivery*, vol. 7, pp. 789-95, 1992.

[84] A. A. Girgis, W. B. Chang, and E. B. Makram, "A digital recursive measurement scheme for on-line tracking of power system harmonics," *IEEE Transactions on Power Delivery*, vol. 6, pp. 1153-1160, 1991.

[85] A. A. Girgis and F. M. Ham, "A quantitative study of pitfalls in the FFT," *IEEE Transactions on Aerospace and Electronic Systems*, vol. AES-16, pp. 434-9, 1980.

[86] F. Zhang, Z. Geng, and W. Yuan, "The algorithm of interpolating windowed FFT for harmonic analysis of electric power system," *IEEE Transactions on Power Delivery*, vol. 16, pp. 160-164, 2001.

[87] D. D. Shipp, W. S. Vilcheck, M. E. Swartz, and N. H. Woodley, "Expert system for analysis of power system harmonics," Houston, TX, USA, 1992.

[88] P. K. Dash, S. K. Panda, A. C. Liew, B. Mishra, and R. K. Jena, "A new approach to monitoring electric power quality," *Electric Power Systems Research*, vol. 46, pp. 11-20, 1998.

[89] W. M. Al-Hasawi, H. K. M. Youssef, and K. M. El-Naggar, "A genetic algorithm for on-line identification and tracking of power system harmonics," presented at Proceedings of 2000 Conference on Power and Energy Systems (PES 2000), 19-22 Sept. 2000, Marabella, Spain, 2000.

[90] R. A. Macedo, D. da Silva, D. V. Coury, and A. C. P. L. F. de Carvalho, "A new technique based on genetic algorithms for tracking of power system harmonics," Pernambuco, Brazil, 2002.

[91] C. Z. Janikow and Z. Michalewicz, "Experimental comparison of binary and floating point representations in genetic algorithms," San Diego, CA, USA, 1991.

[92] S. Caorsi, A. Massa, and M. Pastorino, "A computational technique based on a real-coded genetic algorithm for microwave imaging purposes," *IEEE Transactions on Geoscience and Remote Sensing*, vol. 38, pp. 1697-708, 2000.

[93] H. BOUZEBOUDJA, A. CHAKER, A. ALLALI, and B. NAAMA, "Economic dispatch solution using a real-coded genetic algorithm," *Acta Electrotechnica et Informatica*, vol. 5, 2005.

[94] C. S. Moo, Y. N. Chang, and P. P. Mok, "A digital measurement scheme for time-varying transient harmonics," *IEEE Transactions on Power Delivery*, vol. 10, pp. 588-94, 1995.

[95] F. J. Harris, "On the use of windows for harmonic analysis with the discrete Fourier transform," *Proceedings of the IEEE*, vol. 66, pp. 51-83, 1978.

[96] S. Haykin, *Communication Systems*. New York: John wiley & Sons, Inc., 1994.

[97] R. A. De Macedo, D. Da Silva Filho, D. V. Coury, and A. A. De Franca Mendes Carneiro, "An Evolutionary Optimization Approach to Track Voltage and Current Harmonics in Electrical Power Systems," presented at 2003 IEEE Power Engineering Society General Meeting, Jul 13-17 2003, Toronto, Ont., Canada, 2003.

[98] "Report IEEE Power System Relaying Committee working Group D15 "High impedance fault detection technology"," GE Power management web site 2001.

[99] B. D. Russell, R. P. Chinchali, and C. J. Kim, "Behaviour of low frequency spectra during arcing fault and switching events," *IEEE Transactions on Power Delivery*, vol. 3, pp. 1485-92, 1988.

[100] N. Zamanan and J. K. Sykulski, "Modelling arcing high impedance faults in relation to the physical processes in the electric arc," *WSEAS Transactions on Power Systems*, vol. 1 (8), pp. 1507-1512, 2006.

[101] "Distribution Fault Current Analysis," EPRI Report RP-1209-1, Vol. 1-2, Prepared by Power Technologies Inc.1983.

[102] S. Guggenmoos, "Effects of tree mortality on power line security," *Journal of Arboriculture*, vol. 29(4), pp. 181-196, 2003.

[103] N. Zamanan, J. Sykulski, and A. K. Al-Othman, "A digital technique for online identification and tracking of power system harmonics based on Real Coded Genetic Algorithm," Rhodes, Greece, 2006.

[104] N. Zamanan, J. K. Sykulski, and A. K. Al-Othman, "Real Coded Genetic Algorithm Compared to the Classical Method of Fast Fourier Transform in Harmonics Analysis," presented at the 41st International Universities Power Engineering Conference, Newcastle upon Tyne, UK. , 2006.

[105] N. Zamanan, J. K. Sykulski, and A. K. Al-Othman, "Arcing High Impedance Fault Detection Using Real Coded Genetic Algorithm," presented at the third IASTED Asian Conference Power and Energy Systems, Phuket, Thailand, 2007.

[106] E. A. Atwell, A. W. Shaffer, D. I. Jerrings, and J. R. Linders, "Performance testing of the Nordon high impedance ground fault detector on a distribution feeder," Orlando, FL, USA, 1990.